

Delft University of Technology
Master's Thesis in Electrical Engineering

Uniform Gain Beamforming in 60 GHz Communications

Anggrit Dewangkara Yudha Pinangkis



Uniform Gain Beamforming in 60 GHz Communications

Master's Thesis in Electrical Engineering

Embedded Software Section
Faculty of Electrical Engineering, Mathematics and Computer Science
Delft University of Technology
Mekelweg 4, 2628 CD Delft, The Netherlands

Anggrit Dewangkara Yudha Pinangkis
anggritdewangkarayudhapinangkis-1@student.tudelft.nl

5th August 2017

Author

Anggrit Dewangkara Yudha Pinangkis (anggritdewangkarayudhapinangkis-1@student.tudelft.nl)

Title

Uniform Gain Beamforming in 60 GHz Communications

MSc presentation

5th August 2017

Graduation Committee

prof. dr. K. Langendoen (chair) Delft University of Technology

dr. Przemyslaw Pawelczak Delft University of Technology

dr. Morteza Alavi Delft University of Technology

Abstract

Wireless data traffic is growing rapidly as the number of mobile devices increase and video contents become more popular. As 2.4 GHz and 5 GHz band communications only provide limited bandwidth, these frequency bands cannot support the demand of ultra-high data rate. Millimeter-wave (mmWave) communications promise massive available bandwidth to support the next generation of wireless communications (e.g. 5G and the next Wi-Fi standard) such as 60 GHz band that offers 7 GHz available bandwidth. This extremely high frequency (EHF) band not only provides large available bandwidth, but it also experiences more losses than in 2.4 GHz and 5 GHz band communications. With such excessive path loss challenge, mmWave communications employ beamforming to compensate the losses. Switched beamforming, which is performed in the media access layer (MAC), is preferred due to its low computational complexity compared to adaptive beamforming. However, to avoid high beam training overhead, beam-searching algorithm in the MAC layer beamforming must be chosen appropriately.

Beam-searching protocol in IEEE 802.15.3c and IEEE 802.11ad, which exploit two-level of beam-searching, still can experience high training overhead if narrow beams are used. Therefore, hierarchical beam-searching algorithms are proposed to reduce training packet overhead. In our approach, hierarchical beam-searching approach with two beam candidates at each level of beam-searching is chosen to minimize the number of training packets. These beam candidates then transmit training packets giving signal quality information of each beam so that the best beam can be selected.

Some beamforming techniques have already been proposed to follow hierarchical beam-searching algorithm. However, the prior beamforming techniques do not consider non-isotropic array element beam pattern. As a result, the gain follows array element beam pattern where the gain weakens at the angle direction close to the end-fire direction following beam pattern of a single patch antenna element. In this thesis, we propose a beamforming technique that has uniform gain within the scanning coverage even with the non-isotropic element patterns. To the best of our knowledge, our proposed beamforming is the first work that considers a realistic element beam pattern in mmWave communications. The proposed beamforming requires flexible antenna weight vectors (AWVs) and more antenna elements than IEEE 802.15.3c or discrete Fourier transform (DFT) based beamforming. Due to the flexibility value of AWVs, the AWVs must be done in the digital domain. However, digital beamforming requires a large number of radio frequency (RF) chains. Therefore, hybrid beamforming is chosen to solve the problem. We show that we achieve uniform gains with reasonable complexity.

Preface

First of all, I would like to thank my daily supervisor, Dr. Kishor Chandra, for guiding me finishing the thesis project and understanding me during the difficult times. I also have to thank my supervisor, Dr. RangaRao Venkatesha Prasad, for giving me advices and feed back on the thesis project. Next, I would like to thank Prof. dr. Koen Langendoen for accepting me to join Embedded Software group.

Special thanks go to my family, especially my parents, for the sincere and irreplaceable support. I want to thank my beloved country, Indonesia, that gives me scholarship support through Indoesia Endowment Fund for Education (LPDP) with their taxes. I also really appreciate my academic counsellor, Agaby Masih, and my student psychologist, Paula Meesters, for helping me through the tough times. Last but not least, thanks to my friends who always support and help me.

Anggrit Dewangkara Yudha Pinangkis

Delft, The Netherlands

5th August 2017

Contents

Preface	v
1 Introduction	1
1.1 Background	1
1.2 Problem Description	4
1.3 Contribution	5
1.4 Outline	6
2 Beamforming in 60 GHz	7
2.1 Array Antenna	7
2.2 MAC Layer Beamforming	12
2.3 Beam-Searching Algorithm	12
2.3.1 IEEE 802.15.3c Beam-Searching Algorithms	12
2.3.2 IEEE 802.11ad Beam-Searching Algorithm	14
2.3.3 Hierarchical Beam-Searching Algorithm	15
2.4 Codebook Designs	17
2.4.1 IEEE 802.15.3c Codebook	17
2.4.2 Digital Fourier Transform (DFT) Based Codebook	18
2.4.3 Fourier Series Method with Kaiser Window (FSM-KW) Codebook	19
2.5 Beamforming Architectures	22
2.5.1 Analog Beamforming	23
2.5.2 Digital Beamforming	23
2.5.3 Hybrid Beamforming	23
2.6 Limitations in the Existing Works	30
3 Designing Uniform Gain Beamforming	33
3.1 Uniform Gain Beamforming	33
3.1.1 Beam-Broadening Factor	40
3.1.2 Sidelobe Attenuation Coefficient in FSM-KW Beam- forming	41
3.2 Beamforming Design Methodology	43

3.2.1	Solving the Highest Level Beamforming Parameters (Beamwidth and Beam Position)	44
3.2.2	Defining Lower Level Beamforming Parameters (Beamwidth and Beam Position)	49
3.2.3	Constructing Beamforming Codebook for Fully-Digital Beamforming Architecture	51
3.2.4	Constructing Beamforming Codebook for Hybrid Beamforming Architecture	54
4	Beamforming Realization	61
4.1	Beamforming in Different Element Patterns	61
4.2	Beamforming for Different Scanning Coverage	66
4.3	Beamforming for Different Number of Antenna Elements	68
4.4	Beamforming in Hybrid Architecture for Different Number of RF Chains	69
4.5	Beamforming in Hybrid Architecture Performing Simultaneous Beams	72
5	Beamforming Performance	75
5.1	Gain Variations	75
5.2	Received Signal Quality Analysis	80
6	Conclusion and Future Work	87
6.1	Conclusion	87
6.2	Future Work	88
	Appendices	91
A	Finest Beam Candidates	93
A.1	Scanning Coverage $\Delta\theta_c = 120^\circ$	93
A.2	Scanning Coverage $\Delta\theta_c = 60^\circ$	96
B	Pseudo Algorithms	99
B.1	Hybrid Beamforming Algorithm	99
B.2	Hierarchical Beam-searching Algorithm in the Proposed Beamforming	101

Chapter 1

Introduction

1.1 Background

The demand for the high data rate wireless communications is rapidly increasing due to the proliferation in use of mobile devices and bandwidth hungry applications e.g. video contents. Based on Cisco report [1], while global IP traffic will grow threefold, global mobile data traffic is predicted to grow enormously eightfold from 2015 to 2020. By 2020, mobile devices and Wi-Fi will contribute to 66% of IP traffic [1]. The rapid growing of IP traffic comes from video traffic that is expected to be 82% of all internet traffic in 2020 [1].

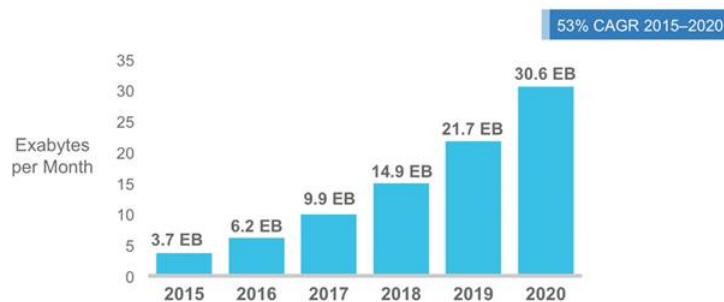


Figure 1.1: Global mobile data traffic in 2015-2020 [1]

Although optical fiber transmission can support up to 255 Tbps [2], wireless transmission is still far below that number e.g. theoretically IEEE 802.11n that works at 2.4 GHz and 5 GHz can reach up to 600 Mbps [3] while IEEE 802.11ac that works at 5 GHz can achieve up to 2.34 Gbps [4]. Thus, there is a huge bottleneck between fiber optic network and wireless link. Moreover, the 2.4 GHz band is heavily congested with a lot of interferences which not only

come from the neighboring wireless network but also from other household electronics e.g. LCD TVs, microwave ovens, and cordless phones.

Two industrial, scientific, and medical (ISM) frequency bands widely used in Wi-Fi which are 2.4 GHz and 5 GHz only occupy 90 MHz and 5 GHz of bandwidth respectively. This narrow bandwidth limits the performance to achieve high data rate. Some techniques such as multiple-input and multiple-output (MIMO) and orthogonal frequency-division multiplexing (OFDM) are implemented to boost up the data rate with such given limited frequency bandwidth. However, the data rate is still not enough to follow the demand of ultra-high throughput, especially in the data-hungry video transmission. Uncoded 4K or 8K video have data rate vary from 3.182 Gbps to 127.4 Gbps while 8K video with 32 bpp that implements advanced coding requires data rate ranging from 10 to 20 Gbps [5]. Thus, higher bandwidth is a must to accommodate ultra-high data rate. Consequently, higher frequency band needs to be used in order to support wider available bandwidth.

Wireless transmission faces some challenges limiting the communication performance such as free space loss, multipath condition, and blockage issue. Theoretically, higher frequency carrier can support higher data rate. However, high frequency also faces significant path loss. Comparing 60 GHz with 2.4 GHz and 5 GHz, the 60 GHz gives additional 28 dB and 21.6 dB of losses respectively. Moreover, the 60 GHz band is also known as an oxygen absorption band that gives 15dB/km of additional losses due to the presence of oxygen [6]. This frequency band is also prone to blockage. It can suffer 40 to 80 dB of attenuation from the brick wall [7].

The 60 GHz band becomes interesting because this unlicensed ISM band is available in most countries as seen in Figure 1.2. It also can offer 10 times until 100 times more spectrum than is currently available spectrum in the ISM bands e.g. 900 MHz, 2.4 GHz, and 5 GHz [8]. Thus, it can support ultra-high data transmission. This frequency band is divided into four channels; each has 2.16 GHz of bandwidth. The four center frequencies are 58.32 GHz, 60.48 GHz, 62.64 GHz and 64.8 GHz [9].

Despite having path loss issue, the 60 GHz band is still really interesting in short range communication (≈ 10 m) [10] to provide multi-gigabit wireless communication. Currently, there are two released IEEE standards in 60 GHz frequency band, IEEE 802.11ad and IEEE 802.15.3c, which run for short range communication. The IEEE 802.15.3c can support data rate up to 5.8 Gbps while the IEEE 802.11ad can achieve up to 7 Gbps [9].

As high losses in the 60 GHz is unavoidable, a directional antenna using narrow pencil beams is needed to achieve ultra-high data rate. Directional beam not only leads to high gain, which compensates the high path loss incurred at 60 GHz, but it also reduces interference level by focusing the

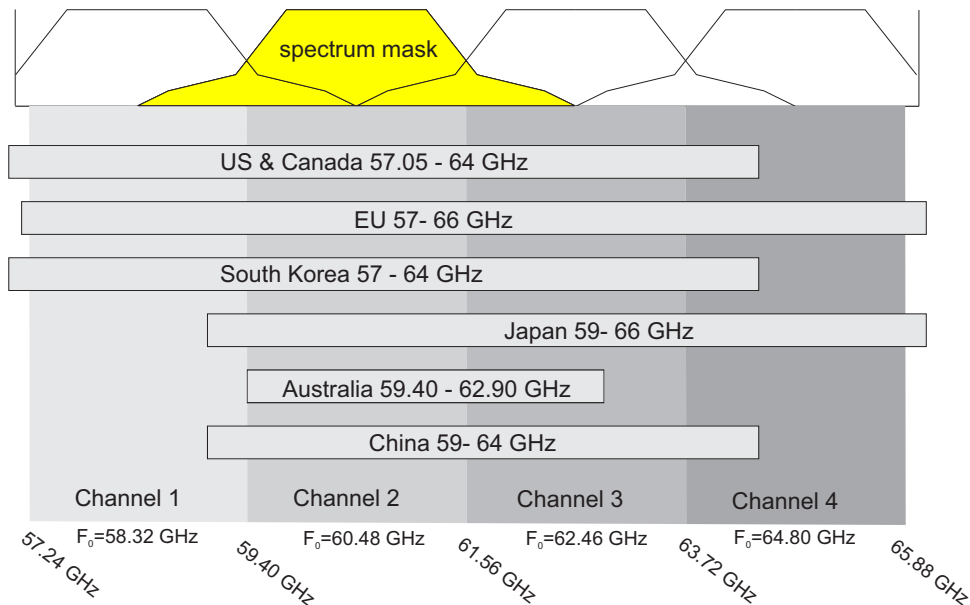


Figure 1.2: Channelization and availability of 60 GHz frequency band in some country regions[8]

transmission into the desired direction. Thus, beamforming is a necessity in the 60 GHz communications. Thanks to the small wavelength in 60 GHz, beamforming implementation using antenna array that consists of a large number of antenna elements in 60 GHz is made feasible. For example, an array antenna that has interspace element distance $\lambda/2$ enables 64 antenna elements to be packed into around 16 cm length of size.

In general, there are two types of beamforming: (i) adaptive beamforming and (ii) switched beamforming. The former one uses adaptive signal processing to create the beam so that maximum signal quality can be obtained. However, this beamforming requires high computational complexity. To minimize the complexity, the later beamforming is used in IEEE 802.15.3c and IEEE 802.11ad. In the switched beamforming, searching process is done by selecting the best beam among the predefined beam candidates. The predefined beam candidates are controlled by assigning codebook at the array antenna elements. The codebook represents the predefined antenna weight vectors (AWVs) of array antenna. The beam quality of each beam is measured sequentially following the beam-searching protocol.

In the switched beamforming, two devices that want to initiate beamforming need to exchange training packets to get information which best beam pair should be selected. These training packets give signal quality information by using such specific beam. By measuring the signal quality from each beam, communication using the best beam pair can be established. As the beam

resolution increases, the number of training packets also increases. Thus, to avoid high overhead in the beam-searching, protocol how to exchange the training packets should be defined properly.

Usually, instead of using fully exhaustive beam-searching, two-level beam-searching is performed to improve the efficiency of training packets as in IEEE 802.11ad and IEEE 802.15.3c. Both IEEE standards use two-level of beam-searching that consists of coarse level and fine level. Beam-searching protocol in IEEE 802.11ad performs better than the one in IEEE 802.15.3c regarding the low number of packet training that should be sent. Nevertheless, this two-level beam-searching still incurs beam training overhead, especially in the high beam resolution. Hence, hierarchical beam-searching that exploits binary search-like is preferred [11, 12, 13, 14, 15]. Instead of employing two-level beamforming as in IEEE 802.15.3c and IEEE 802.11ad, the hierarchical approach performs multi-level beamforming where in our approach at each level there are two beam candidates to minimize number of training packets.

1.2 Problem Description

Prior beamforming approaches generally only consider isotropic radiation pattern in the element antenna. By assuming isotropic element pattern, IEEE 802.15.3c, DFT-based, and FSM-KW based beamforming have the same maximum gain for each beam candidates. Even FSM-KW based beamforming in [12] has equal gain for its all beam candidates. Nevertheless, isotropic assumption is not realistic.

An antenna element always has higher gain in a particular direction. Array phased antenna in 60 GHz communication usually exploits patch antenna for a compact design and ease of manufacture reason [16]. A patch antenna is a directional antenna that has maximum beam in the direction perpendicular to its plane. The beam pattern degrades at low angle direction. Consequently, a steered beam approaching end-fire direction also weakens following the beam degradation of element pattern as shown in Figure 1.3, and so does the received signal quality. Therefore, to improve the signal quality in the direction close to end-fire, we propose to use beamforming that has uniform gain in all direction within the scanning coverage.

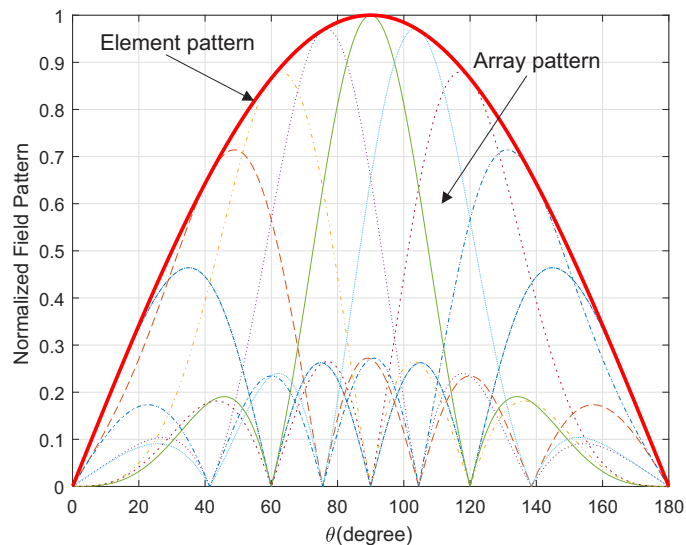


Figure 1.3: The array patterns drop following the element pattern as the beams are steered

1.3 Contribution

This thesis focuses on designing beamforming technique in 60 GHz communications. Switched beamforming is chosen due to its simplicity over adaptive beamforming. Predefined beams in the switched beamforming are assigned by codebook matrix that represents the antenna weight vectors (AWVs).

Prior beamforming techniques which generally assume isotropic antenna element radiation suffers beam degradation at the edge of scanning coverage when the non-isotropic antenna element radiation is taken into account. This beam degradation affects the received signal quality. Therefore, the proposed beamforming design must be able to generate relatively the same gain for all predefined beam candidates.

We identify that the main objective of this thesis is

Designing beamforming technique with uniform gain for 60 GHz communications irrespective of the beam direction.

Beside achieving the main goal, this thesis also gives some contributions as follows

- Identify the beam-searching algorithm, beamforming design, and beamforming architecture that must be used in the proposed beamforming.
- Designing algorithm that can define codebook for the proposed beam-

forming so that the beamforming can be set for any arbitrary limited scanning coverage.

- Evaluate the proposed beamforming by comparing the signal received quality in the proposed beamforming with the existing beamforming techniques that also uses hierarchical beamforming

1.4 Outline

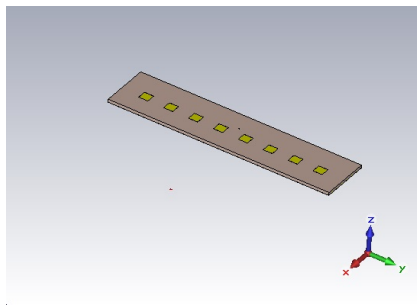
Explanation about beamforming mechanisms especially in the 60 GHz standards i.e. IEEE 802.15.3c and IEEE 802.11ad is described in Chapter 2. Chapter 3 explains about the approach how to design the proposed beams. After that, beamforming for various conditions such as various element beam patterns, various scanning coverages, and various number of antenna elements are presented in Chapter 4. In Chapter 5, the proposed beamforming is evaluated by simulating the received signal quality. Finally, in Chapter 6 the conclusions and future works are discussed.

Chapter 2

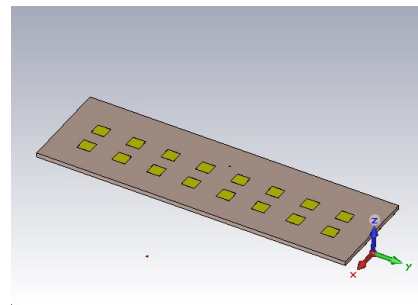
Beamforming in 60 GHz

Beamforming can be realized by adjusting amplitude and phase of signal at each antenna element in the array antenna. As stated in Chapter 1, beamforming is an essential technique to compensate high losses in 60 GHz. Therefore, beamforming mechanism should be designed properly by considering the beamforming application.

2.1 Array Antenna



(a) 1x8 linear array



(b) 2x8 planar array

Figure 2.1: Array antenna structure

Array antenna is a structure composed of several antenna elements as shown in Figure 2.1. A straight line array antenna in Figure 2.1a is called linear array antenna while a two dimension array antenna in Figure 2.1b is named planar antenna. The array antenna is an important part in the 60 GHz communications as this wireless communication systems require beamforming to compensate high Friis loss in high frequency or short wavelength as shown

in Eq. 2.1.

$$PL = 20 \log \left(\frac{4\pi d}{\lambda} \right) \quad (2.1)$$

where PL is Friis free space loss (dB), d is the distance between transmitter and receiver (m), and λ is wavelength (m).

Array antenna depicted in Figure 2.1 is composed by patch antenna elements. Patch antenna is preferred as an antenna element in the mmWave beamforming application since this antenna has a compact size and is easy to manufacture [16]. This antenna element focuses energy direction perpendicular to its ground plane as illustrated in Figure 2.2.

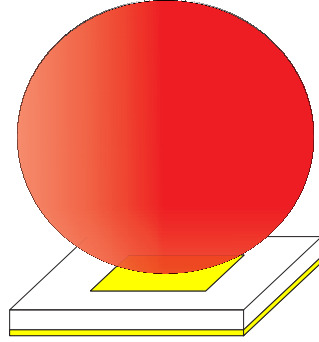


Figure 2.2: Illustration of beam pattern in a single antenna patch element

Incoming electromagnetic waves at the antenna elements experience different phase due to spacing between antenna elements in the array antenna. There will be constructive and destructive interference as a result of combining the fields from each antenna element. Therefore, by adjusting the antenna weight vectors (AWVs), consisting phase and amplitude changes, the radiation can be focused into the desired direction. In this thesis, we only focus on uniform linear array antenna that has uniform spacing between the antenna elements as shown in Figure 2.3 due to its simplicity in the beamforming design.

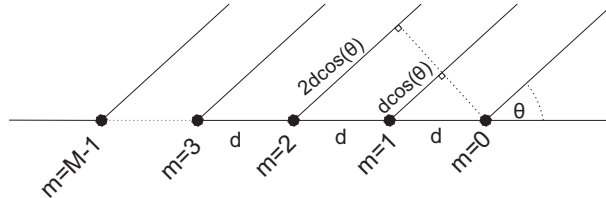


Figure 2.3: Geometry of a linear array antenna consisting of M antenna elements

Total field received by antenna array from θ direction ($E_{total}(\theta)$) that has M identical antenna elements can be defined as the sum of the field received by M antenna elements. If each antenna element receives field $E_0(\theta)$ from θ direction, the total field received by array antenna from θ direction will be

$$E_{total}(\theta) = E_0(\theta) \sum_{m=0}^{M-1} e^{jm \frac{2\pi}{\lambda} d \cos \theta} \quad (2.2)$$

where θ denotes the elevation direction from the antenna plane (XY plane) to the Z axis as seen in Figure 2.1.

If we adjust the weight vectors (amplitude and phase shift) of each antenna element with $w(m)$, the total field received by the array antenna becomes

$$E_{total}(\theta) = E_0(\theta) \sum_{m=0}^{M-1} w_m e^{jm \frac{2\pi}{\lambda} d \cos \theta} \quad (2.3)$$

where θ denotes the elevation angle and m is the antenna element index. The weight vector, \mathbf{w} , is in the normalized form such that $\|\mathbf{w}\| = 1$. It means that the total input power in the array antenna is normalized to one of unit power. Therefore, the antenna input power will be independent to the number of antenna element.

From Eq. 2.3, the total field can be seen as a product of the field from a single element (E_0) and the array factor (AF) [17, 18, 19]

$$E_{total}(\theta) = E_0(\theta) AF(\theta) \quad (2.4)$$

where

$$AF(\theta) = \sum_{m=0}^{M-1} w_m e^{jm \frac{2\pi}{\lambda} d \cos \theta} \quad (2.5)$$

Eq. 2.4 gives an interpretation that the radiation strength will depend on the array factor. Thus, \mathbf{w} must be set so that the antenna will receive signals from the desired direction only. By doing so, there will be antenna gain advantage in the desired direction and interference rejection in the undesired direction. Figure 2.4 depicts the array beam pattern as a result of multiplication between the element pattern and the array factor.

Planar array gives more concentrated beam than linear array. By using the same antenna orientation as in Figure 2.1, the 3D array factor of both linear array antenna and planar array antenna can be seen in Figure 2.5. In this case, we set such that each antenna element has a uniform amplitude and there are no phase shift changes.

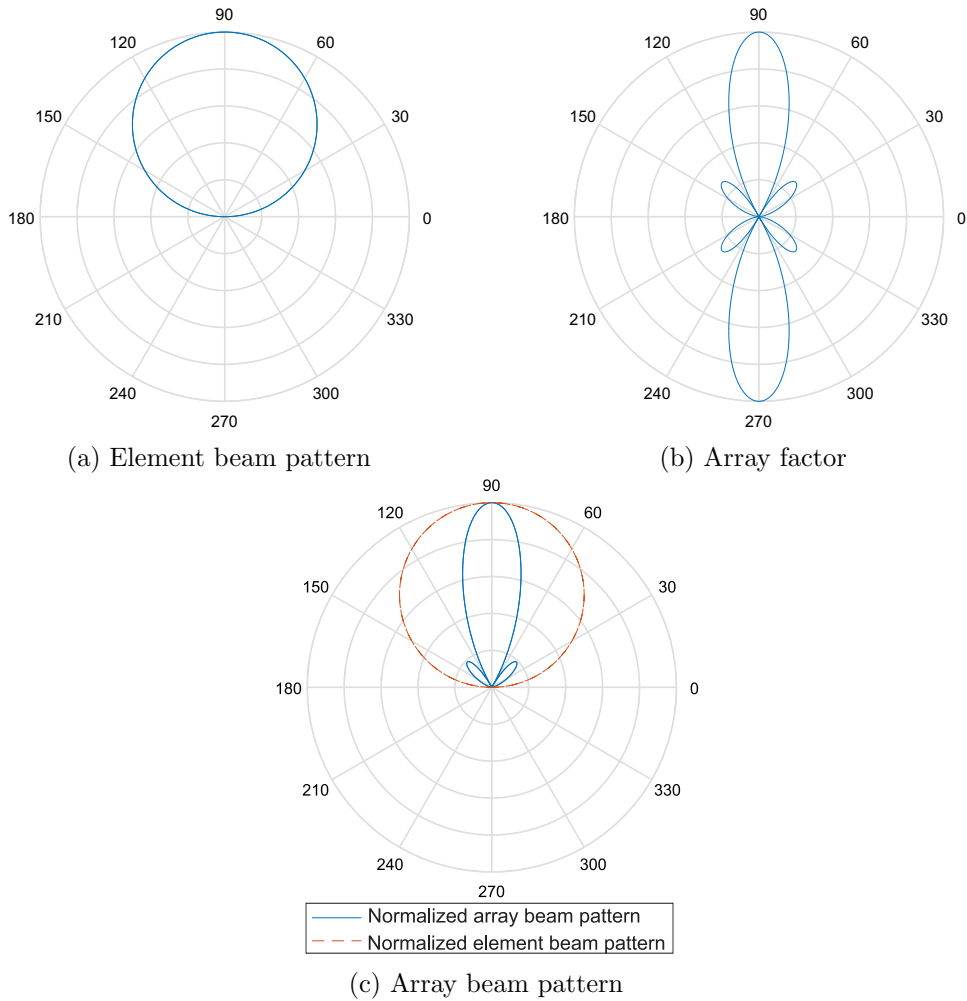


Figure 2.4: Illustration of beamforming in array antenna (number of antenna elements $M = 4$)

In order to avoid multiple maxima or grating lobe as seen in Figure 2.6 and to minimize the coupling effect, the inter-element spacing is set to half of wavelength [17, 20]. Therefore, in our approach, the spacing is also set to half of wavelength.

Antenna performance is usually described in directivity or gain. Directivity is defined as the ratio between the radiation intensity in a given direction and the average radiation intensity over all directions [17]. If we use directivity in the array antenna, Eq. 2.4 can be written as

$$D(\theta) = D_0(\theta)[AF(\theta)]^2 \quad (2.6)$$

where $D(\theta)$ is the directivity of array antenna at θ direction and $D_0(\theta)$ is the directivity of an antenna element at θ direction. By comparing Eq. 2.4

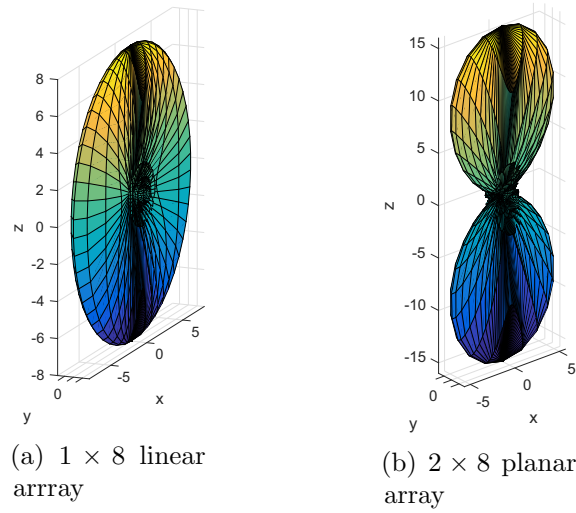


Figure 2.5: Array factor in the array antenna

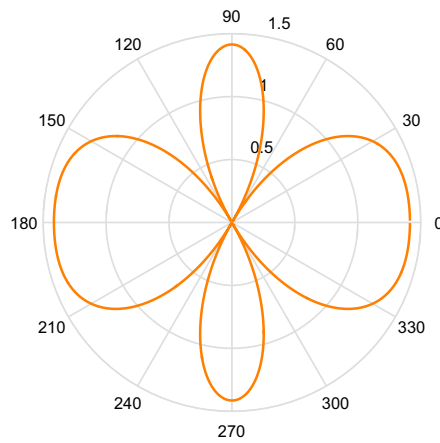


Figure 2.6: Grating lobes when $d = \lambda$

and Eq. 2.6, we can say that directivity is proportional to the square of field.

When antenna radiation efficiency (ϵ), which is a ratio between the radiated power and the input power, is taken into account, gain (G) can be used to describe the antenna performance. Gain is closely related to directivity, and it can be written as

$$G = \epsilon D \tag{2.7}$$

2.2 MAC Layer Beamforming

In general, beamforming can be classified as switched beamforming and adaptive beamforming. In adaptive beamforming, AWVs are calculated based on channel state information (CSI) to estimate the angle of arrival (AOA). These signal processing calculations lead to massive computational complexity and beam training overhead.

In order to reduce the computation complexity, switched beamforming is preferred in IEEE 802.15.3c and IEEE 802.11ad. In the both IEEE standards, beamforming is performed in media access control (MAC). Therefore, this beamforming mechanism is also called as MAC layer beamforming. By using MAC layer, two devices that want to communicate can exchange training packets to determine the best appropriate transmit and receive beam. Instead of using an exhaustive beam-searching mechanism, both standards perform two-level of beamforming: sector level and beam level, which can reduce the number of training packets.

Beam patterns in the switched beamforming are based on the predefined AWVs, which are called as beam codebook. This predefined codebook adjusts the signal amplitude and phase shift at each antenna element so that the desired beam pattern can be obtained.

2.3 Beam-Searching Algorithm

2.3.1 IEEE 802.15.3c Beam-Searching Algorithms

IEEE 802.15.3c is a standard for wireless personal access networks (WPANs) for high data rate in 60 GHz [21]. This standard is based on Piconet network that organizes communication between devices (DEVs) through Piconet controller (PNC). PNC is a DEV that has the capability to control the network.

Before starting beamforming, PNC will transmit beacon by using its quasi-omni beam and will be waiting for DEVs to join the network. IEEE 802.15.3c exploits two-level beamforming mechanism. The first level is sector level, which is a coarse level needed to find the area of interest and to find the best sectors for both devices. It will be followed by beam level where some beams level are covered by one sector. The beam level then will select the best beam pair among the beam candidates covered in the best-selected sector.

Beam training mechanism in IEEE 80215.3c is illustrated in Figure 2.7 where DEV1 and DEV2 consist of N_1^s and N_2^s sector candidates respectively. During

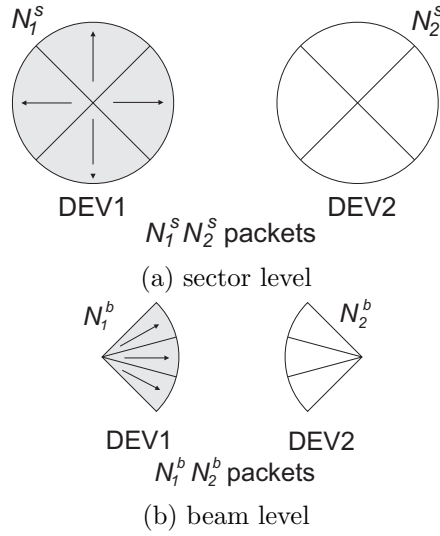


Figure 2.7: Beamforming mechanism in IEEE 802.15.3c (symmetrical channel condition)

one cycle, DEV1 will send N_2^s repetitions of a sector training in the same direction by using the same sector while DEV2 will sweep its all sector. These packet repetition will be transmitted repeatedly through all its N_1^s sector. After finishing N_1^s sector training sequences, DEV2 shall get the information of the best sector pair in the DEV1-DEV2 link. This sector pair is the best transmit sector of DEV1 and the best receive sector of DEV2.

Considering the possibilities of unsymmetrically of transmit and receive channels, sector training in the opposite direction should be performed. In the symmetrical channel the best transmit sector is also the best receive sector, but in the unsymmetrical channel, this condition is not guaranteed. Hence, DEV2 should also transmit training packets to DEV1 in order to get the best sector pair of the DEV2-DEV1 link.

DEV2 transmits training packets to DEV1 in the similar mechanism as in the training sector transmission from DEV1 to DEV2. By doing sector training, the best pair of transmit and receive sector both for the DEV1-DEV2 link and the DEV2-DEV1 link can be known. Hence, in total there will be $N_1^s N_2^s$ number of sector training packets in symmetrical channel condition and $2N_1^s N_2^s$ number of sector training packets in unsymmetrical channel condition.

The beam level training will follow the sector level training. The training exchange between DEV1 and DEV2 is similar with the one in the sector level. DEV1 transmits beam level training sequences, which consist of N_2^b cycles and in each cycle, the training is repeated for N_1^b times. During each cycle,

DEV2 will sweep its beam candidates. In unsymmetrical channel condition, this process is then repeated for the DEV2-DEV1 link where DEV2 will transmit N_2^b cycles of training packet and there are N_1^b packet repetitions in each cycle.

By doing sector level beamforming and beam level beamforming, the total training packets will be

$$N = \alpha(N_1^s \times N_2^s + N_1^b \times N_2^b) \quad (2.8)$$

where $\alpha=1$ when the channel is symmetrical and $\alpha = 2$ when the channel is asymmetrical.

2.3.2 IEEE 802.11ad Beam-Searching Algorithm

Instead of calling a device as a DEV as in IEEE 802.15.3c, IEEE 802.11ad calls the device as a station (STA). Henceforth, STA will be used to mention a device/station in our approach. Before starting beamforming, STA1 will transmit beacons to initiate communication with STA2. The beacons are transmitted through its quasi-omni beam.

Similar to IEEE 802.15.3c, IEEE 802.11ad also exploits two-level beam-training mechanism [22]. However, instead of using exhaustive beam-searching at each level of beam-searching as in IEEE 802.153c, IEEE 802.11ad uses its best sector or its best beam to receive the training packets. The beam-training mechanism is shown in Figure 2.8.

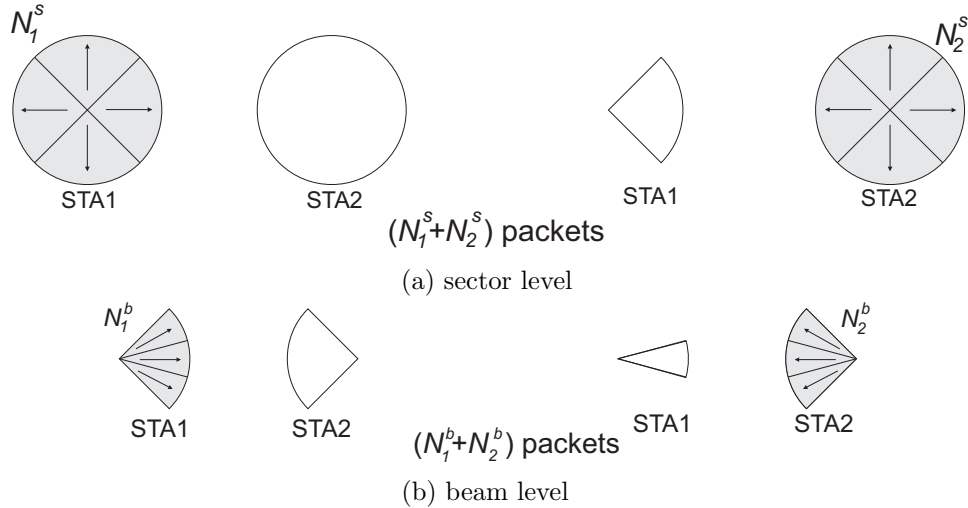


Figure 2.8: Beam-searching mechanism in IEEE 802.11ad (symmetrical channel condition)

In IEEE 802.11.ad, STA1 will transmit training packets through its N_1^s number of sector candidates while STA2 will receive through a quasi-omni. During the packet training from STA1 to STA2, STA2 will obtain information giving the best transmit sector of STA1. STA2 will then give acknowledgment to STA1 giving the information which sector of STA1 that will give the best transmission. After that, STA1 will change its beam into its best transmit sector while STA2 will change its beams into beam level consisting of N_2^s number of beams. For the unsymmetrical channel, training packet then will perform in the STA2-STA1 link where STA2 will transmit N_2^s number of training packets. Therefore, the best pair sectors for the STA1-STA2 link and the STA2-STA1 link can be known.

Sector level training will be followed by beam level training. One sector in STA1 and STA2 will cover N_1^b and N_2^b number of beams, respectively. Training packets mechanism in beam level will be done in a similar way with the one in sector level training.

The total training packets in IEEE 802.11ad will be

$$N = \alpha(N_1^s + N_2^s + N_1^b + N_2^b) \quad (2.9)$$

where $\alpha = 1$ when the channel is symmetrical and $\alpha = 2$ when the channel is asymmetrical.

2.3.3 Hierarchical Beam-Searching Algorithm

The best beam among two beam candidates at each level of beam-searching is selected to minimize the number of training packets. Thus, the beam-searching will perform hierarchical approach as being used in [11], [12], [13], [14] and [15]. This algorithm is quite similar to IEEE 802.11ad, but instead of only using two-level beam-searching, this algorithm performs multi-level beam-searching. Another difference is that at each level, either in sector level or beam level, IEEE 802.11ad has several beam candidates, but in the hierarchical approach there will be only two beam candidates as seen in Figure 2.9. Therefore, the total number of packet training can be reduced to be

$$N = \alpha(2\log_2 N_1 + 2\log_2 N_2) \quad (2.10)$$

where N_1 is number of possible finest beams in STA1, N_2 is number of possible finest beams in STA2, $\alpha = 1$ when the channel is symmetrical, and $\alpha = 2$ when the channel is asymmetrical. If N_1 and N_2 is associated with N_1^s , N_1^b , N_2^s and N_2^b in the IEEE 802.15.3c and IEEE 802.11ad beam training mechanism, they will be equivalent with $N_1 = N_1^s \times N_1^b$ and $N_2 = N_2^s \times N_2^b$.

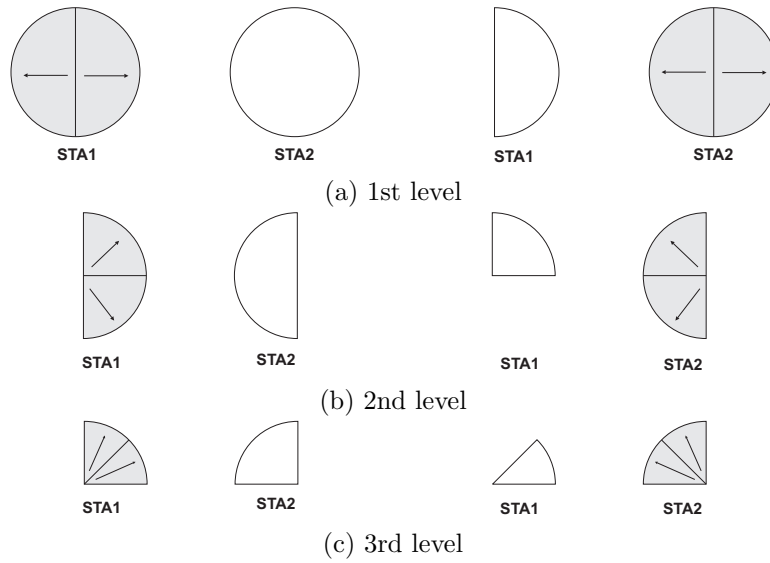


Figure 2.9: Illustration of beam-searching mechanism in the hierarchical beam-searching approach (symmetrical channel condition)

The comparison of number of training packets between the hierarchical approach and the other beam-searching techniques is shown in Table 2.1. It can be seen that for a high number of beamforming resolutions, the hierarchical approach experiences the advantage of beam training packets reduction.

Table 2.1: Illustration of training packet numbers in IEEE 802.15.3c, IEEE 802.11ad and hierarchical approach, taking assumption that the channel is symmetric and both devices have the same number of sectors and beams

Number of sectors	Number of beams per sector	Number of training packets (symmetrical channel)		
		IEEE 802.15.3c	IEEE 802.11ad	Hierarchical approach
4	2	20	12	12
4	4	32	16	16
8	8	128	32	24
8	16	320	48	28

2.4 Codebook Designs

Codebook is a matrix that represents the antenna weighting vectors (AWVs) to adjust the amplitude and phase shift of signal at the array antenna. In switched beamforming the beam candidates are predefined, therefore the codebook should be fixed and predefined. IEEE 802.15.3c employs specific codebook, but there is no specific codebook defined in IEEE 802.11ad.

A matrix of codebook $\mathbf{w} \in \mathbb{C}^{M \times K}$ that consists of M antenna elements and K possible beams is shown in Eq. 2.11. Each matrix column represents one beam candidate.

$$\mathbf{w} = \begin{bmatrix} w_{1,1} & w_{1,2} & \dots & w_{1,K} \\ w_{2,1} & w_{2,2} & \dots & w_{2,K} \\ \dots & \dots & \dots & \dots \\ w_{M,1} & w_{M,2} & \dots & w_{M,K} \end{bmatrix} \quad (2.11)$$

2.4.1 IEEE 802.15.3c Codebook

To simplify the beamforming mechanism, IEEE 802.15.3c [21] and J. Wang et al. [23] use analog beamforming where there are only 2-bits of phase shifter ($0, \pi/2, \pi, 3\pi/2$). In their beamforming design, there is no amplitude adjustment to keep the beamforming mechanism simple.

Nevertheless, by using only 2-bit of phase shift resolution, the codebook faces limitations. Some beams cannot reach maximum gain as shown in Figure 2.10. Moreover, there is a gap between two adjacent beams, and it will give an additional loss. This loss is called as cusping loss. Beamforming resulted from this codebook is shown in Figure 2.10.

In the case when K number of beams is more than M number of antenna elements, the codebook is given as

$$w(m, k) = j^{fix\{\frac{m \times mod[k+(K/2), K]}{K/4}\}} \text{ for } m = 0 : M - 1 \text{ and } k = 0 : K - 1 \quad (2.12)$$

for a special case when $K = M/2$

$$w(m, k) = \begin{cases} (-j)^{mod(m, k)}, & \text{for } m = 0 : M - 1 \text{ and } k = 0 \\ (-1)^{fix\{\frac{m \times mod[k+(K/2), K]}{K/4}\}} & \text{for } m = 0 : M - 1 \text{ and } k = 1 : K - 1 \end{cases} \quad (2.13)$$

However, to keep the gain loss intersection low, the number of beam candidates is usually set to two times of the number antenna elements [23].

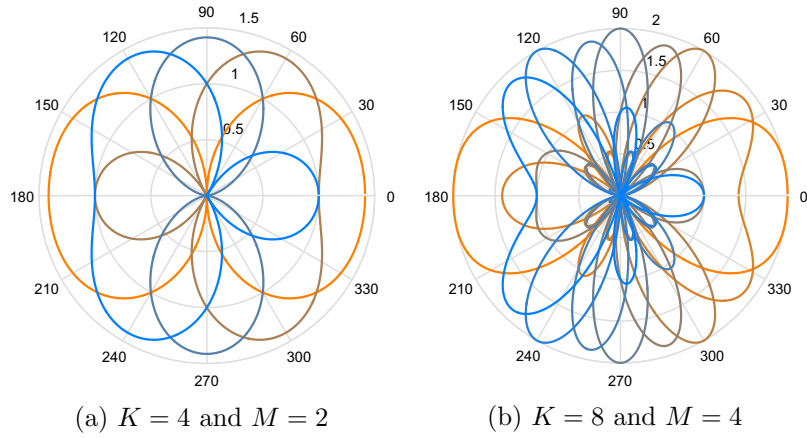


Figure 2.10: Array factor pattern in IEEE 802.15.3c beamforming

2.4.2 Digital Fourier Transform (DFT) Based Codebook

DFT based codebook is intended to maximize the beam gain by using more flexible phase shifter instead only uses two bits of phase shift resolution [24]. DFT based codebook can be formulated as

$$w(m, k) = e^{-j2\pi mk/K} \text{ for } m = 0 : M - 1 \text{ and } k = 0 : K - 1 \quad (2.14)$$

where M is the number of antenna elements and K is the number of possible beams. In DFT-based codebook, phase shifter resolution will follow the number of beam candidates. When there are K number of beams, the phase shift resolution will be $b = \log_2(K)$ bits. Thus, when $K > 4$, DFT-based beamforming needs higher phase shift resolution than IEEE 802.15.3c beamforming.

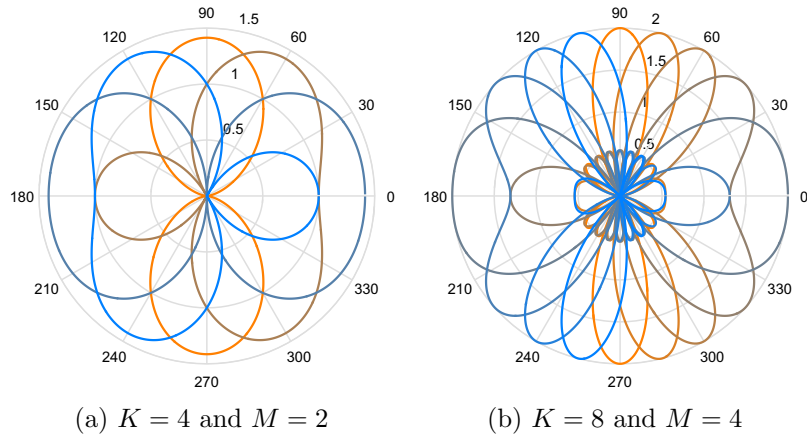


Figure 2.11: Array factor pattern in DFT-based beamforming

Table 2.2: Cusping loss in IEEE 802.15.3c and DFT based codebook

Number of Possible Beams (K)	Maximum Cusping Loss at Intersection (dB)	
	IEEE 802.15.3c Codebook	DFT Based Codebook
4	0.69	0.69
8	1.55	0.86
16	1.85	0.90
32	1.98	0.91

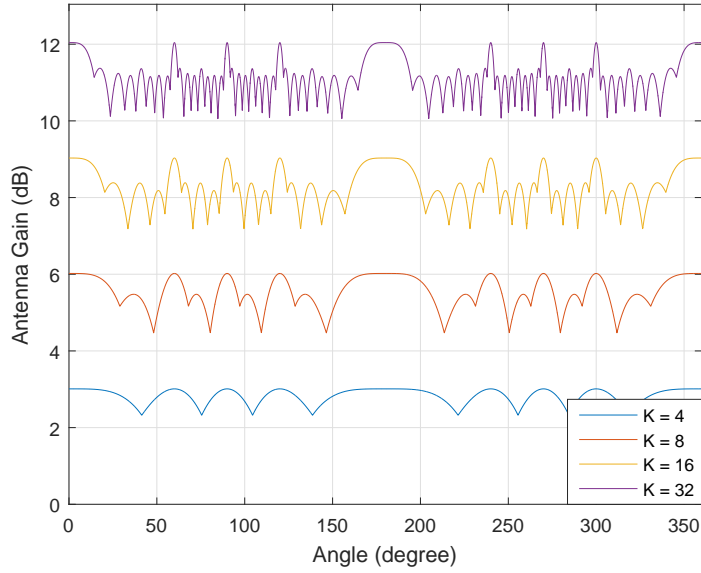
By using more flexible phase shift and assuming isotropic beam pattern of the antenna element, all beams can reach maximum gain as shown in Figure 2.11. However, there is still cusping loss, where the loss value can be seen in Table 2.2, due to beam overlapping between the adjacent beams. Comparison of beam fluctuation in DFT-based beamforming and IEEE 802.15.3c can be seen in Figure 2.12 where DFT-based beamforming has less fluctuation than IEEE 802.15.3c.

When isotropic element pattern is taken as an assumption, beamforming in IEEE 802.15.3c with $K = 32$ suffers cusping loss 1.98 dB or it loses about 36% of its power as seen in Table 2.2. If this beamforming is used in both DEV1 and DEV2, it potentially reduces 3.96 dB or 60% of its received power. It can be seen that DFT codebook can minimize the losses where there is only 0.91 dB of loss. However, if both DEV1 and DEV2 suffers maximum cusping loss, it might still have 1.92 dB of losses or about 35% of its power in total .

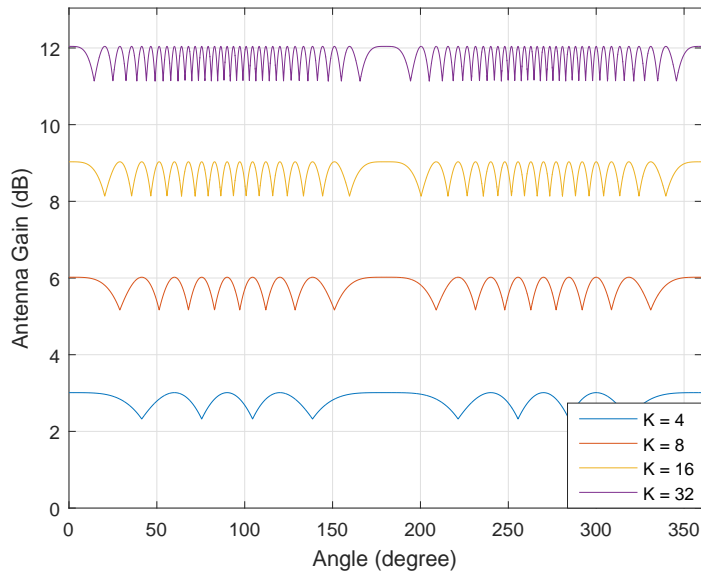
2.4.3 Fourier Series Method with Kaiser Window (FSM-KW) Codebook

Beamforming can be seen as the same problem in the digital bandpass filter design as illustrated in Figure 2.13. Window sample length is associated with the number of antenna elements (M) in beamforming. As Fourier series method in the beamforming design results in the beam ripples [17, 18], Kaiser window is used to reduce the ripples [25]. Kaiser window is chosen because the trade-off between sidelobe attenuation and beam transition width can be controlled. The higher the attenuation parameter is given, the wider the beam transition width will be obtained. Thus, the attenuation parameter should be set so that the beamwidth fits with the desired beam direction. By using this beamforming approach, a relatively flat array pattern within the desired scanning coverage can be achieved.

If we want to design a beam that has beam coverage between θ_1 and θ_2 and



(a) IEEE 802.15.3c beamforming



(b) DFT-based beamforming

Figure 2.12: Gain fluctuation in IEEE 802.15.3c beamforming and DFT based beamforming with several numbers of possible beams K . Isotropic element pattern is taken as an assumption

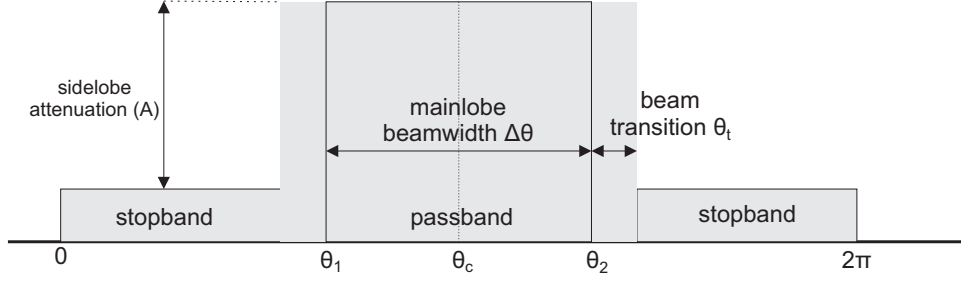


Figure 2.13: Beamforming design associated with bandpass filter

beam center direction at θ_c with the FSM-KW beamforming approach, the beamforming codebook can be defined as

$$w(m) = w_{window}(m)e^{-j\beta\psi_o} \frac{\sin(\beta\psi_b)}{\pi\beta} \text{ for } m = 0, 1, \dots, M-1 \quad (2.15)$$

where $w_{window}(m)$ is the Kaiser window sample and $\beta = m - (M-1)/2$ while ψ_o and ψ_b are given as

$$\psi_o = \frac{\pi}{2}(\cos\theta_1 + \cos\theta_2) \quad (2.16)$$

$$\psi_b = \pi \sin\theta_c \sin\frac{\Delta\theta}{2} + \frac{\pi D}{M-1} \quad (2.17)$$

The D -factor can be defined from the sidelobe attenuation A (dB)

$$D = \begin{cases} \frac{A-7.95}{14.36} & \text{if } A > 21 \\ 0.922 & \text{if } A \leq 21 \end{cases} \quad (2.18)$$

The γ factor can be calculated as

$$\gamma = \begin{cases} 0.11(A-8.7) & \text{if } A \geq 50 \\ 0.58(A-21)^{0.4} + 0.079(A-21) & \text{if } 21 < A < 50 \\ 0 & \text{if } A \leq 21 \end{cases} \quad (2.19)$$

The Kaiser window samples itself are given as

$$w_{window}(m) = \frac{I_0(\gamma\sqrt{1-4\beta^2})}{I_0(\gamma)} \quad (2.20)$$

where I_0 is the zero-th order modified Bessel function of the first kind.

To create such flat beams, FSM-KW beamforming requires more antenna elements than IEEE 802.15.3c and DFT based beamforming. The desired flat beam shape is approached by Fourier series. Consequently, to achieve nearly ideal desired beam shape, more samples or antenna elements are needed.

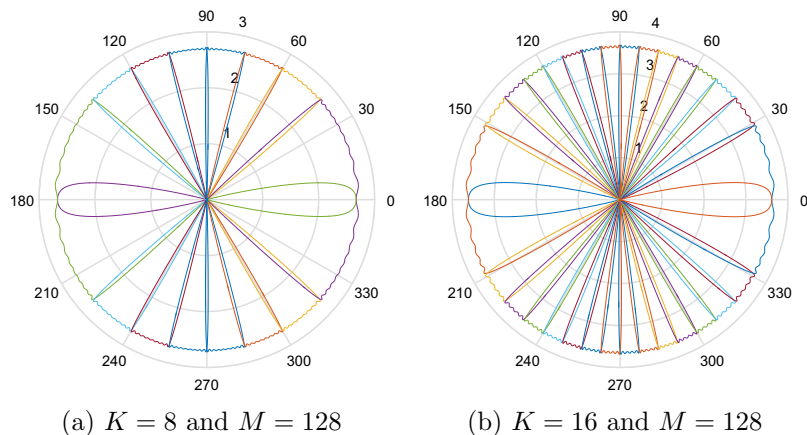


Figure 2.14: FSM-KW beamforming with fully-digital beamforming

FSM-KW beamforming also not only requires phase shift adjustment as in IEEE 802.15.3c beamforming or DFT beamforming, but it also requires amplitude adjustments. This complexity pushes up the requirement of digital signal processing to adjust the phase shift and amplitude.

The FSM-KW based beamforming designed in [12] with fully-digital beamforming architecture is shown in Figure 2.14 where there are $K = 8$ and $K = 16$ possible finest beams. These beams are composed of $M = 128$ antenna elements and 40 dB of sidelobe attenuation. To avoid cusping loss, each beam should have a beamwidth that fits with its adjacent beam.

With a large number of antenna elements, digital beamforming is power hungry and costly since each antenna element needs one RF chain consisting of down-converter, analog to digital converter (ADC), digital to analog converter (DAC), and so on. Therefore, digital beamforming in FSM-KW beamforming becomes impractical. As an alternative, hybrid-beamforming is used as in [12], [26], [27], [28], and [29].

2.5 Beamforming Architectures

Based on the architecture, there are three types of beamforming which are analog beamforming, digital beamforming, and hybrid beamforming. Each of beam architecture has its own advantages and disadvantages. Therefore, the preference which beamforming should be selected depends on the applications.

2.5.1 Analog Beamforming

Analog beamforming uses only one RF chain for all antenna elements to minimize the complexity. Since the signal is processed in the analog domain, there will be limitations in changing antenna weighting (phase shift and amplitude adjustment) where the antenna weighting can be done only in the discrete number. This beamforming is used in IEEE 802.15.3c where in this case, there are only 2-bits of phase shifter [21]. The limitation to adjust the phase and amplitude brings a lack of beamforming flexibility.

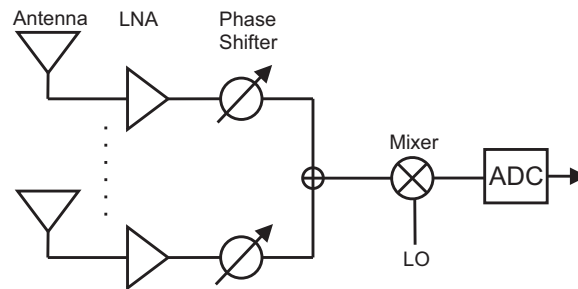


Figure 2.15: Analog beamforming architecture

2.5.2 Digital Beamforming

In digital beamforming shown in Figure 2.16, the signal at each antenna element is digitized using an analog-to-digital converter (ADC). Digital beamforming offers a flexible adjustment of phase shift and amplitude since the signal processing can be done in the digital domain. As a result, beam patterns also can be set more flexible in the digital beamforming than in the analog beamforming. Unlike analog beamforming that can only perform a single beam, digital beamforming can create simultaneous beams to communicate with several devices simultaneously.

Nevertheless, since the adjustment is done in the digital domain, each antenna element requires one RF chains, consisting ADC/DAC (digital-to-analog converter) and other RF components, which are power hungry and expensive. Therefore, it is impractical to implement digital beamforming with a lot number of antenna elements.

2.5.3 Hybrid Beamforming

Hybrid beamforming is a combination between analog beamforming and digital beamforming. It takes the benefit of simplicity architecture from analog beamforming and the advantage of flexibility from digital beamforming

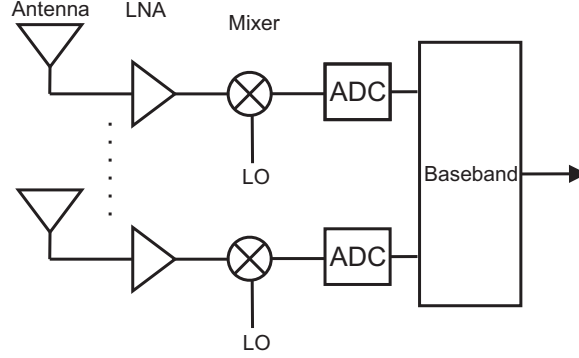


Figure 2.16: Digital beamforming architecture

(beam design flexibility and multiple simultaneous beams), although the flexibility is lower than the digital beamforming. In hybrid beamforming, to reduce the number of RF chains, several antenna elements are served by only one RF chain simultaneously as shown in Figure 2.17 where there are M number of antenna elements and N_{RF} number of RF chains ($M > N_{RF}$).

Predefined codebook in the fully digital beamforming ($\mathbf{w} \in \mathbb{C}^{M \times 1}$) can be approached by the multiplication between the predefined RF codebook ($\mathbf{w}_{RF} \in \mathbb{C}^{M \times N_{RF}}$) and the predefined baseband codebook ($\mathbf{w}_{BB} \in \mathbb{C}^{N_{RF} \times 1}$)

$$\mathbf{w} = \mathbf{w}_{RF} \mathbf{w}_{BB} \quad (2.21)$$

Since each element of \mathbf{w}_{RF} is restricted by the feasible RF codebook $\mathbf{w}_{RF_{can}}$ due to hardware constraint, we need to find \mathbf{w}_{RF}^{opt} and \mathbf{w}_{BB}^{opt} that can satisfy

$$\begin{aligned} (\mathbf{w}_{RF}^{opt}, \mathbf{w}_{BB}^{opt}) &= \arg \min_{\mathbf{w}_{RF}, \mathbf{w}_{BB}} \|\mathbf{w} - \mathbf{w}_{RF} \mathbf{w}_{BB}\|_2 \\ &s.t. \mathbf{w}_{RF_{i,j}} \in \mathbf{w}_{RF_{can}} \text{ where } i = 1, \dots, M \text{ and } j = 1, \dots, N_{RF} \\ &\|\mathbf{w}_{RF} \mathbf{w}_{BB}\|_2^2 = 1 \end{aligned} \quad (2.22)$$

Orthogonal matching pursuit (OMP) algorithm can be used to achieve the solution in Eq. 2.22 [26, 28, 29]. In the OMP algorithm, restricted RF codebook candidate ($\mathbf{w}_{RF_{can}}$) can be taken from the predefined codebook in IEEE 802.15.3c. Nevertheless, to accommodate higher phase shift resolution, codebook with b -bits phase shift resolution [30], as shown in Eq. 2.23, also can be used.

$$\mathbf{w}_{RF_{can}}(m, k) = e^{j \frac{2\pi}{2^b} \text{fix} \left\{ \frac{m \times \text{mod}((m-1) + (K/2), K)}{K/2^b} \right\}} \quad (2.23)$$

where $m = 0, 1, \dots, M - 1$, $k = 0, 1, \dots, K - 1$, M is number of antenna elements, and $K = M$.

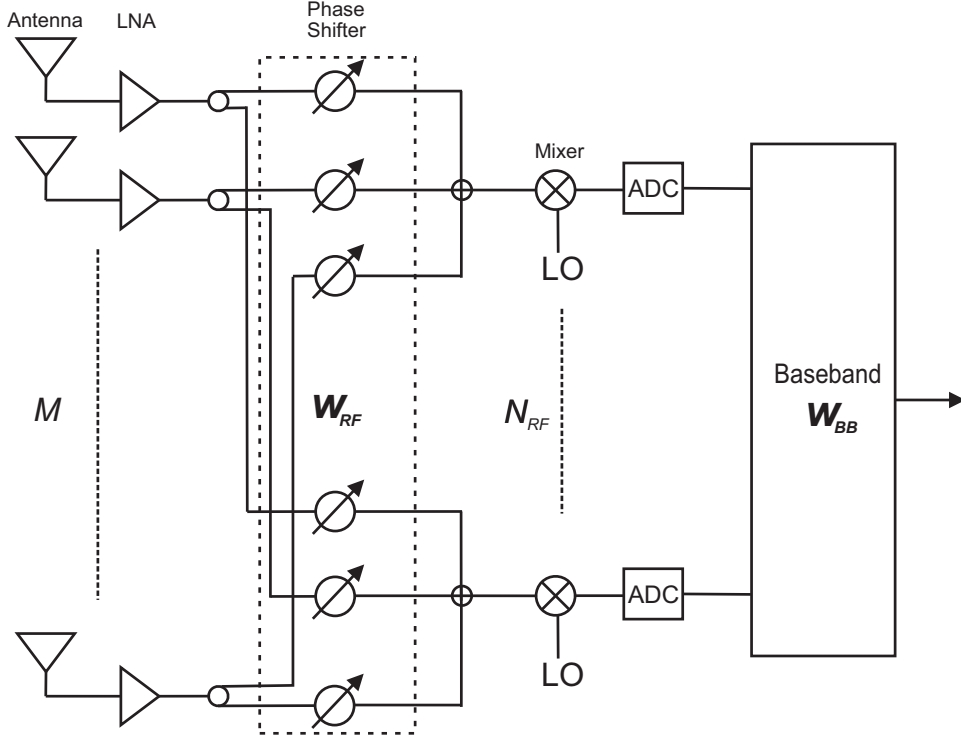


Figure 2.17: Hybrid beamforming architecture

Orthogonal matching pursuit with dynamic dictionary learning (DDL-OMP) algorithm [12] modifies OMP algorithm by iteratively updating the RF codebook candidate $\mathbf{w}_{RF_{can}}$. At each iteration, the codebook candidate is updated with a column vector which are highly likely to generate the digital codebook.

While OMP algorithm and DDL-OMP algorithm rely on the predefined RF codebook candidate, geometric approach algorithm [31] does not use any predefined RF codebook candidate. Thus, the performance of geometric approach algorithm does not depend on the selected codebook candidate $\mathbf{w}_{RF_{can}}$.

Algorithm 1 shows the process how to approach the hybrid-beamforming codebook. This beamforming accommodates the ability of hybrid beamforming to transmit N_s multiple beams simultaneously where $N_s \leq N_{RF} \leq M$. The ideal fully-digital codebook $\mathbf{w} \in \mathbb{C}^{M \times N_s}$ will be approximated with the RF codebook $\mathbf{w}_{RF} \in \mathbb{C}^{M \times N_{RF}}$ and the baseband codebook $\mathbf{w}_{BB} \in \mathbb{C}^{N_{RF} \times N_s}$.

First, the RF codebook \mathbf{w}_{RF} and the residual matrix \mathbf{w}_{res} are initialized. The algorithm selects the residual column \mathbf{w}_{res} with maximum norm and appends its mapped version $S(\mathbf{w}_{res})$ to the current RF codebook \mathbf{W}_{res} .

$S(\mathbf{v})$ is an operator that maps the vector \mathbf{v} into the closest vector attainable with 2-bit RF phase shifter.

The algorithm then updates the residual matrix \mathbf{W}_{res} with the objective to make $\mathbf{W}_{res} = \mathbf{W}_{res} - \delta S(\mathbf{W}_{res})$ close to zero. It means that we need to find $\delta \in \mathbb{C}$ so that

$$\mathbf{W}_{res}(i) - \delta S(\mathbf{W}_{res})(i) \approx 0 \quad \forall i \leq M \quad (2.24)$$

The algorithm finds δ as equivalent to find the good center for the set points $\frac{\mathbf{W}_{res}}{S(\mathbf{W}_{res})(i)}$ distributed over $\pi/2$ circular sector as seen in Figure 2.18. Each $\frac{\mathbf{W}_{res}(i)}{S(\mathbf{W}_{res})(i)}$ has a complex modulus $|\mathbf{W}_{res}(i)|$ and argument between $-\pi/4$ and $\pi/4$ as $S(\mathbf{W}_{res})$ maps \mathbf{W}_{res} to the closest points with 2-bit RF phase shifter. The algorithm divide the $\pi/2$ circular sector into two sub-sector which are north pole and south pole. The border line between the north pole and the south pole is $(w_{max} + w_{min})/2$ where $w_{max} = \max_i |\mathbf{W}_{res}(i)|$ and $w_{min} = \min_i |\mathbf{W}_{res}(i)|$. The points are in the north pole if the modulus is more than or equal to $(w_{max} + w_{min})/2$ while the rests are located in the south pole. The algorithm focuses on finding \mathbf{W}_{res} locating in the south pole and calculates their mean value δ' . If δ' is in the north pole, δ is set to be $\delta = \frac{\delta'}{|\delta'|} \frac{w_{max} + w_{min}}{2}$. Line 15-19 then updates the residual matrix.

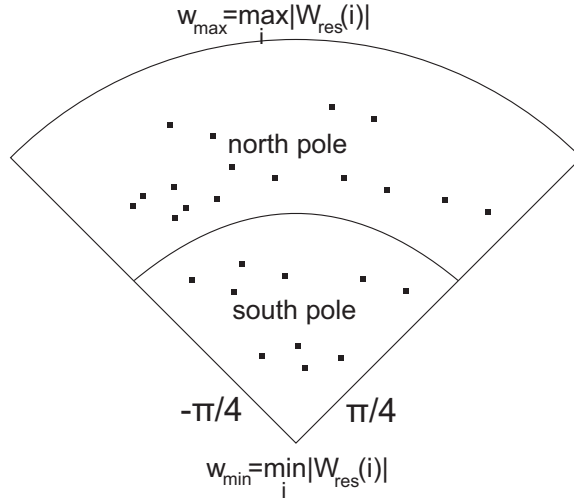


Figure 2.18: Illustration of the geometric approach to find the δ parameter

The process is repeated until all N_{RF} codebook vectors are selected. At last, the algorithm normalizes \mathbf{w}_{BB} to satisfy $\|\mathbf{w}_{RF}[\mathbf{w}_{BB}]_{:,i}\|_2^2$.

The comparative results of hybrid beamforming between OMP algorithm, DDL-OMP algorithm, and geometric approach algorithm can be seen Figure 2.19. It can be seen from Figure 2.19 that hybrid beamforming with

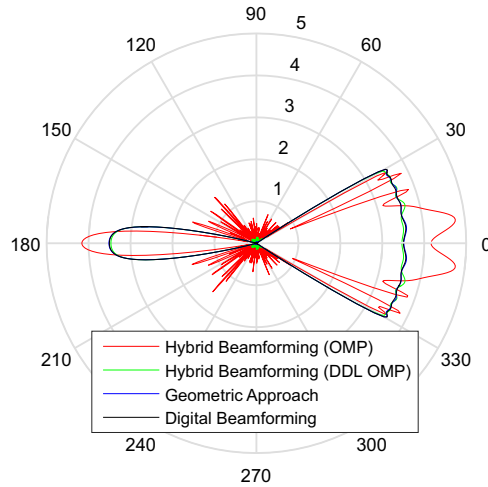


Figure 2.19: Array factor pattern in FSM-KW with beamwidth between $-30^\circ \leq \theta \leq 30^\circ$. The beams are designed with $M = 128$ antenna elements in fully digital beamforming and hybrid beamforming (OMP, hybrid, and geometric approach algorithm) with $N_{RF} = 8$ number of RF chains

DDL-OMP and geometric approach algorithm almost give the same beam pattern. These two algorithms outperform OMP algorithm. By using only 8-RF chains, DDL-OMP algorithm and geometric approach algorithm can create almost the same pattern with fully-digital beamforming. On the other hand, beam created in OMP algorithm still has higher fluctuations than DDL-OMP or geometric approach algorithm.

In hybrid beamforming, the number of antenna elements and RF chains should be chosen wisely considering the trade-off between hardware complexity and beam performance. As the number of RF chains is getting higher, the root mean square error (RMSE) between fully digital codebook \mathbf{w} and predefined codebook in hybrid beamforming $\mathbf{w}_{RF}\mathbf{w}_{BB}$ will be less as depicted in Figure 2.20. Nevertheless, choosing the optimal number of antenna elements and RF chains is outside of our research area.

Minimizing $\|\mathbf{w} - \mathbf{w}_{RF}\mathbf{w}_{BB}\|_2$ in Eq. 2.22 means that the beam in the hybrid architecture should be as close as possible to the one in the fully digital architecture. To show the performance comparison between OMP, DDL-OMP, and geometric approach algorithm, we measure $\|\mathbf{w} - \mathbf{w}_{RF}\mathbf{w}_{BB}\|_2$ when a beam with beamwidth between $-30^\circ \leq \theta \leq 30^\circ$ designed in FSM-KW beamforming (as seen in Figure 2.19) is approached with those three hybrid beamforming method. The beam is constructed with $N = 128$ number of antenna elements. In this case, we measure $\|\mathbf{w} - \mathbf{w}_{RF}\mathbf{w}_{BB}\|_2$ for various number of RF chains from $N_{RF} = 1$ until $N_{RF} = 128$.

It can be seen in Figure 2.20 that DDL-OMP algorithm and geometric

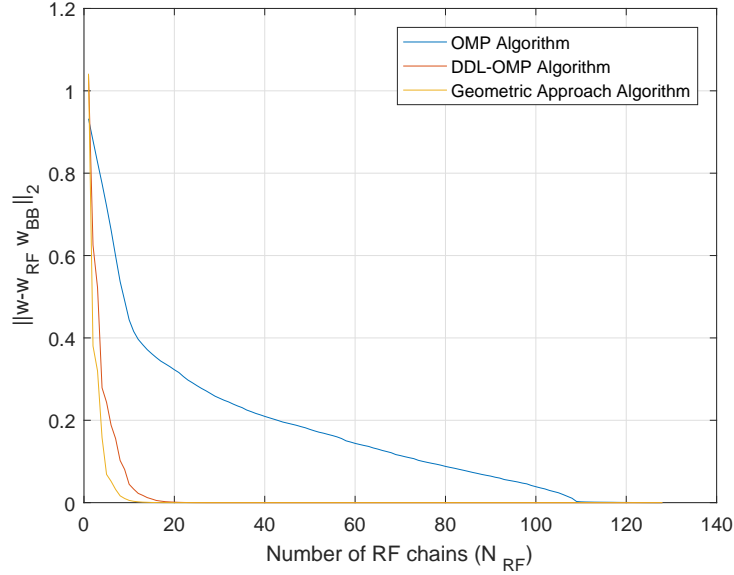


Figure 2.20: Comparison of root mean square error (RMSE), $\|w - w_{RF} w_{BB}\|_2$, with various number of RF chains in OMP algorithm, DDL-OMP algorithm and geometric approach algorithm. In this case the beam is created based on the FSM-KW beamforming with beamwidth between -30° and 30° , $A = 40$ dB, and $M = 128$

approach algorithm give lower RMSE than OMP algorithm. This low RMSE leads the beam patterns in DDL-OMP and geometric approach algorithm highly close to the beam pattern in the fully digital architecture. Nevertheless, geometric approach algorithm still gives a bit lower RMSE than DDL-OMP algorithm. Therefore, in our approach, the hybrid beamforming will be designed based on the geometric approach algorithm.

The algorithm complexity is not taken into account in the beamforming analysis since the proposed beamforming uses switched beamforming where the beam candidates is already defined. Therefore, the beamforming process does not need to find w_{RF} and w_{BB} at each beam-searching level, but they are already predefined instead. Nevertheless, geometric approach algorithm is claimed having lower computational complexity than OMP-based approaches [31, 32].

Algorithm 1: Geometric approach algorithm for hybrid beamforming [31]

Input : Ideal digital predefined codebook \mathbf{w} , restricted RF codebook candidate \mathbf{w}_{RFcan}

Output : Predefined RF codebook \mathbf{w}_{RF} , predefined baseband codebook \mathbf{w}_{BB}

- 1: $\mathbf{w}_{RF} =$ empty matrix
- 2: $\mathbf{w}_{res} = \mathbf{w}$
- 3: **for** $i \leq N_{RF}$ **do**
- 4: $k = \arg \max_k \|\mathbf{w}_{res}(:, k)\|_2^2$
- 5: $\mathbf{W}_{res} = \mathbf{w}_{res}(:, k)$
- 6: $\mathbf{w}_{RF} = [\mathbf{w}_{RF}, S(\mathbf{W}_{res})]$ $\{S(\mathbf{v})$ is an operator that maps the vector \mathbf{v} into one close vector attainable with b -bit RF phase shifters $\}$
- 7: $w_{max} = \max_i |\mathbf{W}_{res}(i)|, w_{min} = \min_i |\mathbf{W}_{res}(i)|$
- 8: $J = \text{find} [|\mathbf{W}_{res}| \geq \frac{w_{max} + w_{min}}{2}]$
- 9: $\delta' = \text{mean} [\mathbf{W}_{res}(J) / S(\mathbf{W}_{res}(J))]$
- 10: **if** $|\delta'| > \frac{w_{max} + w_{min}}{2}$ **then**
- 11: $\delta = \frac{\delta'}{|\delta'|} \frac{w_{max} + w_{min}}{2}$
- 12: **else**
- 13: $\delta = \delta'$
- 14: **end if**
- 15: $\mathbf{W}_{res} = \mathbf{W}_{res} - \delta S(\mathbf{W}_{res})$
- 16: $\mathbf{w}_{res}(:, k) = \mathbf{W}_{res}$
- 17: **for** $j \leq N_s, j \neq k$ **do**
- 18: $\mathbf{w}_{res}(:, j) = \mathbf{w}_{res}(:, j) - S(\mathbf{W}_{res} \frac{[S(\mathbf{W}_{res})]^H \mathbf{w}_{res}(:, j)}{\|S(\mathbf{w}_{res})\|_2^2})$
- 19: **end for**
- 20: **end for**
- 21: $\mathbf{w}'_{BB} = (\mathbf{w}_{RF}^H \mathbf{w}_{RF})^{-1} \mathbf{w}_{RF}^H \mathbf{w}$
- 22: **for** $i \leq N_s$ **do**
- 23: $\mathbf{w}_{BB}(:, i) = \frac{\mathbf{w}'_{BB}(:, i)}{\|\mathbf{w}_{RF} \mathbf{w}'_{BB}\|_2}$
- 24: **end for**

2.6 Limitations in the Existing Works

IEEE 802.11ad and IEEE 802.15.3c perform two-level beamforming that causes high training packet overhead in the high beam resolution. To reduce the number of training packets, hierarchical beamforming with two beam candidates at each beamforming level is proposed [11, 12, 13, 14, 15]. Nevertheless, existing beamforming designs generally assume isotropic antenna element radiation in their beamforming design.

In the isotropic assumption, FSM-KW based beamforming [12], that employs hierarchical beamforming, has better beam pattern than IEEE 802.15.3c and DFT-based beamforming. Compared to IEEE.802.153c and DFT based beamforming, beam pattern in FSM-KW beamforming in [12] has less intersection area between the adjacent beams and less cusping loss. However, isotropic radiation pattern is not realistic.

Patch antennas which are generally used as antenna elements of array antenna have lower gain near to end-fire direction than the one at broadside direction. As the array antenna beam is the multiplication product of array factor and antenna element beam pattern, the array antenna beam degrades following beam degradation in the antenna element pattern. If we take sinusoidal pattern in Figure 3.12 as the antenna element radiation pattern, array beamforming pattern for IEEE 802.15.3c, DFT-based, and FSM-KW based beamforming in [12] can be seen in Figure 2.21, Figure 2.22, and Figure 2.23, respectively.

In Figure 2.21, Figure 2.22, and Figure 2.23 we can see that the existing switched beamforming techniques face gain degradation at the low angle direction. To avoid signal quality degradation when the communication is performed by using the beam close to end-fire direction, in this thesis, we proposed beamforming that has relatively flat radiation throughout its scanning coverage. The scanning coverage is limited to $\Delta\theta_c = 120^\circ$ taking assumption that in general array antenna has maximum scanning coverage of 120° [18, 33]. As the proposed beamforming is also designed based on the FSM-KW design, that needs a large number of antenna elements, hybrid beamforming architecture is used in the proposed beamforming to reduce the number of RF chains.

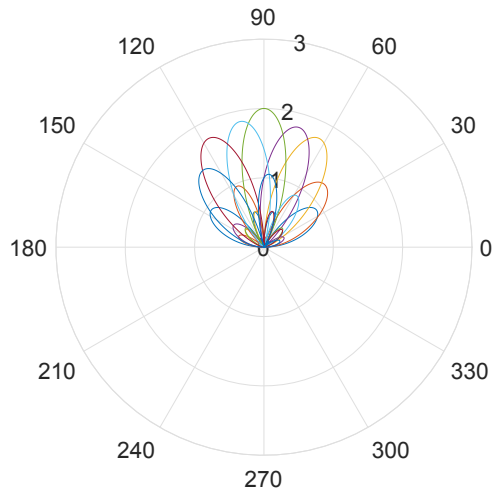


Figure 2.21: Beamforming degradation in IEEE 802.15.3c beamforming ($K = 8, M = 4$) taking assumption sinusoid antenna element radiation pattern

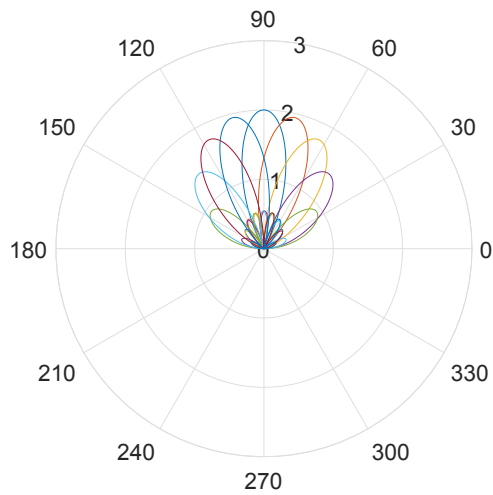


Figure 2.22: Beam degradation in IEEE 802.15.3c beamforming ($K = 8, M = 4$) taking assumption sinusoid antenna element radiation pattern

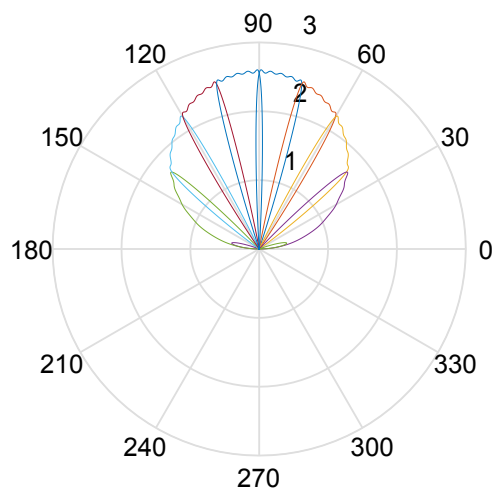


Figure 2.23: Beam degradation in the FSM-KW based beamforming [12] ($K = 8$, fully-digital beamforming with $M = 64$) taking assumption sinusoid antenna element radiation pattern

Chapter 3

Designing Uniform Gain Beamforming

FSM-KW beamforming seems able to generate an almost ideal beam with a relatively flat gain and a small beam intersection. However, this beamforming approach takes an assumption that the antenna elements have an isotropic element pattern which is not realistic. A patch antenna, which is commonly used as an element of array antenna [16], has low gain in low elevation angle. Therefore, the array beam pattern in the FSM-KW beamforming does not have such ideal flat beam, but it follows the element beam pattern where the beam steered towards end-fire direction will have low gain.

Since FSM-KW beamforming has flexibilities to design a beam with a specific beamwidth and to adjust the trade-off between the ripple and the beam transition, this beamforming is chosen as a design base in the proposed approach. By using FSM-KW beamforming, we can create a beam that has flat array factor within the desired beamwidth. To support the design flexibility, FSM-KW beamforming not only requires a lot of antenna elements but it also needs flexible phase shift and amplitude adjustment. Therefore, it is not be feasible if this beamforming is implemented in analog beamforming. Since digital beamforming requires a huge number of RF chains, which is the same as the number of antenna elements, hybrid beamforming is the solution for practical implementation.

3.1 Uniform Gain Beamforming

The proposed beamforming must be able to follow hierarchical beamforming and is expected to have uniform gain for all beam candidates. A simple illustration showing beamforming that follows hierarchical approach is depicted

in Figure 3.1. Each circular sector represents one beam candidate and at the k -th beam-searching level there will be 2^k beam candidates. Each beam is expected to have the same gain and to have only one beam area. A beam from the lower level will cover exactly two beams at the higher level i.e. a beam at the 1st level covers two beams at the 2nd level.

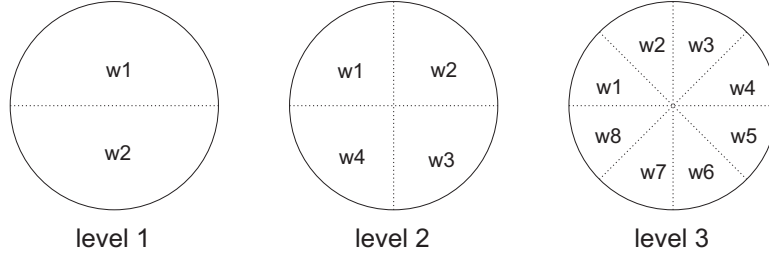


Figure 3.1: Ideal multi-level beamforming when the number of beam-searching level is three

Nevertheless, covering 360° with only one array patch antenna system is not feasible. A patch antenna element only has beam pattern above its patch plane and the beam at the end-fire direction is significantly lower than the one at the broadside direction as already shown in the Chapter 2.1. Usually, for a practical reason, scanning coverage of array antenna is limited maximum to $\pm 60^\circ$ from the broadside direction or it has scanning coverage $\Delta\theta_c = 120^\circ$ [18, 33]. Therefore, the proposed beamforming will have limited scanning coverage and if the proposed beamforming is intended to cover 360° , multiple antenna systems must be employed on the device.

The objective of our beamforming design is to create a flat beamforming as depicted in Figure 3.2. We want to create beams with minimum overlap between the adjacent beams and with the same gain for all beam candidates at each beamforming level. Fourier series method with Kaiser window (FSM-KW) will be used as our based design as it offers beamforming flexibility to

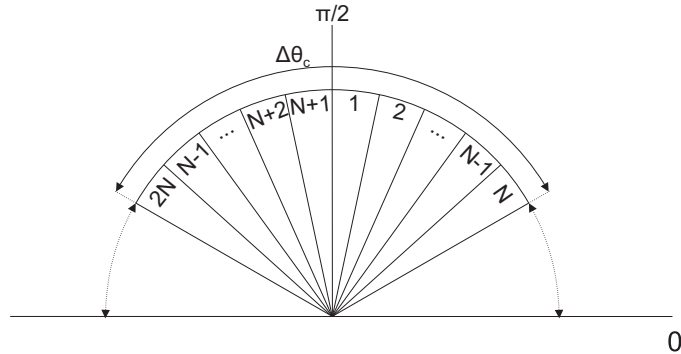


Figure 3.2: Proposed beamforming for K number of possible beams ($K = 2N$)

adjust the beam position and the beamwidth.

FSM-KW beamforming designs the beam by approaching the array factor with the truncated version of the infinite Fourier series. Array factor written in Eq. 2.5 has antenna element index $m = 0, 1, \dots, M - 1$ with M is the number of antenna elements. If we change the element index to be $m = 0, \pm 1, \pm 2, \dots, \pm \frac{(M-1)}{2}$ for odd number of antenna elements in order to have symmetry with respect to the array center, array factor can be written in the wavenumber domain $\psi = \frac{2\pi}{\lambda}d \cos \theta$ as

$$AF(\psi) = \sum_{m=-\frac{M-1}{2}}^{\frac{M-1}{2}} w_m e^{jm\psi} \quad (3.1)$$

If the number of antenna elements is even with antenna element index $m = \pm 1, \pm 2, \dots, M/2$, the array factor can be written as

$$AF(\psi) = \sum_{m=1}^{M/2} [w_m e^{j(m-1/2)\psi} + w_{-m} e^{-j(m-1/2)\psi}] \quad (3.2)$$

We can see Eq. 3.1 and Eq. 3.2 as the truncated version of the infinite Fourier series [25] where for odd case we have

$$AF(\psi) = \sum_{m=-\infty}^{\infty} w_m e^{jm\psi} \quad (3.3)$$

and the Fourier coefficient can be obtained as

$$w_m = \frac{1}{2\pi} \int_{-\pi}^{\pi} AF(\psi) e^{-jm\psi} d\psi, \text{ for } m = 0, \pm 1, \pm 2, \dots \quad (3.4)$$

For even case we have

$$AF(\psi) = \sum_{m=1}^{\infty} [w_m e^{j(m-1/2)\psi} + w_{-m} e^{-j(m-1/2)\psi}] \quad (3.5)$$

and the Fourier coefficient will be

$$w_{\pm m} = \frac{1}{2\pi} \int_{-\pi}^{\pi} AF(\psi) e^{\mp j(m-1/2)\psi} d\psi, \text{ for } m = 0, 1, 2, \dots \quad (3.6)$$

Beamforming is a spatial filtering so we can see beamforming as a bandpass filter in the wavenumber ψ domain with array factor center ψ_o and bandwidth $2\psi_b$. The ideal bandpass response in the ψ domain can be written as

$$AF_{BP}(\psi) = \begin{cases} 1, & \psi_o - \psi_b \leq \psi \leq \psi_o + \psi_b \\ 0, & \text{otherwise} \end{cases} \quad (3.7)$$

Therefore, we can obtain the ideal weights of the bandpass filter for odd case from Eq. 3.4 as

$$\begin{aligned}
w_{BP}(m) &= \frac{1}{2\pi} \int_{-\pi}^{\pi} AF_{BP}(\psi) e^{-jm\psi} d\psi \\
&= \frac{1}{2\pi} \int_{\psi_o - \psi_b}^{\psi_o + \psi_b} 1 \cdot e^{-jm\psi} d\psi \\
&= e^{-jm\psi_o} \frac{\sin(\psi_b m)}{\pi m}, \text{ for } m = 0, \pm 1, \pm 2, \dots \pm \frac{M-1}{2}
\end{aligned} \tag{3.8}$$

while for even case, from Eq. 3.6 we can obtain

$$\begin{aligned}
w_{BP}(\pm m) &= \frac{1}{2\pi} \int_{-\pi}^{\pi} AF_{BP}(\psi) e^{\mp j(m-1/2)\psi} d\psi \\
&= \frac{1}{2\pi} \int_{-\pi}^{\pi} 1 \cdot e^{\mp j(m-1/2)\psi} d\psi \\
&= e^{\mp j(m-1/2)\psi_o} \frac{\sin(\psi_b(m-1/2))}{\pi(m-1/2)}, \text{ for } m = 1, 2, \dots, M/2
\end{aligned} \tag{3.9}$$

If we change the antenna element index in Eq. 3.8 and Eq. 3.9 to be antenna element index $m = 0, 1, \dots, M-1$, both equations give the same equation as follow

$$w_{BP}(m) = e^{-j\beta\psi_o} \frac{\sin(\psi_b\beta)}{\pi\beta}, \quad m = 0, 1, \dots, M-1 \tag{3.10}$$

where $\beta = m - \frac{M-1}{2}$.

Kaiser window allow the flexibility to choose sidelobe attenuation A . This sidelobe attenuation define the D -factor as follow

$$D = \begin{cases} \frac{A-7.95}{14.36}, & \text{if } A > 21 \\ 0.922, & \text{if } A \leq 21 \end{cases} \tag{3.11}$$

and the γ factor

$$\gamma = \begin{cases} 0.11(A - 8.7) & \text{if } A \geq 50 \\ 0.58(A - 21)^{0.4} + 0.079(A - 21) & \text{if } 21 < A < 50 \\ 0 & \text{if } A \leq 21 \end{cases} \tag{3.12}$$

The Kaiser window samples with length of M itself are given as

$$w_{window}(m) = \frac{I_0(\gamma\sqrt{1 - \frac{4\beta^2}{(M-1)^2}})}{I_0(\gamma)} \quad m = 0, 1, \dots, M-1 \tag{3.13}$$

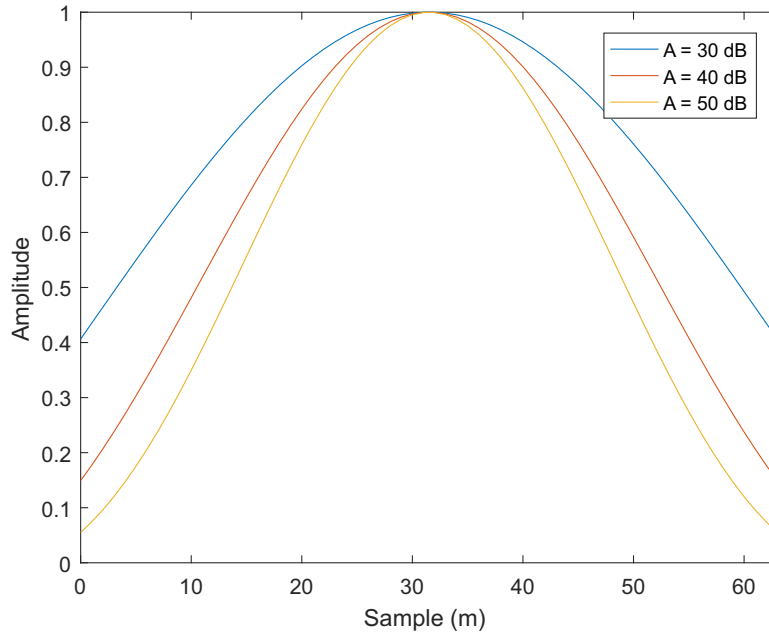


Figure 3.3: Kaiser window impulse response for various sidelobe attenuation A with $M = 64$ window length

where I_0 is the zero-th order modified Bessel function of the first kind and $\beta = m - \frac{M-1}{2}$. For example, if we are using $M = 64$, the Kaiser window impulse response for various sidelobe attenuation is shown in Figure 3.3 .

Since we want to design filter in the angular domain θ while Eq. 3.10 still has ψ_o and ψ_b , which are still in the ψ domain, we need to map ψ_o and ψ_b into angular domain θ .

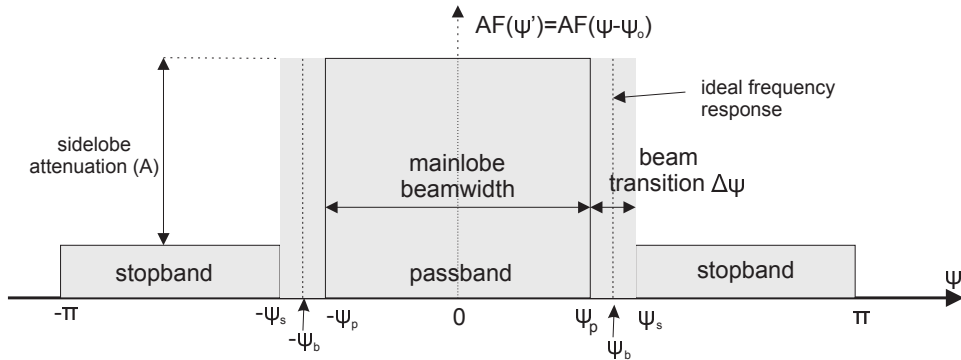


Figure 3.4: Lowpass filter design equivalent

Designing bandpass filter in the ψ domain with bandwidth $2\psi_b$ is equivalent

to designing a lowpass filter with cut-off frequency ψ_b in the ψ' domain where $\psi' = \psi - \psi_o$ depicted in Figure 3.4

$$AF_{LP}(\psi') = \begin{cases} 1, & -\psi_b \leq \psi' \leq \psi_b \\ 0, & \text{otherwise} \end{cases} \quad (3.14)$$

Therefore, we can obtain the ideal weights of lowpass filter for the odd case as follow

$$\begin{aligned} w_{LP}(m) &= \frac{1}{2\pi} \int_{-\pi}^{\pi} AF_{LP}(\psi') e^{-jm\psi'} d\psi' \\ &= \frac{1}{2\pi} \int_{-\psi_b}^{\psi_b} 1 \cdot e^{-jm\psi'} d\psi' \\ &= \frac{\sin(\psi_b m)}{\pi m}, \text{ for } m = 0, \pm 1, \pm 2, \dots \pm N \end{aligned} \quad (3.15)$$

while for the even case

$$\begin{aligned} w_{LP}(\pm m) &= \frac{1}{2\pi} \int_{-\pi}^{\pi} AF_{LP}(\psi') e^{\mp j(m-1/2)\psi'} d\psi' \\ &= \frac{1}{2\pi} \int_{-\psi_b}^{\psi_b} 1 \cdot e^{\mp j(m-1/2)\psi'} d\psi' \\ &= \frac{\sin(\psi_b(m-1/2))}{\pi(m-1/2)}, \text{ for } m = 1, 2, \dots, N \end{aligned} \quad (3.16)$$

By seeing Eq.3.8 with Eq.3.15 and also Eq.3.9 with Eq. 3.16, we can see that $w_{BP}(m) = e^{-jn\psi_o} w_{LP}(m)$.

In the θ domain, the ideal beam array factor must be flat over $\theta_1 - \theta_2$ which is the the desired beam coverage

$$AF(\theta) = \begin{cases} 1, & \theta_1 \leq \theta \leq \theta_2 \\ 0, & \text{otherwise} \end{cases} \quad (3.17)$$

We define the beam center position θ_c and the beamwidth θ_b as follows

$$\begin{aligned} \theta_c &= \frac{1}{2}(\theta_1 + \theta_2) \\ \theta_b &= \theta_2 - \theta_1 \end{aligned} \quad (3.18)$$

so that we can obtain θ_1 and θ_2 as follows

$$\begin{aligned} \theta_1 &= \theta_c - \frac{1}{2}\theta_b \\ \theta_2 &= \theta_c + \frac{1}{2}\theta_b \end{aligned} \quad (3.19)$$

As $\psi' = \psi - \psi_o = kd \cos \theta - \psi_o$, θ_1 and θ_2 can be mapped onto lowpass passband $(\psi_p, -\psi_p)$ in ψ' as follows

$$\begin{aligned}\psi_p &= kd \cos \theta_1 - \psi_o \\ -\psi_p &= kd \cos \theta_2 - \psi_o\end{aligned}\quad (3.20)$$

From Eq. 3.20, we can obtain ψ_o and ψ_p

$$\psi_o = \frac{1}{2}kd(\cos \theta_1 + \cos \theta_2) \quad (3.21)$$

$$\psi_p = \frac{1}{2}kd(\cos \theta_1 - \cos \theta_2) \quad (3.22)$$

By using Eq. 3.19, Eq. 3.22, and some trigonometry identities, ψ_p is equivalent with

$$\psi_p = kd \sin(\theta_c) \sin\left(\frac{\psi_b}{2}\right) \quad (3.23)$$

The ideal cutoff frequency ψ_b can be taken as the middle between the passband ψ_p and the stopband ψ_s frequencies

$$\begin{aligned}\psi_b &= \frac{1}{2}(\psi_p + \psi_s) \\ &= \psi_p + \frac{1}{2}\Delta\psi\end{aligned}\quad (3.24)$$

where by defining the transition width $\Delta\psi$ as $\Delta\psi = \frac{2\pi D}{N-1}$ and using Eq 3.23, we can define the cut off frequency as follow

$$\psi_b = kd \sin(\theta_c) \sin\left(\frac{\psi_b}{2}\right) + \frac{2\pi D}{M-1} \quad (3.25)$$

Finally, FSM-KW codebook can be obtained as the windowed array weights $w(m) = w_{window}(m)w_{BP}(m)$

$$w(m) = w_{window}(m)e^{-j\beta\psi_o} \frac{\sin(\beta\psi_b)}{\pi\beta} \text{ for } m = 0, 1, \dots, M-1 \quad (3.26)$$

where $w_{window}(m)$ is the Kaiser window sample and $\beta = m - (M-1)/2$ while ψ_o and ψ_b are given in the Eq. 3.21 and Eq. 3.25, respectively.

In our proposed beamforming design, we will rely on the beam position and the beamwidth to adjust the array factor of FSM-KW beamforming. Therefore, we need to consider beam-broadening factor when the broadside beam is steered into end-fire direction. As FSM-KW beamforming requires a predefined sidelobe attenuation parameter A , that will affect on the window transition region and the beam ripples reduction [25], we also need to consider what the appropriate sidelobe attenuation is.

3.1.1 Beam-Broadening Factor

Beam at the broadside direction or $\theta = \pi/2$ will broaden if it is steered into end-fire direction [18, 19] as depicted in Figure 3.5 where the broadside beam is steered into $\theta = \pi/4$. It can be seen that the steered beam has wider beamwidth than the broadside beam, but these two beams still have the same array factor directivity.

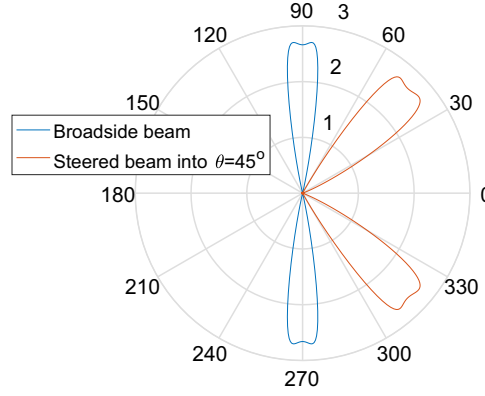


Figure 3.5: Broadside beam is steered into $\theta = 45^\circ$

The relation between the beam direction and the beamwidth, which is called as beam-broadening factor, can be approached by Eq. 3.27 [18, 19].

$$\Delta\theta(\theta = \theta') = \frac{\Delta\theta(\theta = \pi/2)}{\sin \theta'} \quad (3.27)$$

where $\Delta\theta(\theta = \theta')$ is the beamwidth of beam at $\theta = \theta'$ direction and $\Delta\theta(\theta = \pi/2)$ is the beamwidth of broadside beam at $\theta = \pi/2$ direction. However, the equation is not valid for the beamwidth at end-fire direction as $1/\sin(0) = \infty$.

Steering the beam into $\theta = \theta'$ direction can be done in two ways.

1. The first technique is by multiplying the codebook of broadside beamforming at $\theta = \pi/2$ with the steering factor $e^{-jm\frac{2\pi}{\lambda}d\cos(\theta')}$

$$w_{\theta'}(m) = w_0(m)e^{-jm\frac{2\pi}{\lambda}d\cos \theta'} \quad (3.28)$$

where $w_{\theta'}(m)$ is the codebook for the beam steered into θ' direction, w_0 is the codebook for the broadside beam, and $m = 0, 1, \dots, M - 1$ is the element index for array antenna that consists of M number antenna elements.

2. The second technique of beam steering is by directly designing the beam, where in this term we design with FSM-KW beamforming, with

a specific beam direction and a specific beamwidth. If we define the beamwidth of the steered beam by considering beam broadening factor in Eq. 3.27, we will get the same codebook as in the first beam steering technique. Thus, the scanned beam will be the same as in the one designed using the prior technique.

3.1.2 Sidelobe Attenuation Coefficient in FSM-KW Beamforming

In the Fourier series method beamforming, we can create array factor pattern that will have radiation over a specific coverage angle only. However, by using Fourier series method only, the array factor pattern still has fluctuations. Thus, window technique is applied to reduce the fluctuations [12, 25].

Compared to other window functions, Kaiser window has a flexibility to adjust the sidelobe attenuation parameter, considering the trade-off between beam transition width and beam ripple [12]. Hence, our proposed beamforming will be based on the Fourier series method with Kaiser window (FSM-KW). In Figure 3.6 we can see that as the sidelobe attenuation parameter A increases, the ripples will decrease but the beam will slightly widen. Thus, we need to choose an appropriate sidelobe attenuation for the proposed beamforming. Based on the trade-off between the percentage of power radiated by main

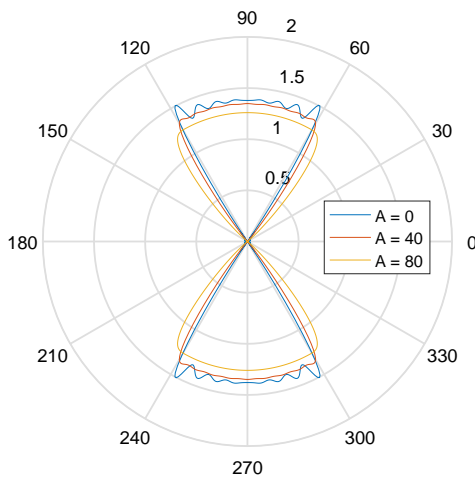


Figure 3.6: Array factor in FSM-KW beamforming for various sidelobe attenuation A (designed in fully-digital beamforming with $M = 128$)

lobe and the attenuation loss at the edge of beam coverage, as shown in

Figure 3.7 and Figure 3.8 respectively, selecting 40 dB of sidelobe attenuation in the proposed beamforming is justifiable.

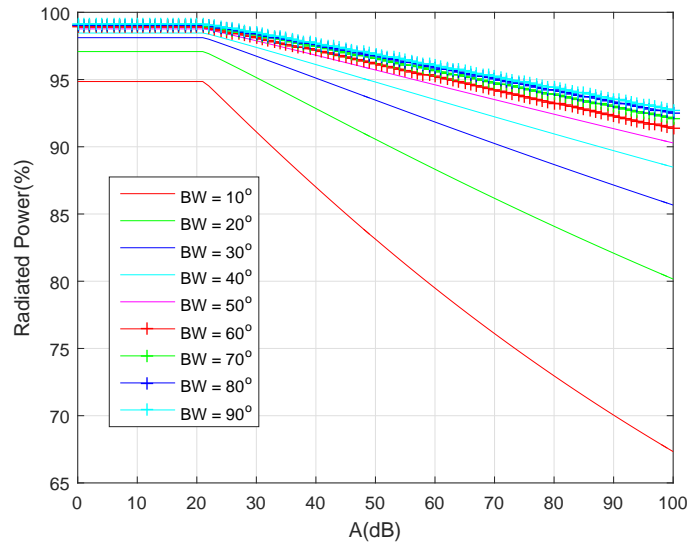


Figure 3.7: Percentage of power radiated by mainlobe at various beamwidth (BW) with $M=128$ number of antenna elements

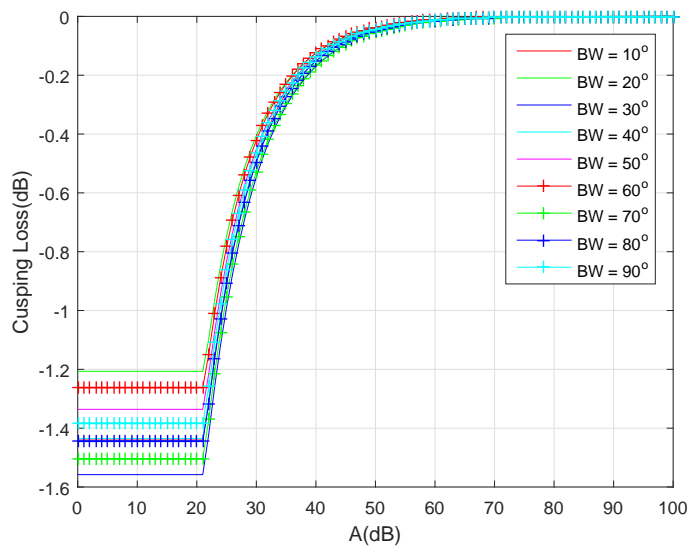


Figure 3.8: Beam attenuation at the edge of beamwidth at various beamwidth (BW) with $M = 128$ number of antenna elements

3.2 Beamforming Design Methodology

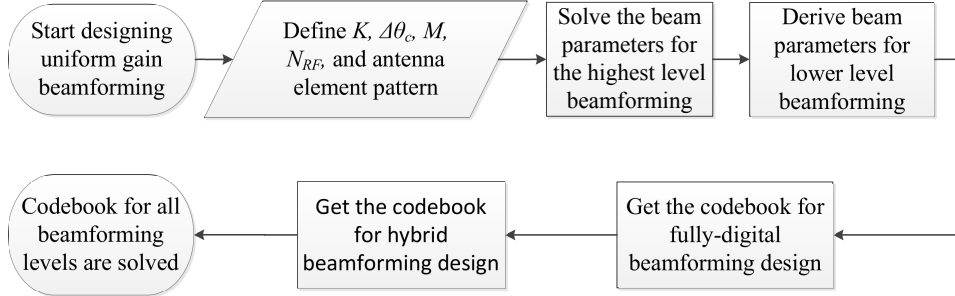


Figure 3.9: An overview flowchart of the beamforming design

In general, the process of designing the proposed beamforming codebook until we obtain beamforming codebook that is ready to be implemented can be done following flowchart in Figure 3.9.

1. First, we need to define the beamforming parameters, consisting number of beams in the highest beam level (K) and beam scanning coverage ($\Delta\theta_c$), that want to be designed. We also need to characterize the hardware limitation parameters which are antenna element pattern, number of antenna elements (M), and number of RF chains in the hybrid beamforming design (N_{RF}).
2. Secondly, we need to solve the beam parameters (beam position and beamwidth) of the highest level beams. The beam parameters will depend on K , $\Delta\theta_c$, and antenna element pattern. We have to solve this parameters (beam position and beamwidth) because low gain at the edge of scanning coverage need to be compensated by giving high array factor directivity while array factor directivity depends on the beamwidth and the beam position. This process will be explained in Subsection 3.2.1.
3. After beam parameters (beamwidth and beam position) for the highest level beam are obtained, we can derive the beam parameters (beamwidth and beam position) for the lower level beam as explained in Subsection 3.2.2.
4. After all beam parameters (beamwidth and beam position) are obtained, we can design the beamforming codebook by using FSM-KW beamforming as depicted in Subsection 3.2.3. The codebook designed in this process is still an ideal codebook that can be implemented only on digital beamforming architecture. Different number of antenna elements M will give different digital codebook.

5. The last process is designing codebook for hybrid beamforming architecture as described in Subsection 3.2.4. Digital beamforming with large number of antenna elements is expensive and power consuming. Therefore, hybrid beamforming architecture is preferred due to its hardware simplicity that can reduce the number of RF chains without losing significantly the beamforming performance. Nevertheless, the number of optimum RF chains is out of our thesis area.

3.2.1 Solving the Highest Level Beamforming Parameters (Beamwidth and Beam Position)

The proposed beamforming design when there are K possible beams (where $K = 2N$) is illustrated in Figure 3.2. We start solving beam parameters (beamwidth and beam position) from the highest level of beamforming. The proposed beamforming has K number of finest beams. The beam design is also symmetrical toward $\theta = \pi/2$; the 1st beam is symmetrical to the $(N + 1)$ -th beam, the 2nd beam is symmetrical to the $(N + 2)$ -th beam, and so on. Therefore, to simplify the equation only the first N beam positions out of K possible beams that need to be analyzed while the rest beams can be defined later.

Since there are N beams that need to be analyzed, in total there will be $2N$ parameters consisting of N beam position parameters and N beamwidth parameters that need to be solved. Hence, we will derive $2N$ equations to solve the beam parameters. The position and the beamwidth of k -th beam are denoted in radian as θ_k and $\Delta\theta_k$, respectively. In general, these $2N$ equations can be derived into following three parts

1. The N equations can be set from the relation between beam position of the k -th beam and the total beamwidth of several beams as illustrated in Figure 3.10.

The sum of the half-beamwidth of the first beam and the position of the first beam is $\pi/2$. The sum of the beamwidth of the first beam, the half-beamwidth of the second beam, and the position of the second beam is $\pi/2$ as well. This relationship is also applicable for the other beams. Therefore, we can set N equations as depicted in Eq. 3.29.

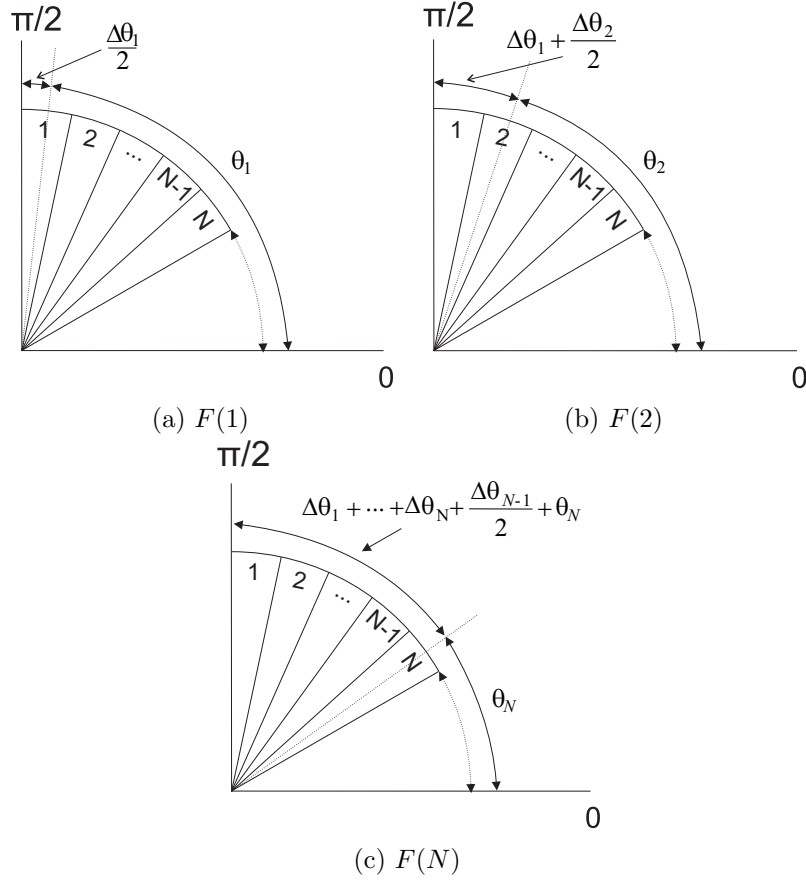


Figure 3.10: Illustration how to get E_{q_1} , E_{q_2} , and E_{q_N}

$$\begin{aligned}
 E_{q_1} &= \frac{\Delta\theta_1}{2} + \theta_1 - \frac{\pi}{2} = 0 \\
 E_{q_2} &= \Delta\theta_1 + \frac{\Delta\theta_2}{2} + \theta_2 - \frac{\pi}{2} = 0 \\
 &\dots\dots \\
 E_{q_N} &= \Delta\theta_1 + \dots + \Delta\theta_{N-1} + \frac{\Delta\theta_N}{2} + \theta_N - \frac{\pi}{2} = 0
 \end{aligned} \tag{3.29}$$

2. The next equation can be obtained from the relation between the total beamwidth of N -beams and the scanning coverage $\Delta\theta_c$ as shown in Figure 3.11.

It can be seen that the total beamwidth of N beam is equal to the scanning coverage $\Delta\theta_c$. Therefore, we can obtain Eq. 3.30 as the $(N + 1)$ -th equation.

$$E_{q_{N+1}} = (\Delta\theta_1 + \dots + \Delta\theta_N) - \Delta\theta_c = 0 \tag{3.30}$$

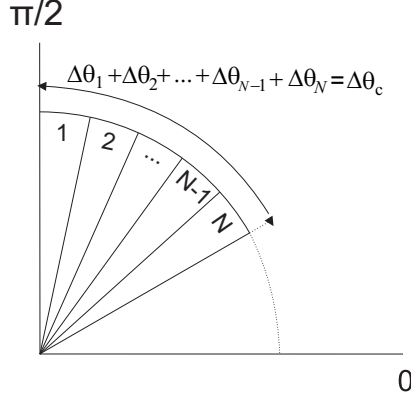


Figure 3.11: Illustration how to get $E_{q_{N+1}}$

3. The rest $(N - 1)$ equations can be set from the relation between the array factor of each beam and the gain of antenna element.

Array radiation pattern is a multiplication between the array factor and the field pattern of antenna element. In the proposed beamforming, each beam is expected to have the same gain or the same radiation strength

$$E_{k^{th} \text{ beam}} = E_{(k+1)^{th} \text{ beam}} \quad (3.31)$$

By using Eq. 2.4 we can derive Eq. 3.31 into Eq. 3.32.

$$E_o(\theta_k) \times AF(\theta_k, \Delta\theta_k) = E_o(\theta_{k+1}) \times AF(\theta_{k+1}, \Delta\theta_{k+1}) \quad (3.32)$$

where $E_o(\theta_k)$ denotes the element field pattern at a given angle direction θ_k while $AF(\theta_k, \Delta\theta_k)$ denotes the array factor function given angle direction θ_k and beamwidth $\Delta\theta_k$. Therefore, to set the rest of equations ($E_{q_{N+2}}$ until $E_{q_{2N}}$) based on Eq. 3.32, the radiation pattern of antenna element and the array factor should have been known.

The proposed beamforming takes into account non-isotropic element pattern, and it is designed for a specific element pattern. Thus, the field pattern of a single antenna element should be known a priori. For example, an useful approximation is that an element pattern can follow a sinusoidal pattern in Eq. 3.33 [19, 34, 35], and this element pattern can be depicted in Figure 3.12. The other element patterns will be considered in Chapter 5.

$$E_{no}(\theta) = \begin{cases} \sin \theta, & \text{for } 0 \leq \theta \leq \pi \\ 0, & \text{otherwise} \end{cases} \quad (3.33)$$

By using FSM-KW beamforming approach, a beam with a particular beam direction and beamwidth can be easily designed. To estimate

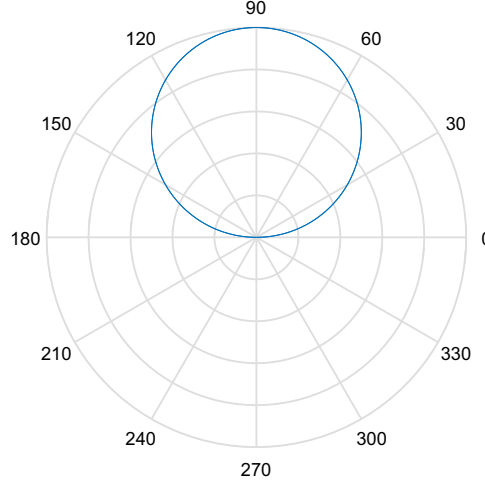


Figure 3.12: Normalized element beam pattern, $E_{no}(\theta) = \sin \theta$

the array factor for a given direction (θ) and beamwidth ($\Delta\theta$), first of all, we need to analyze the array factor of broadside beam for specific beamwidth $\Delta\theta_o$. Thus, we need to get the data of array factor of broadside beam for arbitrary beamwidth in the FSM-KW beamforming. This data is obtained in the modeling when we create broadside beam in the FSM-KW beamforming approach.

The plot between the given beamwidth and the array factor in the broadside direction $\theta = \pi/2$ for arbitrary beamwidth is shown in Figure 3.13. In this case, we use high number of antenna elements which is 128. Since the curve is visually fit to the power function, the curve is estimated by performing curve fitting with a power function $f(x) = ax^b + c$ and it gives $a = 2.685$, $b = -0.2813$, $c = -1.252$ with $RMSE = 0.0548$. The estimated function is written in Eq. 3.34.

$$AF(\Delta\theta_o) = 2.685(\Delta\theta_o)^{-0.2813} - 1.252 \quad (3.34)$$

Eq. 3.34 gives the array factor for a given beamwidth in the broadside direction $\Delta\theta_o$. To find out array factor for an arbitrary beam direction, we should consider beam broadening factor in Eq. 3.27. By joining Eq. 3.27 and Eq. 3.34, we can obtain Eq. 3.35 that gives the array factor for a specific beamwidth $\Delta\theta$ and beam position θ .

$$AF(\theta, \Delta\theta) = 2.685[\theta \sin(\Delta\theta)]^{-0.2813} - 1.252 \quad (3.35)$$

Although the field pattern function in Eq. 3.33 is in the normalized form, it is still relevant with Eq. 3.32. Eq. 3.32 aims to obtain the multiplication between the array factor and the field pattern of antenna

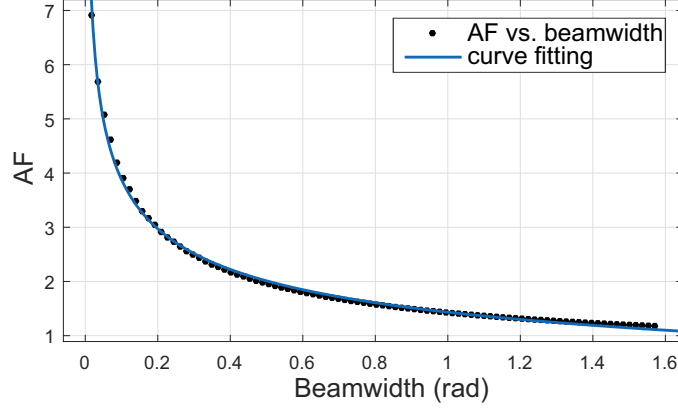


Figure 3.13: Estimating array factor of broadside beam given any beamwidth $0 < \Delta\theta \leq \pi/2$

element for all beams is expected the same. Thus, changing the field pattern with the normalized pattern will not change the equality in Eq. 3.32. By using Eq. 3.33 and Eq. 3.35 in Eq. 3.32 for the first beam until the N -th beam, we can set equations Eq_{N+2} until Eq_{2N} as seen in Eq. 3.36.

$$\begin{aligned}
 Eq_{N+2} &= AF(\theta_1, \Delta\theta_1) \times E_o(\theta_1) - AF(\theta_2, \Delta\theta_2) \times E_o(\theta_2) = 0 \\
 Eq_{N+3} &= AF(\theta_2, \Delta\theta_2) \times E_o(\theta_2) - AF(\theta_3, \Delta\theta_3) \times E_o(\theta_3) = 0 \\
 &\dots \\
 Eq_{2N} &= AF(\theta_{N-1}, \Delta\theta_{N-1}) \times E_o(\theta_{N-1}) - AF(\theta_N, \Delta\theta_N) \times E_o(\theta_N) = 0
 \end{aligned} \tag{3.36}$$

By solving these $2N$ equations (from Eq_1 until Eq_{2N}), we can obtain the desired beam parameters (beam position and beamwidth) for our proposed N beams. In this thesis, we use nonlinear least-square solver(`lsqnonlin`) function in MATLAB to solve these $2N$ equations. Due to its symmetrical position, the other beam parameters can be obtained directly following $\Delta\theta_{(k+N)} = \Delta\theta_k$ and $\theta_{(k+N)} = \pi - \theta_k$ where $k = 1, \dots, N$.

The solutions (beamwidth and beam position parameters) that can satisfy Eq_1 until Eq_{2N} for $K = 8$ number of possible beams and $\Delta\theta_c = 120^\circ$ of scanning coverage are shown in Table 3.1. In this thesis we will focus to design beams that has $\Delta\theta_c = 120^\circ$ since for a practical reason, the scanning coverage of array antenna is limited maximum to $\pm 60^\circ$ from the broadside direction or the maximum scanning coverage is $\Delta\theta_c = 120^\circ$ [18, 33].

Table 3.1: Beam position and beamwidth parameters for $K = 8$ when considering the element pattern $E_o(\theta) = \sin \theta$

Beam Index k	Beam Position θ_k (rad)	Beamwidth $\Delta\theta_k$ (rad)
1	1.419	0.303
2	1.113	0.310
3	0.830	0.256
4	0.613	0.178
5	1.722	0.303
6	2.029	0.310
7	2.311	0.256
8	2.529	0.178

3.2.2 Defining Lower Level Beamforming Parameters (Beamwidth and Beam Position)

In switched beamforming, the beams should be fixed and predefined. Hence, a set of codebook that generates the beams for each level of beam-searching must be set first. In our approach, we start defining beam parameters (beamwidth and beam position) from the highest level of beamforming. Then, the beam parameters at the lower level must be defined based on the beam parameters at the highest level.

Beam in hierarchical beamforming approach must be refined at each level of beamforming where at higher beamforming level, the beam will cover less area. In order to reduce the number of training packets, our beamforming uses hierarchical approach where there will be two beam candidates at each beam-searching level. The beam hierarchy is shown in Table 3.2 where at the higher level the number of possible beams is doubled. In this table, $\mathbf{w}(\ell, k)$ denotes the k -th beam candidate at ℓ -th level of beamforming.

Table 3.2: Beam hierarchy in the proposed beamforming

Beam-searching Level (ℓ)	Codebook Structure							
1	$\mathbf{w}(1, 1)$				$\mathbf{w}(1, 2)$			
2	$\mathbf{w}(2, 1)$		$\mathbf{w}(2, 2)$		$\mathbf{w}(2, 3)$		$\mathbf{w}(2, 4)$	
3	$\mathbf{w}(3, 1)$	$\mathbf{w}(3, 2)$	$\mathbf{w}(3, 3)$	$\mathbf{w}(3, 4)$	$\mathbf{w}(3, 5)$	$\mathbf{w}(3, 6)$	$\mathbf{w}(3, 7)$	$\mathbf{w}(3, 8)$
...	...							
$\log_2 K$	$\mathbf{w}(\log_2 K, 1)$				$\mathbf{w}(\log_2 K, K)$			

At the highest level beamforming (L -th level, where $L = \log_2 K$) there will be $K = 2^L$ beam candidates. The beam at the lower level is the combination

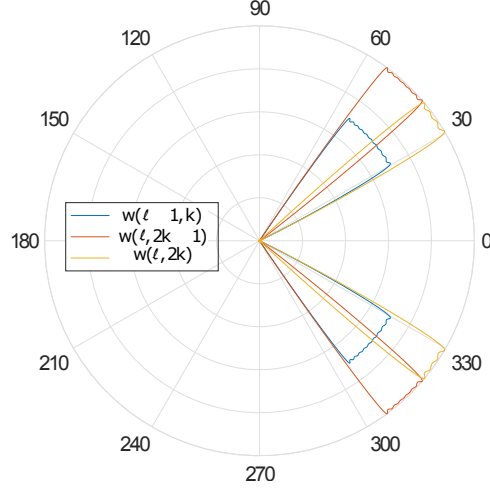


Figure 3.14: Illustration of the proposed beamforming where one beams at lower level covering two beams at higher level

of two adjacent beams at the higher level as illustrated in Figure 3.14. The lower level beam $\mathbf{w}(\ell - 1, k)$ that has direction at $\theta(\ell - 1, k)$ will cover two higher level beams which are $\mathbf{w}(\ell, 2k)$ and $\mathbf{w}(\ell, 2k - 1)$ with beam direction at $\theta(\ell, 2k)$ and $\theta(\ell, 2k - 1)$ respectively. The beamwidth of lower level beam, $\Delta\theta(\ell - 1, k)$, is the combination of these two adjacent beams in the higher level, $\Delta\theta(\ell, 2k - 1)$ and $\Delta\theta(\ell, 2k)$

$$\Delta\theta(\ell - 1, k) = \Delta\theta(\ell, 2k - 1) + \Delta\theta(\ell, 2k) \quad (3.37)$$

where $2 \leq \ell \leq L$ and $k = 1, \dots, 2^\ell$.

The position of the lower level beam, $\theta(\ell - 1, k)$, is at the center of two joined adjacent beams in the lower level

$$\theta(\ell - 1, k) = \begin{cases} \frac{[\theta(\ell, 2k-1) + \Delta\theta(\ell, 2k-1)/2] + [\theta(\ell, 2k) - \Delta\theta(\ell, 2k)/2]}{2} & \text{for } k \leq N \\ \frac{[\theta(\ell, 2k-1) - \Delta\theta(\ell, 2k-1)/2] + [\theta(\ell, 2k) + \Delta\theta(\ell, 2k)/2]}{2} & \text{for } k > N, \end{cases} \quad (3.38)$$

where $2 \leq \ell \leq L$ and $k = 1, \dots, 2^\ell$.

Based on the beam parameters (beamwidth and beam position) in the highest level of beamforming as depicted in Table 3.1, beam parameters for all beam candidates at each level of beam-searching can be defined following Eq. 3.37 and Eq. 3.38 as being explained in Algorithm 2. The beam parameters for all level of beamforming are shown in Table 3.3.

Algorithm 2: Define beam parameters (beamwidth and beam position) in the lower level of beamforming based on the beam parameters in the highest level of beamforming

Input : A set beamwidth parameters and beam position parameters for K possible finest beams
 $[\Delta\theta(\log_2 K, 1), \Delta\theta(\log_2 K, 2), \dots, \Delta\theta(\log_2 K, K)]$ and
 $[\theta(\log_2 K, 1), \theta(\log_2 K, 2), \dots, \theta(\log_2 K, K)]$ respectively

Output: A full set of beamwidth parameters and beam position parameters

$\{[\Delta\theta(1, 1), \Delta\theta(1, 2)], [\Delta\theta(2, 1), \dots, \Delta\theta(2, 4)], \dots, [\Delta\theta(\log_2 K, 1), \dots, \Delta\theta(\log_2 K, K)]\}$
and
 $\{[\theta(1, 1), \theta(1, 2)], [\theta(2, 1), \dots, \theta(2, 4)], \dots, [\theta(\log_2 K, 1), \dots, \theta(\log_2 K, K)]\}$

```

1:  $L = \log_2 K$ 
2:  $\ell = 1$ 
3: while  $\ell < L$  do
4:    $k = 1$ 
5:   while  $k \leq 2^{L-\ell}$  do
6:      $\Delta\theta(L - \ell, k) = \Delta\theta(L - \ell + 1, 2k - 1) + \Delta\theta(L - \ell + 1, 2k)$ 
7:     if  $k \leq 2^{(L-\ell-1)}$  then
8:        $\theta(L - \ell, k) =$ 
          
$$\frac{[\theta(L-\ell+1, 2k-1) + \Delta\theta(L-\ell+1, 2k-1)] + [\theta(L-\ell+1, 2k-1) - \Delta\theta(L-\ell+1, 2k)]}{2}$$

9:     else
10:       $\theta(L - \ell, k) =$ 
          
$$\frac{[\theta(L-\ell+1, 2k-1) - \Delta\theta(L-\ell+1, 2k-1)] + [\theta(L-\ell+1, 2k-1) + \Delta\theta(L-\ell+1, 2k)]}{2}$$

11:    end if
12:     $k ++$ 
13:  end while
14:   $\ell ++$ 
15: end while

```

3.2.3 Constructing Beamforming Codebook for Fully-Digital Beamforming Architecture

After the beam parameters (beamwidth and beam position) for all beamforming levels have been defined, we need to construct the beam by defining the beamforming codebook, which represents the amplitude and phase changes at each antenna element. The beams are designed based on the Fourier series method with Kaiser window (FSM-KW) beamforming with sidelobe attenuation level $A = 40$ dB.

The beam codebook with M number of antenna array elements in the fully-digital beamforming can be designed by using antenna parameters (beamwidth and beam position) in Table 3.3 and recalling Eq. 3.26 as

Table 3.3: Beamwidth and beam position parameters in the proposed uniform beamforming when $K = 8$

Beam searching Level (ℓ)	Beam parameters:							
	AWVs index							
	Beamwidth (rad)				Beam position (rad)			
3	$w(3,1)$	$w(3,2)$	$w(3,3)$	$w(3,4)$	$w(3,5)$	$w(3,6)$	$w(3,7)$	$w(3,8)$
	0.303	0.310	0.256	0.178	0.303	0.310	0.256	0.178
	1.419	1.112	2.529	0.613	1.722	2.029	2.312	2.529
2	$w(2,1)$		$w(2,2)$		$w(2,3)$		$w(2,4)$	
	0.613		0.434		0.613		0.434	
	1.264		0.741		1.877		2.401	
1	$w(1,1)$				$w(1,2)$			
	1.0472				1.0472			
	1.0472				2.094			

follow

$$w(m) = w_{window}(m)e^{-j\beta\psi_o} \frac{\sin(\beta\psi_b)}{\pi\beta} \text{ for } m = 0, 1, \dots, M-1 \quad (3.39)$$

where $w_{window}(m)$ is the Kaiser window sample with window length M and $\beta = m - (M-1)/2$ while ψ_o and ψ_b are given as follows

$$\psi_o = \frac{1}{2}kd(\cos\theta_1 + \cos\theta_2) \quad (3.40)$$

$$\psi_b = kd \sin(\theta_c) \sin\left(\frac{\psi_b}{2}\right) + \frac{2\pi D}{M-1} \quad (3.41)$$

where D is

$$D = \begin{cases} \frac{A-7.95}{14.36}, & \text{if } A > 21 \\ 0.922, & \text{if } A \leq 21 \end{cases} \quad (3.42)$$

θ_c is the beam position, and the beam coverage $\theta_1 - \theta_2$ can be obtained from the beam position θ_c and the beamwidth parameters $\Delta\theta$ as follows

$$\begin{aligned} \theta_1 &= \theta_c - \frac{1}{2}\Delta\theta \\ \theta_2 &= \theta_c + \frac{1}{2}\Delta\theta \end{aligned} \quad (3.43)$$

All beam candidates when the beams are constructed in the digital beamforming architecture with $M = 64$ are shown in Figure 3.15, Figure 3.16, and Figure 3.17 for the first, the second, and the third level of beamforming respectively.

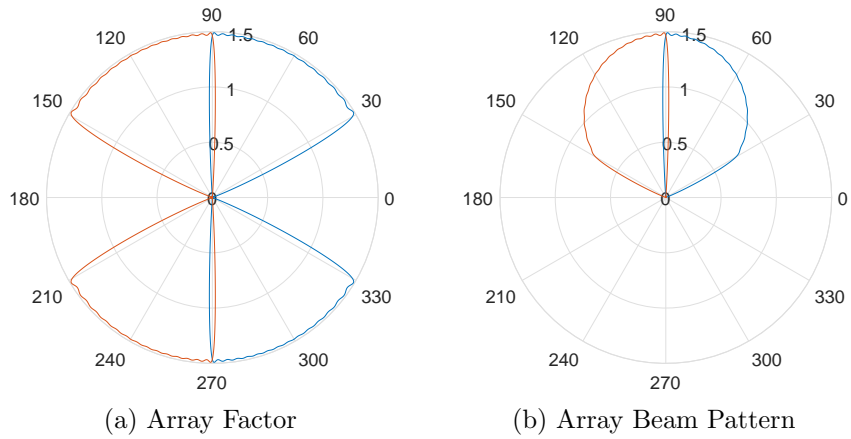


Figure 3.15: The first level of beamforming ($K = 2$) constructed with fully-digital beamforming architecture ($M = 64$)

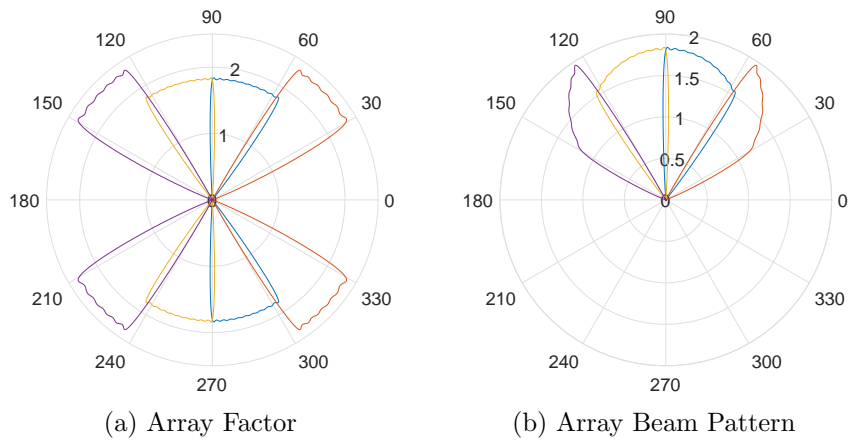


Figure 3.16: The second level of beamforming ($K = 4$) constructed with fully-digital beamforming architecture ($M = 64$)

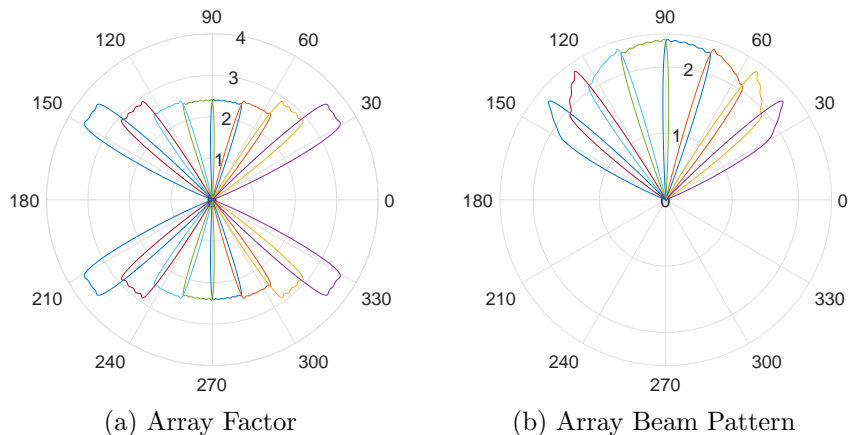


Figure 3.17: The third level of beamforming ($K = 8$) constructed with fully-digital beamforming architecture ($M = 64$)

3.2.4 Constructing Beamforming Codebook for Hybrid Beamforming Architecture

Since the proposed beamforming requires a large number of antenna elements that will lead to a large number of RF chains (as the same as the number of antenna elements), implementation in digital beamforming is not feasible. For example, if we use $M = 64$ number of antenna elements, we require $N_{RF} = 64$ number of RF chains in the digital beamforming. As a solution, the beamforming must be implemented in hybrid beamforming. In our approach, we use geometric approach algorithm [31] shown in Algorithm 1.

First, the algorithm takes the ideal fully-digital codebook for each beam which has been designed in the Subsection 3.2.3 at each level of beamforming. This ideal fully-digital codebook $\mathbf{w} \in \mathbb{C}^{M \times 1}$ with $M = 64$ number of antenna elements will be approached with the RF codebook $\mathbf{w}_{RF} \in \mathbb{C}^{M \times N_{RF}}$ and the baseband codebook $\mathbf{w}_{BB} \in \mathbb{C}^{N_{RF} \times 1}$. In this case, we use $N_{RF} = 8$ to show that with low number of RF chains, the hybrid beamforming can approach almost the same beam quality in the fully-digital beamforming. The optimum number of RF chains is outside our thesis area since the preference of number of RF chains will depend on the hardware cost preference.

In the algorithm, the RF codebook \mathbf{w}_{RF} and the residual matrix \mathbf{w}_{res} are initialized. The algorithm set the residual column \mathbf{w}_{res} with maximum norm and appends its mapped version $S(\mathbf{w}_{res})$ to the current RF codebook \mathbf{W}_{res} . $S(\mathbf{v})$ is an operator that maps the vector \mathbf{v} into the closest vector attainable with 2-bit RF phase shifter.

The algorithm then updates the residual matrix \mathbf{W}_{res} with the objective to make $\mathbf{W}_{res} = \mathbf{W}_{res} - \delta S(\mathbf{W}_{res})$ close to zero. It means that we need to

find $\delta \in \mathbb{C}$ so that

$$\mathbf{W}_{res}(i) - \delta S(\mathbf{W}_{res})(i) \approx 0 \quad \forall i \leq M \quad (3.44)$$

The algorithm finds δ as equivalent to find the good center for the set points $\frac{\mathbf{W}_{res}}{S(\mathbf{W}_{res})(i)}$ which are distributed over $\pi/2$ circular sector as seen in Figure. Each $\frac{\mathbf{W}_{res}(i)}{S(\mathbf{W}_{res})(i)}$ has a complex modulus $\mathbf{W}_{res}(i)$ and complex argument between $-\pi/4$ and $\pi/4$ since $S(\mathbf{W}_{res})$ maps \mathbf{W}_{res} to the closest points with 2-bit RF phase shifter. The algorithm divide the $\pi/2$ circular sector into two sub-sector which are north pole and south pole. The border line between the north pole and the south pole is $(w_{max} + w_{min})/2$ where $w_{max} = \max_i |\mathbf{W}_{res}(i)|$ and $w_{min} = \min_i |\mathbf{W}_{res}(i)|$. The points are located in the north pole if the modulus is greater or equal to $(w_{max} + w_{min})/2$ while the others are located in the south pole. The algorithm focuses on finding \mathbf{W}_{res} locating in the south pole and calculates their mean value δ' . If δ' is in the north pole, δ is set to be $\delta = \frac{\delta'}{|\delta'|} \frac{w_{max} + w_{min}}{2}$. Line 15-19 then updates the residual matrix.

The process is repeated until all N_{RF} codebook vectors are selected. The algorithm normalizes \mathbf{w}_{BB} to satisfy $\|\mathbf{w}_{RF}[\mathbf{w}_{BB}]_{:,i}\|_2^2$. Finally, we get the predefined RF codebook \mathbf{w}_{RF} and the predefined baseband codebook \mathbf{w}_{BB} which are ready to be implemented in the systems.

The result of all possible beam candidates at each level of beamforming by using hybrid beamforming with $N_{RF} = 8$ number RF chains is shown in Figure 3.18, Figure 3.19, and Figure 3.20, respectively for the first, the second, and the third level of beamforming.

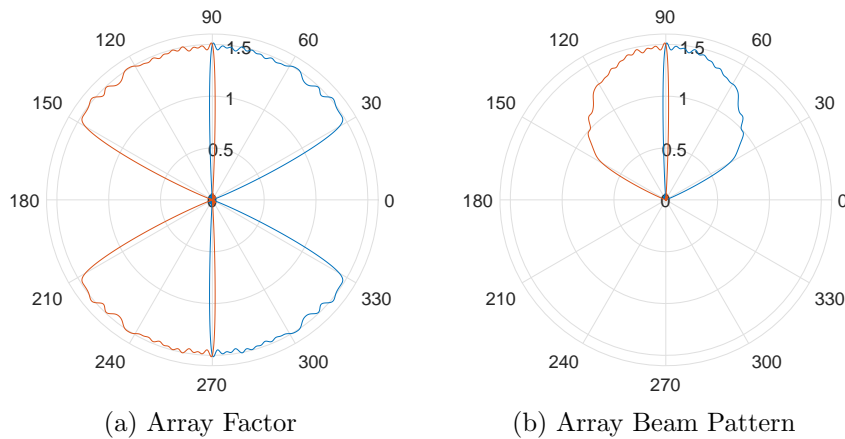


Figure 3.18: The first level of beamforming ($K = 2$) constructed with hybrid beamforming architecture ($M = 64, N_{RF} = 8$)

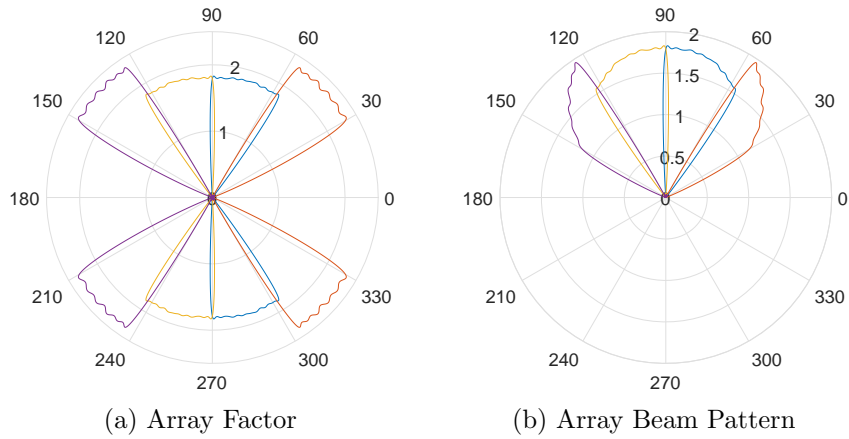


Figure 3.19: The second level of beamforming ($K = 4$) constructed with hybrid beamforming architecture ($M = 64, N_{RF} = 8$)

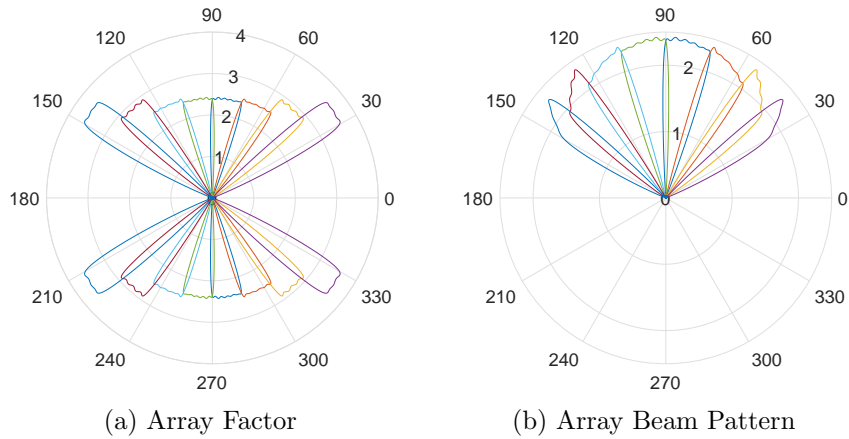


Figure 3.20: The third level of beamforming ($K = 8$) constructed with hybrid beamforming architecture ($M = 64, N_{RF} = 8$)

From the beamforming candidates depicted in Figure 3.18, Figure 3.19, and Figure 3.20, the beamforming will follow hierarchical approach as shown in Figure 3.21 and Figure 3.22. Beamforming starts at the first level where there are two beam candidates that need to be selected. The best selected beam then will be divided into two other beam candidates at higher level following hierarchical beamforming approach until the best beam in the finest level of beamforming is obtained.

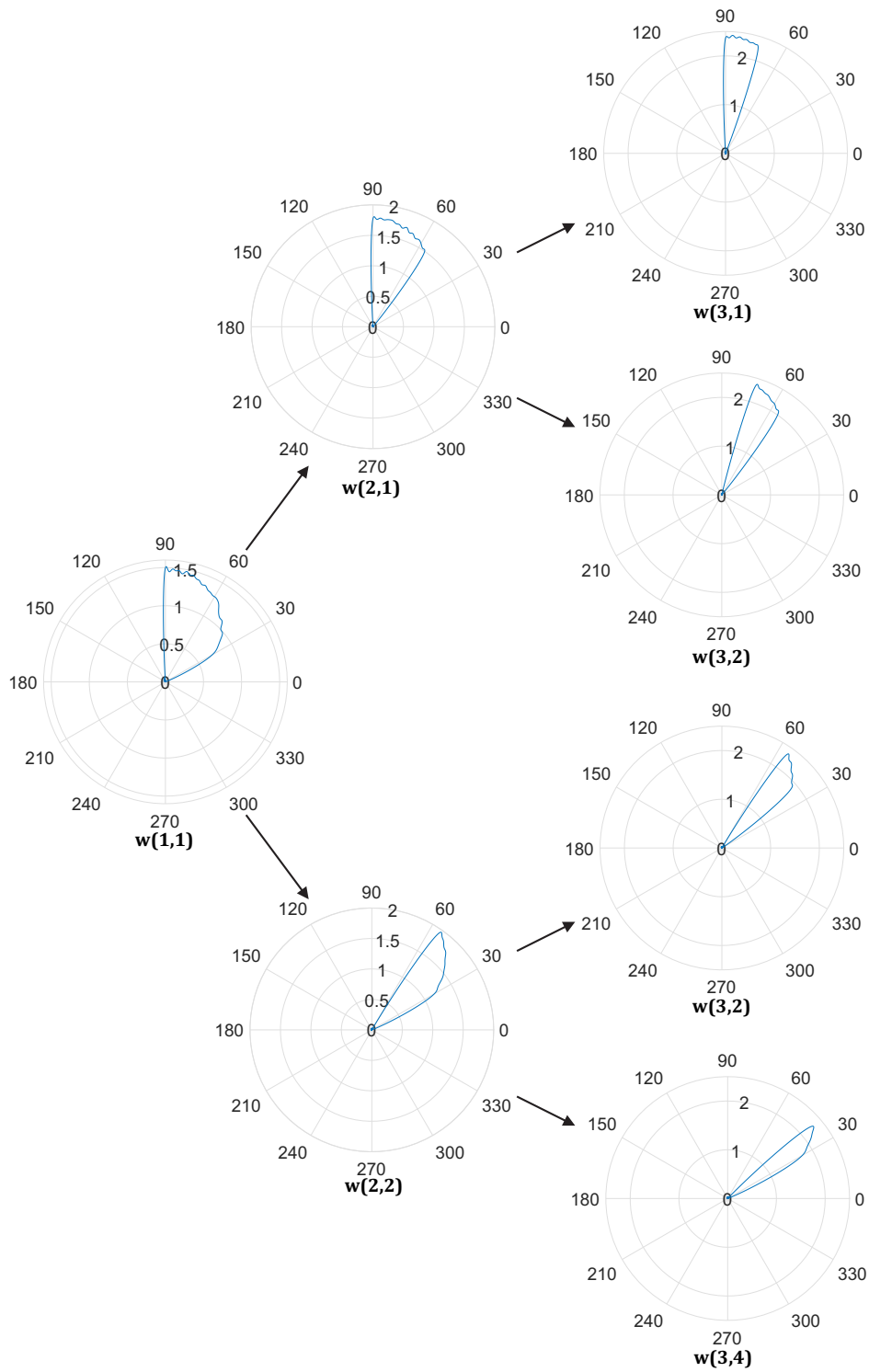


Figure 3.21: Beam-searching in the proposed uniform beamforming when $w(1,1)$ is selected for three level of beamforming (designed in hybrid beamforming architecture with $M = 64$ and $N_{RF} = 8$)

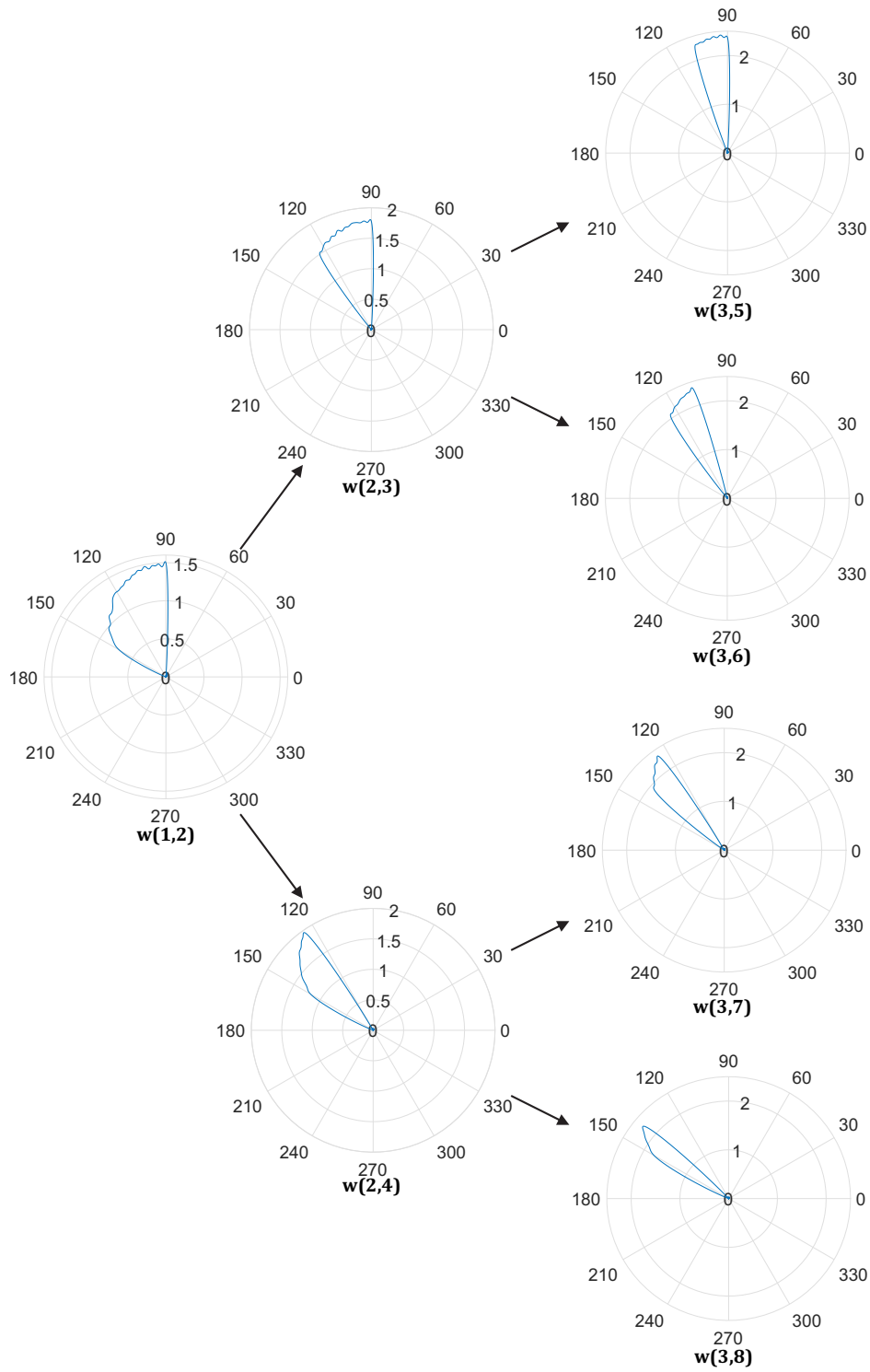


Figure 3.22: Beam-searching in the proposed uniform beamforming when $w(1,2)$ is selected for three level of beamforming (designed in hybrid beamforming architecture with $M = 64$ and $N_{RF} = 8$)

Chapter 4

Beamforming Realization

The proposed beamforming is designed by considering practical element pattern since isotropic element pattern is unrealistic to be achieved. Thus, in Chapter 3, the mechanisms how to design the beams are presented by taking an assumption that the element pattern follows sinusoidal pattern. This sinusoidal assumption is taken for simplicity reason where usually beam pattern in a patch antenna element is close to sinusoidal pattern. Nevertheless, in this chapter, two other element beam patterns, which are more realistic than sinusoidal pattern, are used to design the proposed beamforming following the procedures in Chapter 3. We also design beamforming with different scanning coverage $\Delta\theta_c$. The impact of the number of antenna elements on beam pattern also will be observed in this chapter. Beamforming in the hybrid beamforming design also will be observed for different number of RF chains N_{RF} and different number of simultaneous beams N_s .

4.1 Beamforming in Different Element Patterns

In this section, there are two different element patterns. These two element patterns are based on the real design of 60 GHz antennas. The first element pattern in Figure 4.1 is designed in [36] and it has a maximum gain of 7.2 dBi. This antenna structure design can be seen in Figure 4.2 where it consists of two substrate layers, RO3003 for the upper layer and quartz for the lower layer. With its compact size, $P_\omega = 1.7$ mm and $P_l = 1.2$ mm, this antenna can be implemented in our proposed beamforming that has element spacing of $\lambda/2 = 2.5$ mm.

For the second element pattern in Figure 4.3, we use beam pattern designed in [37] with a maximum gain of 3.8 dBi. The antenna is fabricated in silicone substrate with the structure shown in Figure 4.4. This antenna is

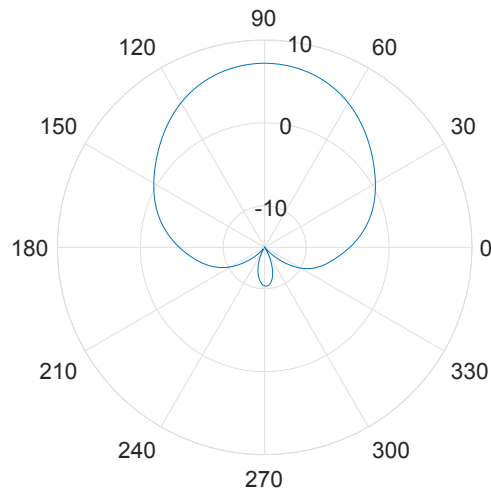


Figure 4.1: Element pattern of the first antenna (dBi)

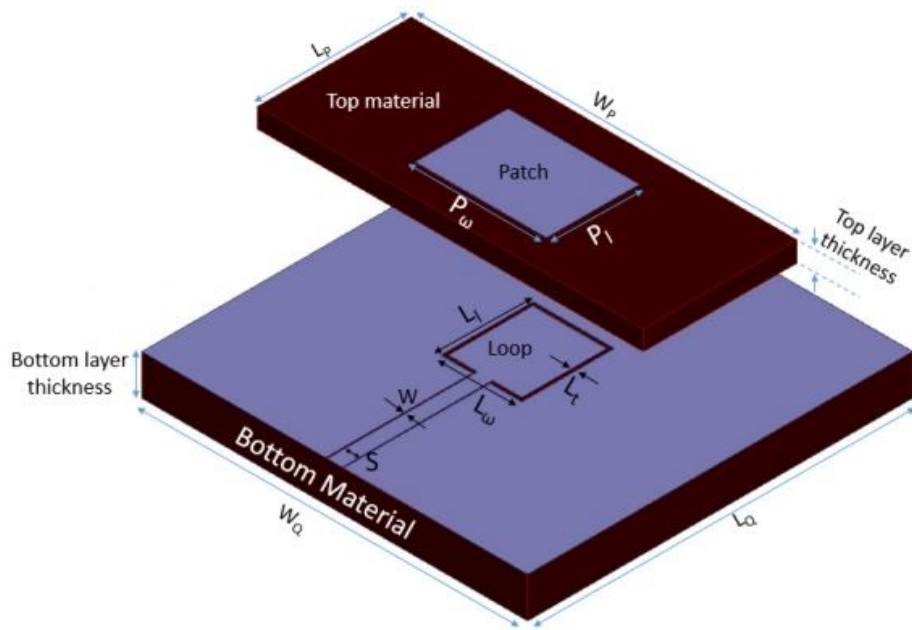


Figure 4.2: Antenna structure of the first antenna element [36]

a half-circle antenna with 0.479 mm of size, so it also can be used in the proposed beamforming with element spacing of $\lambda/2 = 2.5$ mm.

From these two element beam patterns, first of all we need to obtain a function that can give such element pattern in the desired beam pattern angle direction by performing curve fitting along $0 \leq \theta \leq \pi/2$. The curve fitting is done along $0 \leq \theta \leq \pi/2$ only since the element radiation has symmetrical pattern

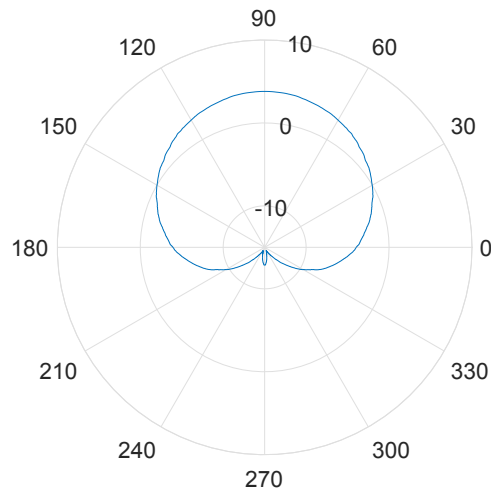


Figure 4.3: Element pattern of the second antenna (dBi)

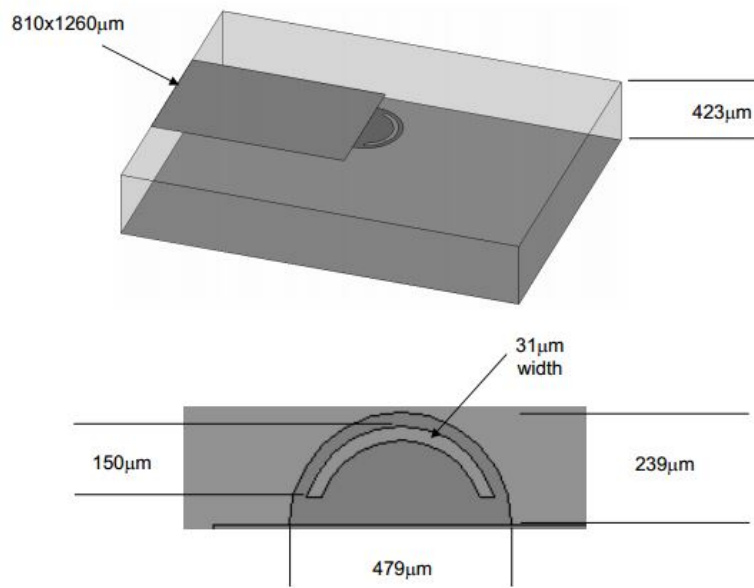


Figure 4.4: Antenna structure of the second antenna element [37]

and it is intended to radiate above the ground plane.

Beam patterns shown in Figure 4.1 and Figure 4.3 are the gain patterns. On the other hand, our approach uses field pattern to design the beams. Therefore, in the beginning, we need to convert the gain pattern into field pattern. Since field is proportional to the square root of gain, we do curve fitting in the square root of gain.

At $\theta = 30^\circ$ (the direction of the lowest gain in 120° of scanning coverage), both antenna elements have 0.42 dBi and -0.02 dBi of gain for the first and the second antenna, respectively. To perform curve fitting, we consider that error must be less than 0.1 dB. If we take 0 dBi (or 1 in linear unit) of element gain as the baseline, 0.1 dB of gain error is equal to 0.02 of gain in linear unit or 0.01 of the square root of gain. Therefore, we define that the curve fitting in the square root of gain have to give root-mean-square error (RMSE) less than 0.01 for both element patterns.

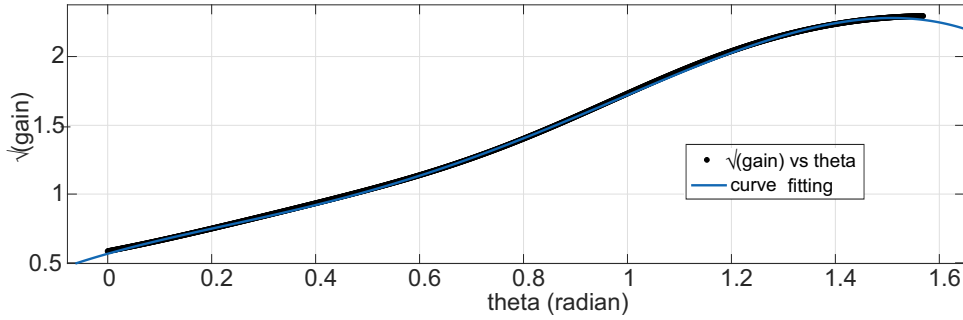


Figure 4.5: Curve fitting of the first antenna field pattern (square root of gain)

The curve fitting for the first antenna element is shown in Figure 4.5. By performing curve fitting in the polynomial function, we get 4th order of polynomial function that can represent the first beam pattern along $0 \leq \theta \leq \pi/2$

$$E'_1(\theta) = p_1\theta^4 + p_2\theta^3 + p_3\theta^2 + p_4\theta + p_5 \quad (4.1)$$

where $p_1 = -0.8841$, $p_2 = 2.138$, $p_3 = -1.168$, $p_4 = 1.067$ and $p_5 = 0.5662$. The 4th order of polynomial is chosen as it can give RMSE = 0.0069, which is less than 0.01.

By using $M = 64$ antenna elements, we design beamforming that consists of $K = 16$ beam patterns as seen in Figure 4.6. This beamforming has scanning coverage $\Delta\theta_c = 120^\circ$ along its broadside direction. It is shown in Figure 4.6a that the array factor in the end-fire direction is higher than the one close to the broadside direction. High array factor in the low angle direction is needed to compensate the gain drop. As a result, the array beam pattern has relatively uniform gain as seen in Figure 4.6b. The beam at $\theta = 90^\circ$ has gain of 16.25 dBi while the beam at $\theta = 0^\circ$ has gain of 13.82 dBi. It means that the gain drop is only 2.43 dB, which is smaller than the gain drop in the element beam pattern. The element pattern has gain of 7.20 dBi at $\theta = 90^\circ$ and 0.41 dBi at $\theta = 30^\circ$, so the gain drop in the element beam pattern is 6.79 dB.

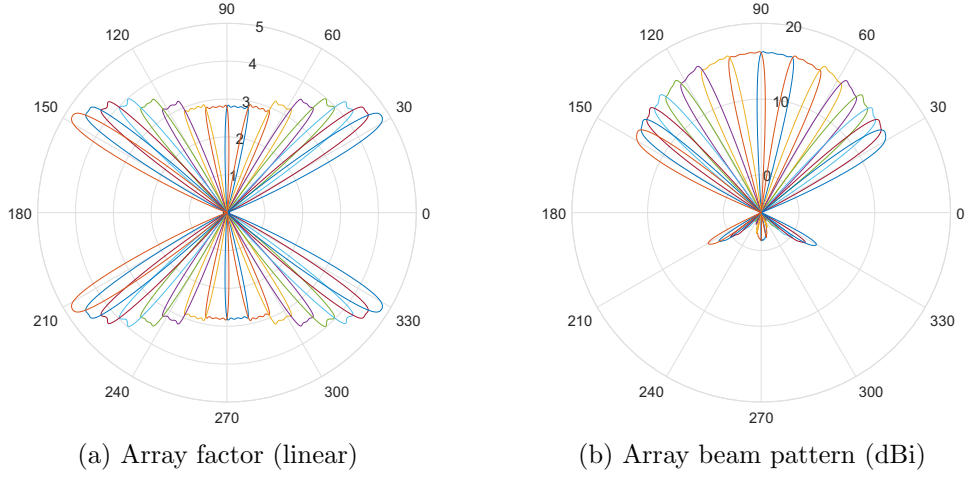


Figure 4.6: Array factor and beam pattern in the proposed beamforming ($K = 16$, $\Delta\theta_c = 120^\circ$) considering element beam pattern I (designed in the fully digital beamforming with $M = 64$)

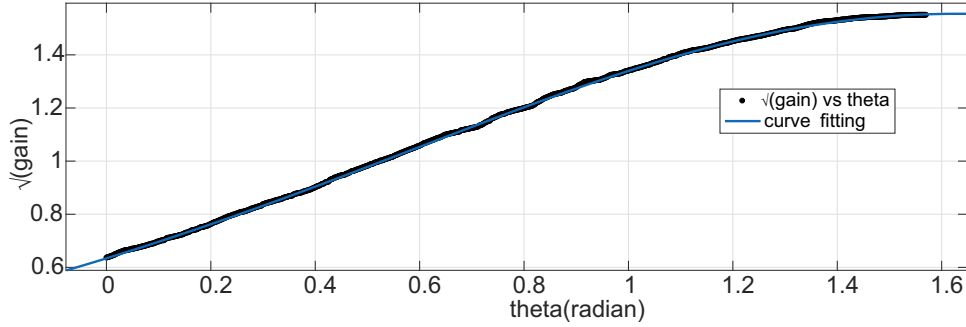


Figure 4.7: Curve fitting of the second antenna field pattern (square root of gain)

For the second element beam pattern, we also perform curve fitting along $0 \leq \theta \leq \pi/2$ by using polynomial function and we obtain the result as

$$E'_1(\theta) = p_1\theta^3 + p_2\theta^2 + p_3\theta + p_4 \quad (4.2)$$

where $p_1 = -0.2323$, $p_2 = 0.389$, $p_3 = 0.5438$, and $p_4 = 0.6383$. This 3rd order polynomial of curve fitting gives $\text{RMSE} = 0.0033$.

Beam patterns that consider the second element pattern are shown in Figure 4.8. This beamforming has gain of 14.29 dBi at $\theta = 90^\circ$ and 12.34 dBi at $\theta = 30^\circ$ which means the gain degradation is 1.95 dB. Compared to its element pattern that has gain of 3.8 dBi at $\theta = 90^\circ$ and -0.02 dBi at $\theta = 30^\circ$ or the gain drop is 3.82 dB, the gain degradation in the proposed beamforming is smaller than the one in the element beam pattern.

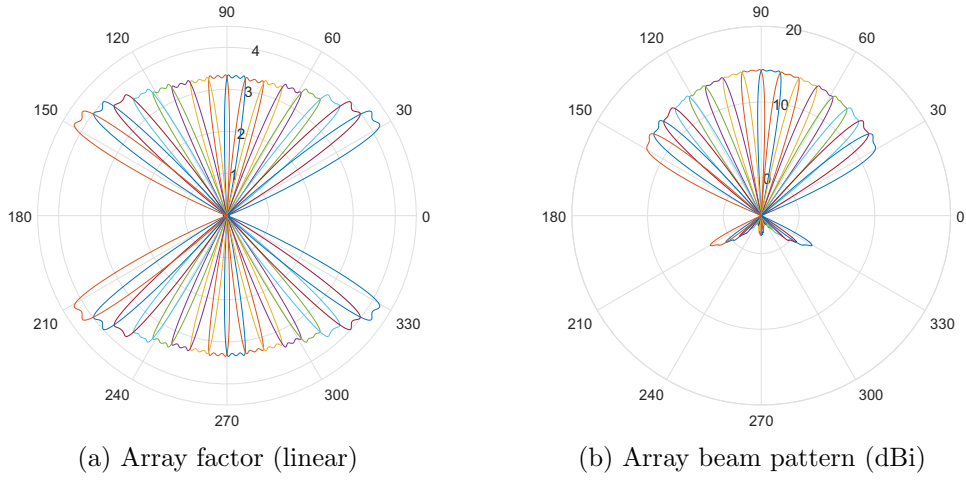


Figure 4.8: Array factor and beam pattern in the proposed beamforming ($K = 16$, $\Delta\theta_c = 120^\circ$) considering element beam pattern II (designed in the fully digital beamforming with $M = 64$)

4.2 Beamforming for Different Scanning Coverage

Beam patterns based on two element patterns in [36] and [37] are shown in Section 4.1. Henceforth, we will only use the first element beam pattern (as seen in Figure 4.1) as the element pattern assumption. Beamforming with scanning coverage $\Delta\theta_c = 60^\circ$ is shown in Figure 4.9 while another beamforming that can cover $\Delta\theta_c = 90^\circ$ is shown in Figure 4.10.

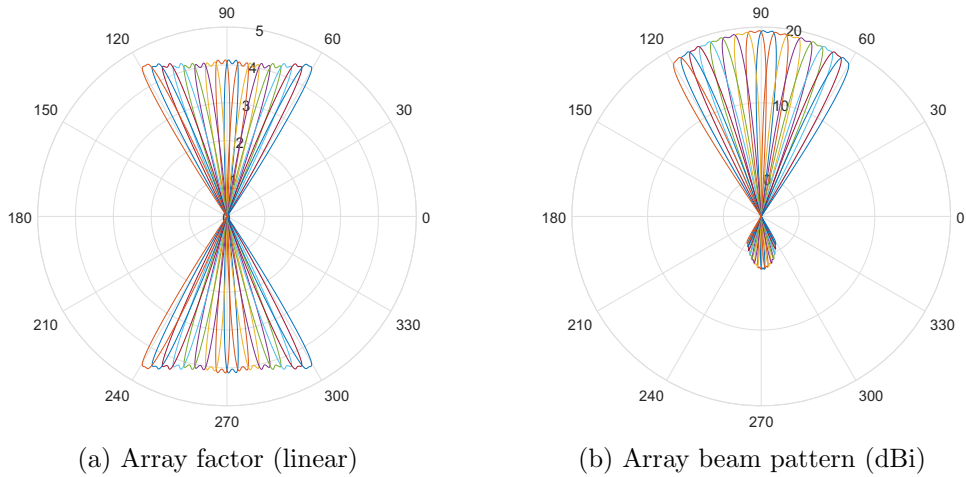


Figure 4.9: Array factor and array beam pattern in the proposed beamforming ($K = 16$, $\Delta\theta_c = 60^\circ$) constructed in the fully digital beamforming ($M = 64$)

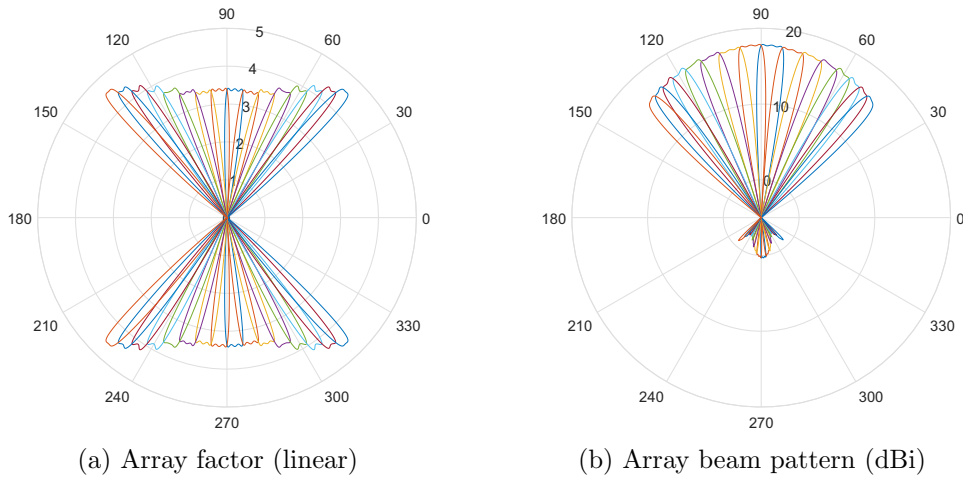


Figure 4.10: Array factor and array beam pattern in the proposed beamforming ($K = 16$, $\Delta\theta_c = 90^\circ$) constructed in the fully digital beamforming ($M = 64$)

Table 4.1: Beamforming gain for various scanning coverage $\Delta\theta_c$

Scanning Coverage $\Delta\theta_c$	Gain at the broadside (dBi)	Gain at the edge of scanning coverage (dBi)	Gain Drop (dB)
60°	19.52	18.11	1.41
90°	17.86	15.80	2.06
120°	16.25	13.82	2.43

We can see from Figure 4.9 and Figure 4.10 that by narrowing scanning coverage, the gain will be higher. Although it gives higher gain, narrowing scanning coverage gives consequence that multiple array antenna systems must be used to cover 360° . By using $\Delta\theta_c = 120^\circ$ of scanning coverage, there are only three antenna systems needed to cover 360° . However, with only $\Delta\theta_c = 90^\circ$ of scanning coverage, there must be four antenna systems.

In Table 4.1 we can see that beamforming with large scanning coverage suffers high gain degradation at low angle since the array antenna cannot compensate low gain in element pattern with high array factor. With a limited number of antenna elements, the antenna system cannot create a very narrow beam that will give high array factor. Larger scanning coverage also has lower gain since each beam will have larger beamwidth than in narrower scanning coverage. As a consequence, gain in the large scanning coverage will decrease.

4.3 Beamforming for Different Number of Antenna Elements

Heretofore we design antenna beamforming using $M = 64$ antenna elements. As already stated before, the larger the number of antenna elements, the more precision beam patterns will be obtained in terms of the desired beamwidth and the small ripple. However, a large number of antenna elements is not preferable as the antenna dimension and the cost will increase.

In this section, we show beamforming with $K = 16$ beam candidates which are constructed using $M = 32$ and $M = 64$ antenna elements as seen in Figure 4.11 and Figure 4.12 respectively. The beamforming has scanning coverage $\Delta\theta_c = 120^\circ$. We can see that as the number of antenna elements increases, beam intersection between adjacent beams decrease.

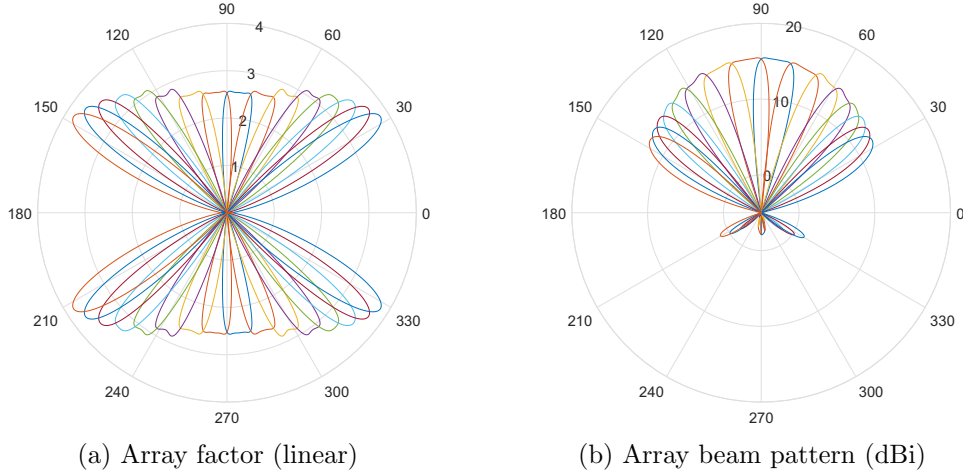


Figure 4.11: Array factor and beam pattern in the proposed beamforming ($K = 16$, $\Delta\theta_c = 120^\circ$) constructed in the fully-digital beamforming ($M = 32$)

Table 4.2 shows the gain degradation from the broadside direction to the edge of beam scanning coverage direction. Beamforming designed with $M = 32$ has lower gain compared to the one created with $M = 128$. It can happen due to beam overlapping that increases when the number of antenna elements is reduced. A small number of antenna elements cannot construct beam with high precision (fit to the desired beamwidth), so the beam transition will be larger.

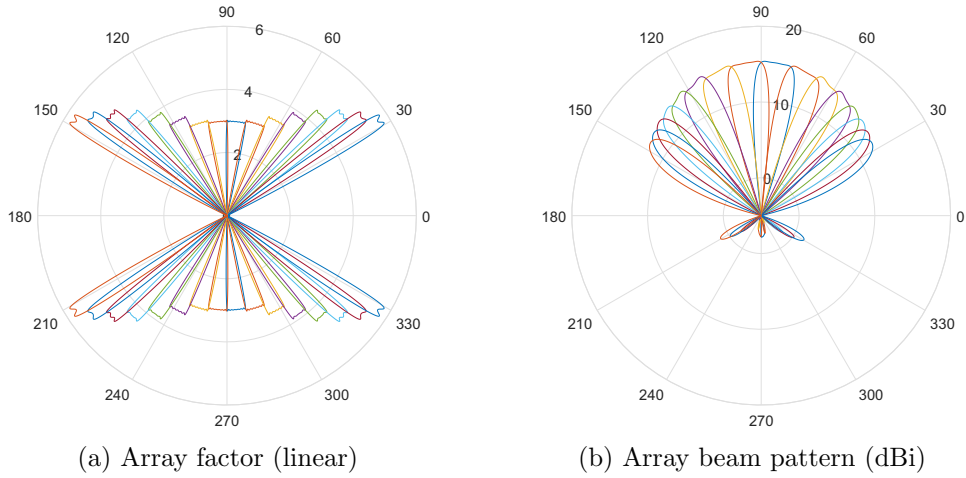


Figure 4.12: Array factor and beam pattern in the proposed beamforming ($K = 16$, $\Delta\theta_c = 120^\circ$) constructed in the fully-digital beamforming ($M = 128$)

Table 4.2: Beamforming gain for various number of antenna elements

Number of Antenna Elements M	Gain at the broadside (dBi)	Gain at the edge of beam (dBi)	Gain Drop (dB)
32	15.38	11.87	3.51
64	16.25	13.82	2.43
128	16.70	15.39	1.31

4.4 Beamforming in Hybrid Architecture for Different Number of RF Chains

The proposed beamforming shown in the Section 4.1, Section 4.2, and Section 4.3 are constructed in the fully-digital architecture. In this section, we will show the proposed beamforming constructed in the hybrid beamforming architecture with various number of RF chains. The beams are designed for scanning coverage $\Delta\theta_c = 120^\circ$, number of finest beams $K = 16$, and number of antenna elements $M = 64$. We investigate various number of RF chains for $N_{RF} = 2$, $N_{RF} = 4$, $N_{RF} = 8$, and $N_{RF} = 16$ which are depicted in Figure 4.13, Figure 4.14, Figure 4.15, and Figure 4.16, respectively.

From Table 4.3 we can see that actually the gain at the edge of scanning coverage and at the broadside direction do not change too much for various number of RF chains (except when $N_{RF} = 2$). However, if we see Figure 4.13, Figure 4.14, Figure 4.15, and Figure 4.16, as the number of RF chains increases, the beams will be closer to the fully digital beamforming depicted

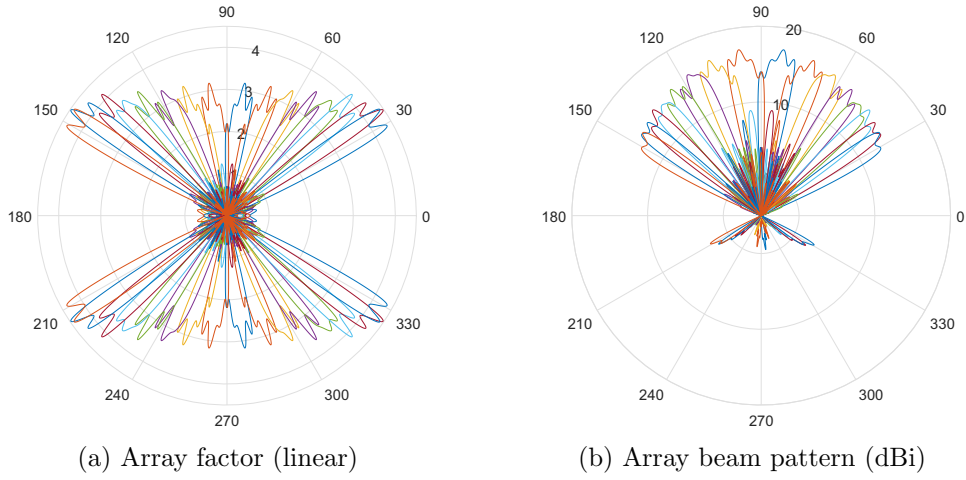


Figure 4.13: Array factor and beam pattern in the proposed beamforming ($K = 16$ and $\Delta\theta_c = 120^\circ$) constructed in the hybrid beamforming architecture ($M = 64$, $N_{RF} = 2$)

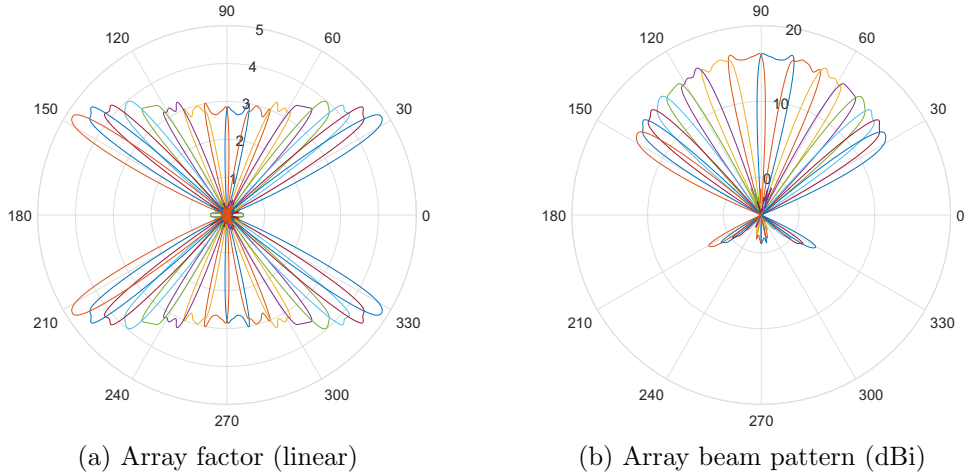


Figure 4.14: Array factor and beam pattern in the proposed beamforming ($K = 16$ and $\Delta\theta_c = 120^\circ$) constructed in the hybrid beamforming architecture ($M = 64$, $N_{RF} = 4$)

in Figure 4.6. We can see that for a small number of RF chains $N_{RF} = 4$, the beams in the hybrid beamforming looks similar with the beams in the fully digital beamforming. Therefore, hybrid beamforming architecture is very effective to reduce the hardware complexity without significantly affecting the beam pattern quality.

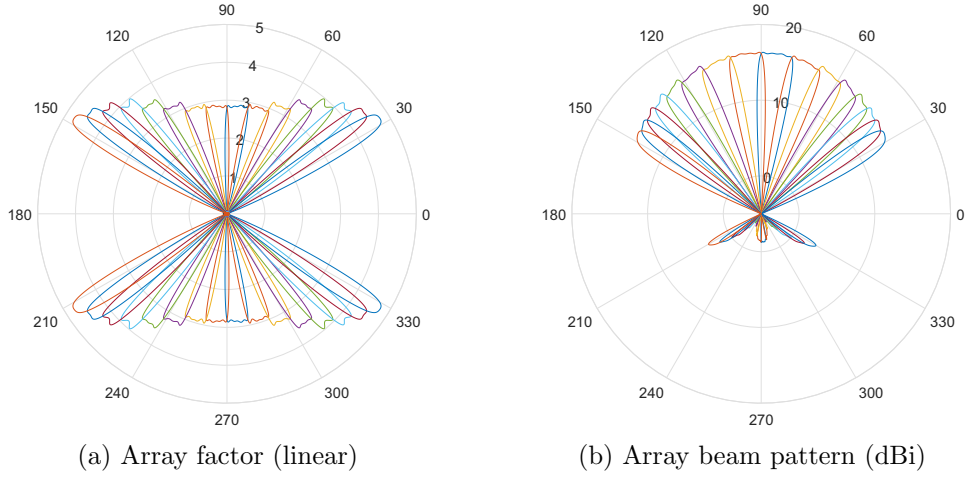


Figure 4.15: Array factor and beam pattern in the proposed beamforming ($K = 16$ and $\Delta\theta_c = 120^\circ$) constructed in the hybrid beamforming architecture ($M = 64$, $N_{RF} = 8$)

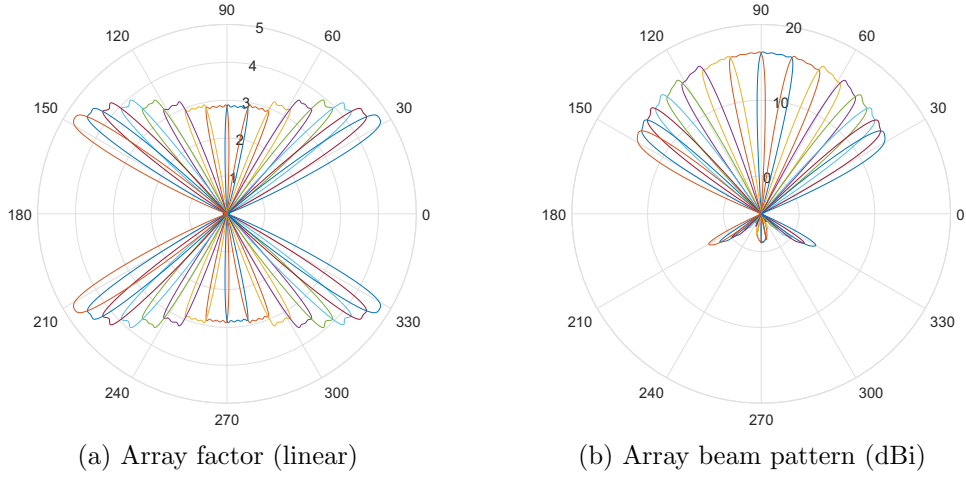


Figure 4.16: Array factor and beam pattern in the proposed beamforming ($K = 16$ and $\Delta\theta_c = 120^\circ$) constructed in the hybrid beamforming architecture ($M = 64$, $N_{RF} = 16$)

Table 4.3: Beamforming gain for various number of antenna elements

Number of RF chains N_{RF}	Gain at the broadside (dBi)	Gain at the edge of beam (dBi)	Gain Drop (dB)
2	17.09	12.72	4.37
4	16.48	13.68	2.80
8	16.32	13.75	2.57
16	16.37	13.72	2.65
64	16.36	13.72	2.64

4.5 Beamforming in Hybrid Architecture Performing Simultaneous Beams

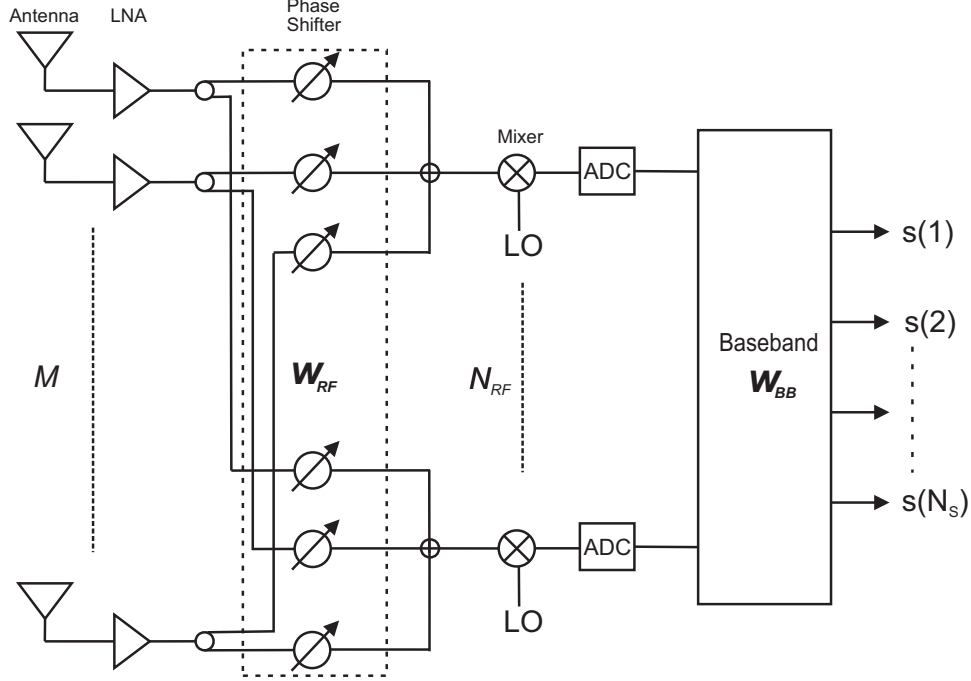


Figure 4.17: Hybrid beamforming architecture showing the ability to transmit multiple beams

Hybrid beamforming has ability to transmit multiple independent beams simultaneously by using only one array antenna system. Therefore, it is possible to communicate with several devices simultaneously by using only one antenna system. Hybrid beamforming architecture with M number of antenna elements and N_{RF} number of RF chains is shown in Figure 4.17. This hybrid beamforming architecture is able to create N_s multiple independent beams simultaneously. These independent beams can be designed with beam codebook $\mathbf{w} \in \mathbb{C}^{M \times N_s}$ where each column vector represents the beam codebook for one independent beam. The beam codebook can be approached by $\mathbf{w} = \mathbf{w}_{RF} \mathbf{w}_{BB}$ where $\mathbf{w}_{RF} \in \mathbb{C}^{M \times N_{RF}}$ is the RF codebook and $\mathbf{w}_{BB} \in \mathbb{C}^{N_{RF} \times N_s}$ is the baseband codebook.

Figure 4.18 shows the third level beamforming examples for several number of simultaneous beams. The beams are designed in the hybrid beamforming with 2-bit of phase shifter resolution, number of antenna elements $M = 64$, and number of RF chains $N_{RF} = 8$. We can see that as the number of simultaneous beams increases, the beam pattern quality will degrade. When number of simultaneous beams $N_s = 5$, the beam patterns are severely

degraded. When we change the number of RF chains to be $N_{RF} = 16$, the beams degrades severely when $N_s > 8$. Therefore, for 2-bit phase shifter resolution, the number of simultaneous beams must be kept $N_s \leq N_{RF}/2$ as also suggested in [31].

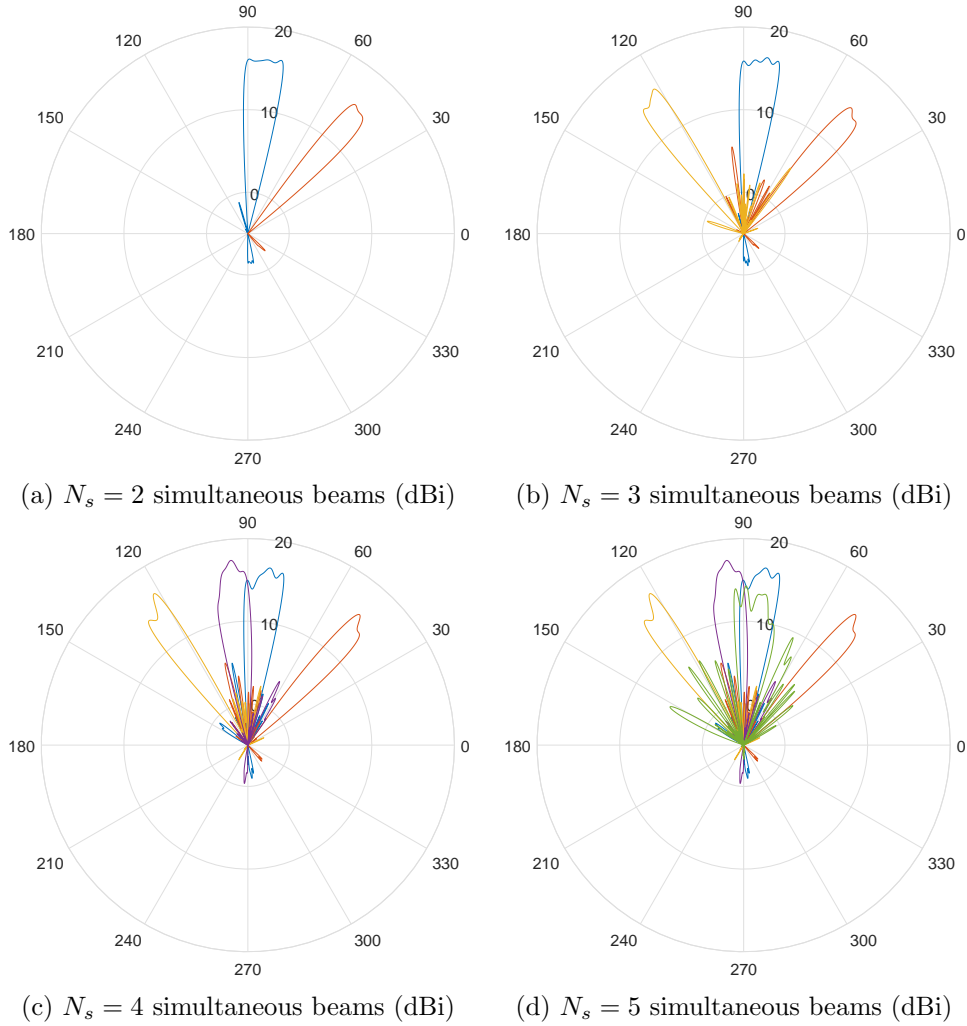


Figure 4.18: Simultaneous beams in the fourth level of beamforming, constructed in the hybrid beamforming architecture ($M = 64, N_{RF} = 8$) for various number of simultaneous beams N_s

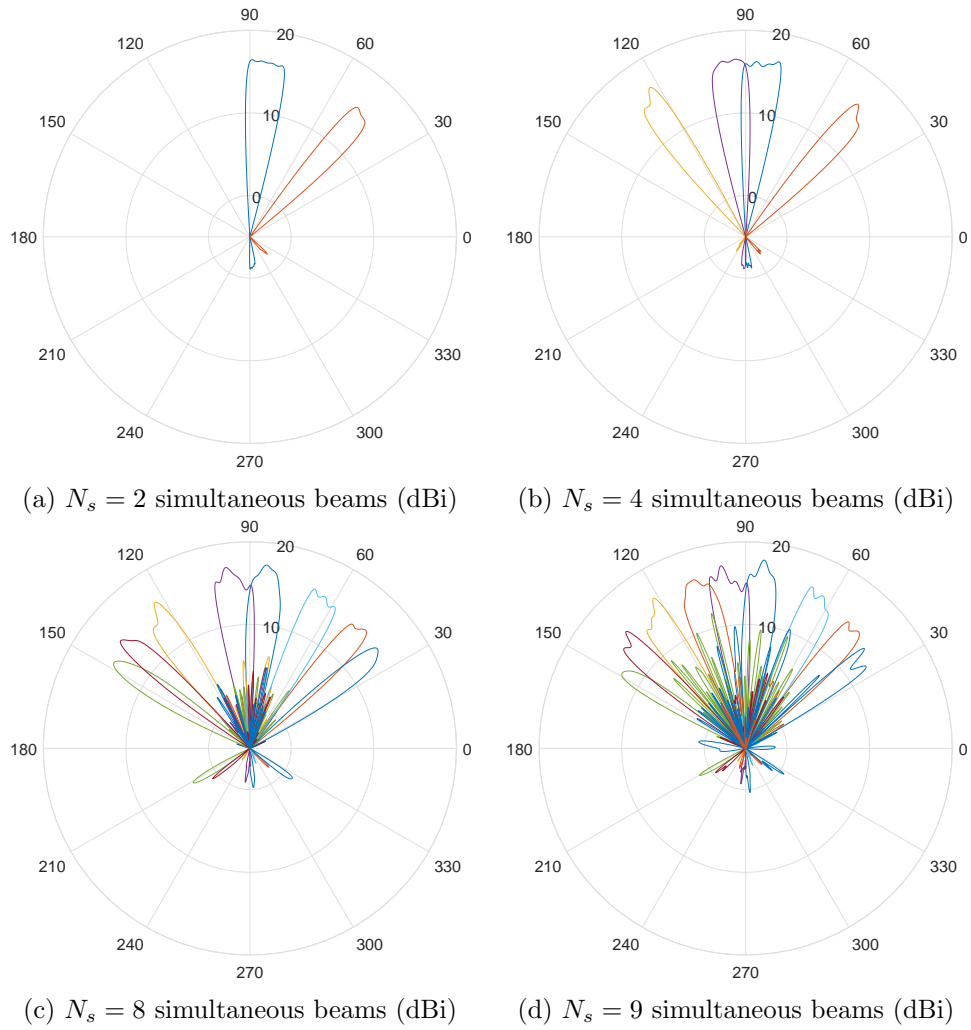


Figure 4.19: Simultaneous beams in the fourth level of beamforming, constructed in the hybrid beamforming architecture ($M = 64, N_{RF} = 16$) for various number of simultaneous beams N_s

Chapter 5

Beamforming Performance

Our proposed beamforming and the other beamforming techniques mentioned in Chapter 2 have different coverage area. Instead of covering 360° with only one antenna systems as in IEEE 802.15.3c, DFT-based, or FSM-KW beamforming, one antenna system in the proposed beamforming has a limited beamforming coverage which is more realistic in the implementation. Hence, to cover 360° more than one antenna systems are needed in the proposed beamforming.

In this chapter, we will analyze the effectiveness of the proposed beamforming compared to the classical FSM-KW beamforming in [12]. In this scenario, beamforming, either in the proposed beamforming approach or in the FSM-KW beamforming approach, has scanning coverage $\Delta\theta_c = 120^\circ$, which is the maximum scanning coverage of array antenna in practical. The beamforming performance is also analyzed by calculating the received SNR considering only large scale fading when the proposed beamforming is designed in hybrid beamforming with the geometric approach algorithm by using $M = 64$ of antenna element number and $N_{RF} = 8$ of RF chains.

5.1 Gain Variations

Ideally, to cover beam searching area there will be K number of finest beam candidates with equal gain at any covered direction. However, in the beamforming design, there will be a gap between the adjacent beams that causes cusping loss especially in IEEE 802.15.3c and DFT-based beamforming. In the Fourier series method there are still some ripples in the beam, though the ripple variations within its beamwidth are not significant. Therefore, the beam gain will vary at different direction.

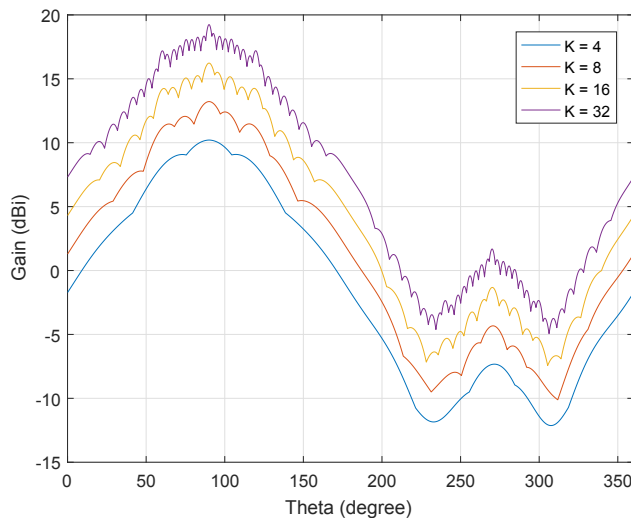


Figure 5.1: Gain variations in IEEE 802.15.3c beamforming

Beamforming designs in mmWave communications do not consider non-isotropic element beam pattern. As a result, the gain will degrade at low angle direction following the beam degradation in the element pattern when the non-isotropic element is taken into account. This phenomenon can be seen in Figure 5.1, Figure 5.2, Figure 5.3, and Figure 5.4 for IEEE 802.15.3c beamforming, DFT beamforming, FSM-KW beamforming, and the proposed beamforming respectively. This beamforming design takes assumption that the element pattern follows the first element pattern in Figure 4.1 with 7.2 dB of maximum gain. In these figures, we plot the best achievable gain at each angle direction for all beam candidates.

We plot the gain in IEEE 802.15.3c and DFT-based beamforming starting from $K = 4$ of number beam candidates at the first level since this is the minimum number of beam candidates that can be obtained in these beamforming techniques. However, we can start beamforming in the FSM-KW and the proposed one with $K = 2$. Comparing these beamforming techniques, IEEE 802.15.3c gain plot shown in Figure 5.1 has the biggest beam variation due to its largest cusping loss. In Figure 5.2, DFT-based beamforming, which requires more flexible phase shift adjustment than IEEE 802.15.3c beamforming, has less gain fluctuation compared to IEEE 802.15.3c beamforming as all beams in DFT-based beamforming can reach the same maximum gain.

FSM-KW beamforming, as seen in Figure 5.3, gives the smallest fluctuations compared to IEEE 802.15.3c and DFT-based beamforming. FSM-KW beamforming also has better spatial filtering, where the beam only has radiation along its desired beamwidth, compared to the other beamforming techniques

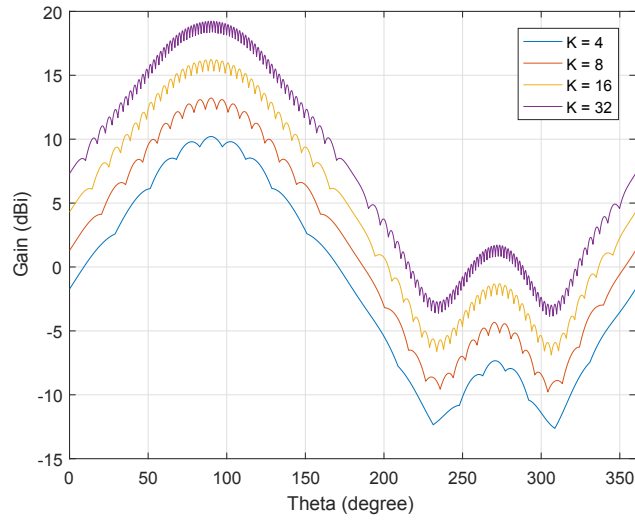


Figure 5.2: Gain variations in DFT beamforming

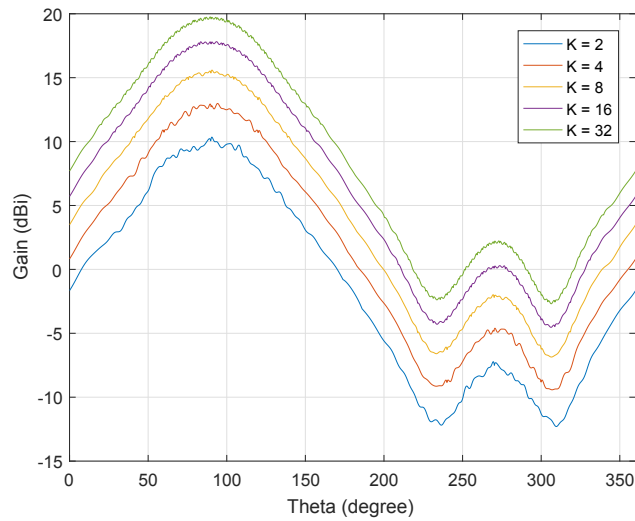


Figure 5.3: Gain variations in FSM-KW beamforming

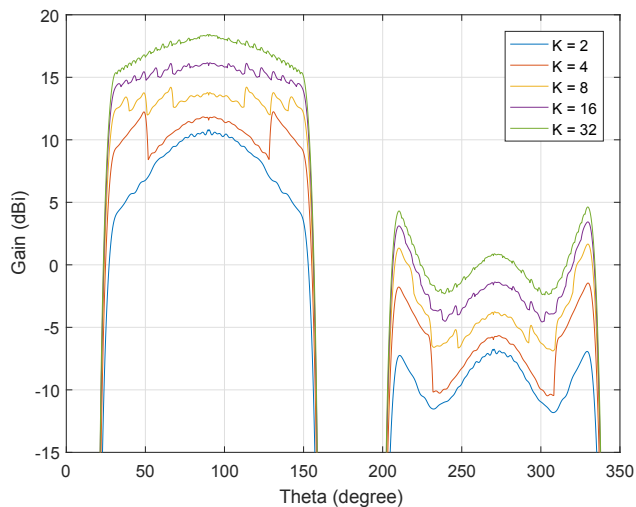


Figure 5.4: Gain variations in the proposed beamforming

Table 5.1: Gain at the broadside direction and the edge of its desired coverage angle in IEEE 802.15.3c beamforming

Number of Beam Candidates K	Gain at $\theta = 90^\circ$ (dBi)	Gain at $\theta = 30^\circ$ (dBi)	Gain Drop (dB)
4	10.21	3.24	6.97
8	13.22	5.66	7.56
16	16.23	8.45	7.78
32	19.24	11.40	7.84

so that the overlapping between the adjacent beams can be minimized. As a result, FSM-KW beamforming has a slightly higher gain than IEEE 802.15.3c and DFT-based beamforming. Nevertheless, FSM-KW beamforming does not consider non-isotropic element beam pattern, so the gain will drop significantly at low beam scanning angle.

The proposed beamforming in Figure 5.4 shows relatively flat beam pattern compared to FSM-KW beamforming. However, in the broadside direction, the proposed beamforming has lower gain than the previous beamforming techniques since the broadside beam in the proposed beamforming has larger beamwidth than the one in the FSM-KW beamforming.

The comparison of gain at the edge of the desired scanning coverage ($\theta = 30^\circ$) and at the broadside direction ($\theta = 90^\circ$) for each beamforming techniques can be seen in Table 5.1, Table 5.2, Table 5.3, and Table 5.4. From these tables, it can be said that in general the gain degradation from the broadside direction ($\theta = 90^\circ$) to the edge of scanning coverage ($\theta = 30^\circ$) for IEEE 802.15.3c beamforming, DFT-based beamforming, and FSM-KW beamforming are

Table 5.2: Gain at the broadside direction and the edge of its desired coverage angle in DFT beamforming

Number of Beam Candidates K	Gain at $\theta = 90^\circ$ (dBi)	Gain at $\theta = 30^\circ$ (dBi)	Gain Drop (dB)
4	10.21	2.84	7.37
8	13.22	6.42	6.80
16	16.23	9.38	6.85
32	19.24	12.15	7.09

Table 5.3: Gain at the broadside direction and the edge of its desired coverage angle in FSM-KW beamforming

Number of Beam Candidates K	Gain at $\theta = 90^\circ$ (dBi)	Gain at $\theta = 30^\circ$ (dBi)	Gain Drop (dB)
2	10.35	2.94	7.41
4	12.98	6.00	6.99
8	15.59	8.68	6.91
16	17.82	11.07	6.75
32	19.75	12.94	6.81

Table 5.4: Gain at the broadside direction and the edge of its desired coverage angle in the proposed beamforming

Number of Beam Candidates K	Gain at $\theta = 90^\circ$ (dBi)	Gain at $\theta = 30^\circ$ (dBi)	Gain Drop (dB)
2	10.80	3.60	7.19
4	12.14	8.75	3.39
8	14.22	11.82	2.40
16	16.29	13.84	2.45
32	18.22	15.12	3.09

close to the gain degradation in the element pattern which is 6.79 dB. By using the proposed beamforming, the beam degradation can be reduced to around 3 dB depending on the beam-searching level.

Beam degradation in the proposed beamforming will reach minimum until a certain level. It will increase again in the high beam-searching level when the beamforming cannot design very narrow beam (to give high array factor) at the edge of scanning coverage direction with a fixed number of antenna elements.

In general, the proposed beamforming has higher gain at the edge of beam than the FSM-KW beamforming. For example, when $K = 32$ at $\theta = 30^\circ$ the proposed beamforming has gain of 15.12 dBi while the FSM-KW beamforming has gain of 12.94 dBi, so there is 2.18 dB of gain improvement. Nevertheless, this improvement should be paid with low gain in the broadside direction. The proposed beam at broadside direction has a slightly lower gain than the FSM-KW beam which are 18.22 dBi and 19.75 dBi for the proposed beamforming and the FSM-KW beamforming respectively.

5.2 Received Signal Quality Analysis

To measure the effectiveness of the proposed beamforming compared to FSM-KW beamforming, we calculate the received signal-to-noise ratio (SNR) where STA1 acts as the transmitter while STA2 is the receiver. In this case we only consider the large scale channel fading in the indoor environment and also there is only a single beam ($N_s = 1$) created at one time. Maximum transmitted power, P_{tx} is set to 10 dBm. The SNR calculations are done for 1000. For all beam-searching level, the beams are designed in hybrid beamforming architecture with $M = 64$ antenna elements and $N_{RF} = 8$ RF chains.

We set such that STA1 and STA2 are separated with 10 m of distance, and these two devices can perform beamforming through its 120° of scanning coverage as seen in Figure 5.5. The STA1 and STA2 orientation is set randomly for each measurement using MATLAB normal distribution pseudo-random generator. However, the STA1 position is always in the 120° scanning coverage of the STA2 and vice versa, the STA2 position is always in the 120° scanning coverage of the STA1. In this case, the STA1 will act as the transmitter while the STA2 is the receiver.

Path-loss model for indoor environment in the large scale channel fading can be expressed as

$$L(d) = L(d_0) + 10n \log_{10} \left(\frac{d}{d_0} \right) + X_\Omega [dB] \quad (5.1)$$

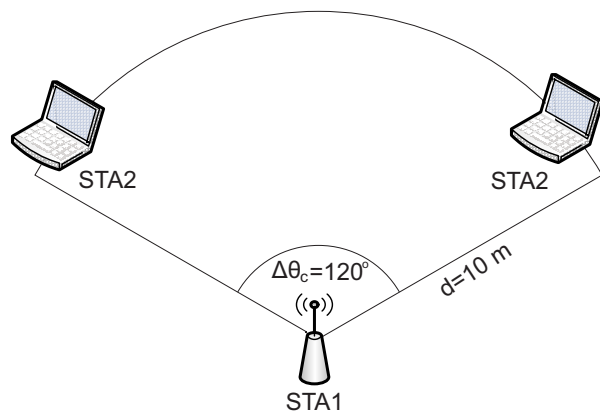


Figure 5.5: Illustration of measuring received signal quality

where $L(d)$ is path loss in dB at distance d , $L(d_0)$ is the reference path loss in dB at distance d_0 , n is path-loss exponent, and X_Ω is shadowing component which has Gaussian distribution with zero mean and Ω standard deviation. For generic LOS condition in indoor environment, $L(d_0) = 68$ dB, $n = 1.7$ and $\Omega = 1.8$ dB [38].

The received SNR can be calculated as

$$SNR = P_{tx} + G_{tx} + G_{rx} - L - [174 \text{ dBm/Hz} + 10\log(B) + NF] \text{ [dB]} \quad (5.2)$$

where P_{tx} is transmitted power which is set to 10 dBm, G_{tx} is transmit antenna gain, G_{rx} is receive antenna gain, B is channel bandwidth which is 2.16 GHz and NF is noise figure which is set to 8 dB.

The average received SNR results are depicted in Figure 5.6 where the proposed beamforming a little bit outperforms FSM-KW beamforming. It can be seen that in average, the proposed beamforming has a slightly higher received SNR than the FSM-KW beamforming due to the coverage angle limitation in the proposed beamforming. However, as the beam-searching level increases, the average received SNR difference between FSM-KW beamforming and the proposed beamforming will be less. This can happen since for a limited number of antenna elements the proposed beamforming cannot accommodate to design a highly narrow beam as the beam-searching level increases where in the high level of beam-searching, the proposed beamforming has to create a very narrow to maintain the gain level equals.

Hybrid beamforming in our simulation scenario that uses $N_{RF} = 8$ number of RF chains nearly does not affect on the beamforming performance (average SNR). We can see that the proposed beamforming, both for hybrid beamforming and fully-digital beamforming, have almost the same average SNR. Thus, we can conclude that the hybrid beamforming really helps reducing the hardware complexity, where in our case fully-digital beamforming must use $M = 64$ number of RF chains and hybrid beamforming only requires $N_{RF} = 8$ number of RF chains, without sacrificing the beamforming quality.

Figure 5.7 and Figure 5.8 show the box plot of received SNR data for the FSM-KW beamforming and the proposed beamforming, respectively. These box plots show the distribution of the received SNR, especially 25th percentile and 75th percentile of the data shown in the blue box of the box plot. The 25th percentile means that 25% of the SNR data is below 25th percentile value, and so does 75th percentile means that 75% of the SNR data is below 75% percentile value. From Figure 5.7 and Figure 5.8, visually we can see that the proposed beamforming has less distance between the 25th percentile and the 75th percentile than the FSM-KW beamforming, which means the variance in the proposed beamforming is less than the FSM-KW beamforming.

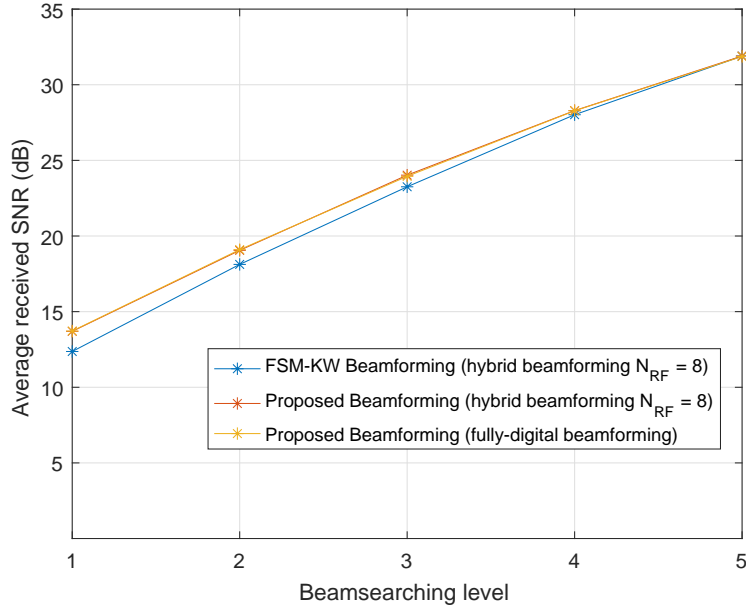


Figure 5.6: Average received SNR for 1000 iterations in the FSM-KW beamforming and the proposed uniform beamforming

The proposed beamforming distribute the beam gain for all beam candidates so that the beam candidates have equal gain. Compared to the FSM-KW beamforming, in the proposed beamforming the gain at the edge of scanning coverage increases with the cost of gain decreasing in the broadside direction. As result, the received signal quality in the same distance for any direction within the scanning coverage is relatively the same.

In the proposed beamforming, the received signal quality in the broadside direction will not be as high as in the FSM-KW beamforming. However, in the direction close to the end-fire, the received signal quality can be maintained not to degrade too much so that in this direction the proposed beamforming has higher SNR than the one in the FSM-KW beamforming. This signal quality improvement for low percentile can be seen in the 25th percentile of received SNR depicted in Table 5.5 where the proposed beamforming has higher 25th percentile SNR than the FSM-KW beamforming with the cost of lower 75th SNR in the proposed beamforming than the one in the FSM-KW beamforming.

The proposed beamforming can achieve the objective to create relatively uniform gain within the desired scanning coverage so that the beam at the edge of coverage will not degrade severely. By maintaining the gain level and implementing several antenna systems to cover 360° , it is expected that for

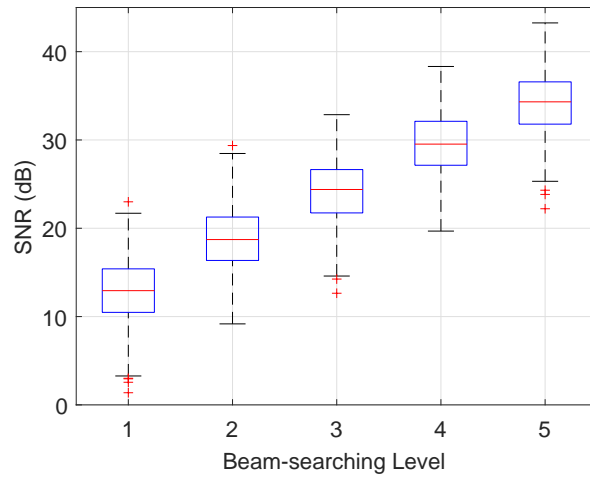


Figure 5.7: Box plot data of the received SNR for 1000 iterations in the FSM-KW beamforming (hybrid beamforming $M = 64, N_{RF} = 8$)

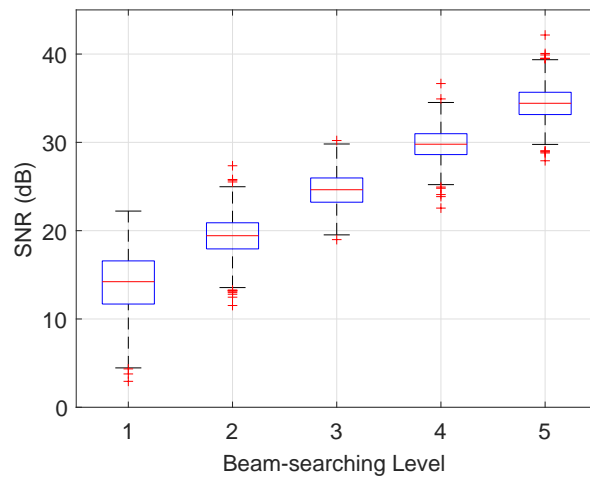


Figure 5.8: Box plot data of the received SNR for 1000 iterations in the proposed beamforming (hybrid beamforming $M = 64, N_{RF} = 8$)

Table 5.5: 25th percentile and 75th percentile comparison of received SNR in the proposed beamforming and the FSM-KW beamforming

Beam-searching Level	Received SNR (dB)			
	25th Percentile		75th Percentile	
	FSM-KW beamforming	Proposed beamforming	FSM-KW beamforming	Proposed beamforming
1	10.48	11.69	15.40	16.58
2	16.36	17.94	21.27	20.89
3	21.74	23.22	26.65	25.97
4	27.14	28.62	32.11	30.98
5	31.79	33.15	36.58	35.67

the same distance the signal quality can be received relatively uniform in all direction. Therefore, the signal quality at the edge of scanning coverage will not degrade too much, and the devices can be put at any orientation without significantly affecting the signal quality.

Chapter 6

Conclusion and Future Work

6.1 Conclusion

Communication in the 60 GHz band offers ultra high data rate. Providing 7 GHz of bandwidth, it can achieve multi-gigabit data rate. However, its high frequency not only provides high bandwidth but also gives greater losses compared to 2.4 GHz and 5 GHz band. Thus, the received signal in the 60 GHz will weaken severely.

Due to its high losses, beamforming becomes an essential technique in the 60 GHz communications by giving additional gain through its narrow beam. Analog beamforming is used in IEEE 802.115.3c and IEEE 802.11ad to simplify the hardware implementation. This analog beamforming limits the beamforming design such as beam intersection between the adjacent beams. To find the best beam pair, these two IEEE standards exploits two-level hierarchical beam-searching approach. However, in the high-resolution narrow beam, the beam-searching mechanism still can cause overhead. Therefore, we consider to use hierarchical beam-searching approach, where there are multi-level of beam-searching, to reduce the number of training packets.

FSM-KW beamforming, which offers design flexibility but requires more complex hardware implementation, can be used in the hierarchical beam-searching approach, where at each stage of beam-searching the interest area is narrowed. FSM-KW beamforming also has small beam intersection that can reduce interference. However, to the best author knowledge, there is no beamforming design in mmWave communications that consider non-isotropic element beam pattern in their design.

Prior beamforming designs take the assumption that element beam pattern is

isotropic, which is unrealistic. As a result, the beamforming that is designed in array antenna consisting of several patch antenna elements will suffer gain degradation in the direction close to end-fire direction. The gain of each beam will vary depending on the angle direction where beam close to the end-fire direction has smaller gain than the one in the broadside direction. Thus, the signal quality will depend on the antenna orientation where the signal quality in the direction near to the end-fire direction will be worse than the one in the broadside direction.

The proposed beamforming is designed based on FSM-KW beamforming due to its flexibilities to set the beamwidth and to reduce the beam ripples. Beamwidth adjustment is needed to accommodate hierarchical beam-searching approach. With Kaiser window in the beamforming, the trade-off between the ripple amplitude and the transition width can be adjusted. FSM-KW beamforming requires a higher number of antenna elements than IEEE 802.15.3c beamforming and DFT-based beamforming. It also needs to adjust the amplitude and phase shift at any arbitrary value. Therefore, it will not be feasible if the proposed beamforming is implemented in digital beamforming, which requires a lot number of RF chains. As an alternative, hybrid beamforming, with a low number of RF chains but with performance close to the digital beamforming, is chosen.

The proposed uniform beamforming offers relatively uniform gain within the scanning coverage, which can be set arbitrarily depending on the beam requirement. The scanning coverage limitation in the proposed beamforming is considered more practical than covering the 360° with only one antenna system since the patch antenna gain will degrade seriously in the direction close to the end-fire direction (low angle direction). Compared to the classical FSM-KW, the proposed beamforming can maintain relatively flat gain within the scanning coverage with non-isotropic element beam pattern assumption. The proposed beamforming can improve the gain at the edge of scanning coverage direction so that it is almost the same with the one in the broadside direction.

6.2 Future Work

This research only focuses on linear array antenna that only facilitates two-dimensional (2D) beamforming where the antenna only steers the beam either into elevation or azimuthal angle, depending on the antenna orientation. Three-dimensional (3D) beamforming can be a future work where theoretically, 3D beamforming can be obtained from a Kronecker product of beamforming in the azimuthal angle and beamforming in the elevation angle. Beam-searching algorithm in the 3D beamforming also can be further

discussed to find the optimal one.

There is still directivity degradation within one beam since the array factor in the desired beamwidth has a flat pattern while the element pattern decline in the low angle direction. As a consequence, the array factor cannot compensate the directivity degradation. If the array factor within the same beam can be designed such that within the same beam the array factor increases in the low angle direction, the directivity degradation within one beam can be minimized.

Appendices

Appendix A

Finest Beam Candidates

In this appendix, finest beam candidates for various scanning coverages and different number of beam candidates. The beams are designed with number of antenna elements $M = 128$ in the digital beamforming architecture. The element pattern assumption is taken from the first element pattern model in [36].

A.1 Scanning Coverage $\Delta\theta_c = 120^\circ$

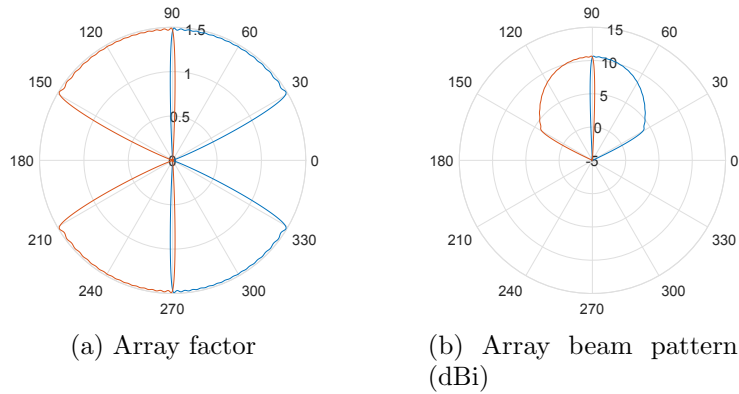


Figure A.1: 2 beam candidates in the proposed beamforming covering 120°

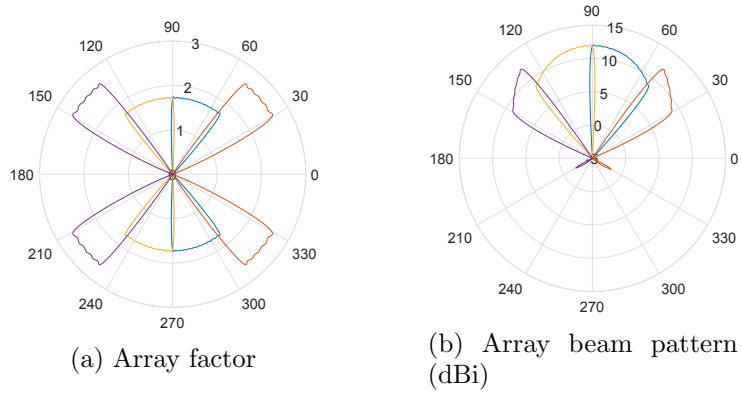


Figure A.2: 4 beam candidates in the proposed beamforming covering 120°

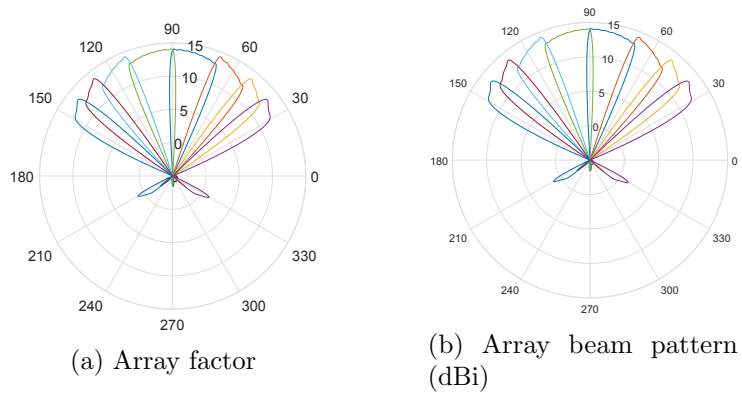


Figure A.3: 8 beam candidates in the proposed beamforming covering 120°

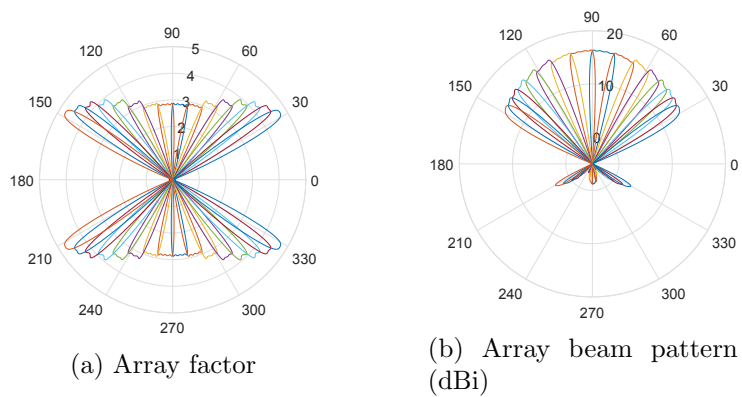
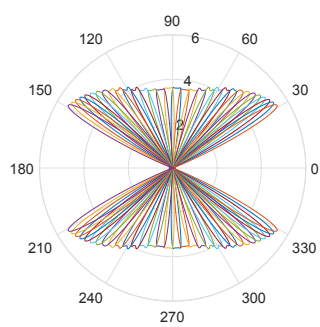
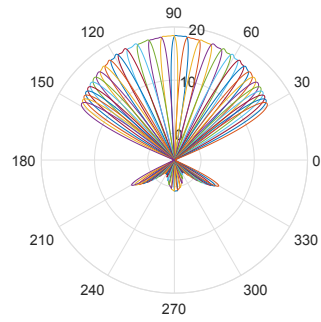


Figure A.4: 16 beam candidates in the proposed beamforming covering 120°



(a) Array factor



(b) Array beam pattern (dB)

Figure A.5: 32 beam candidates in the proposed beamforming covering 120°

A.2 Scanning Coverage $\Delta\theta_c = 60^\circ$

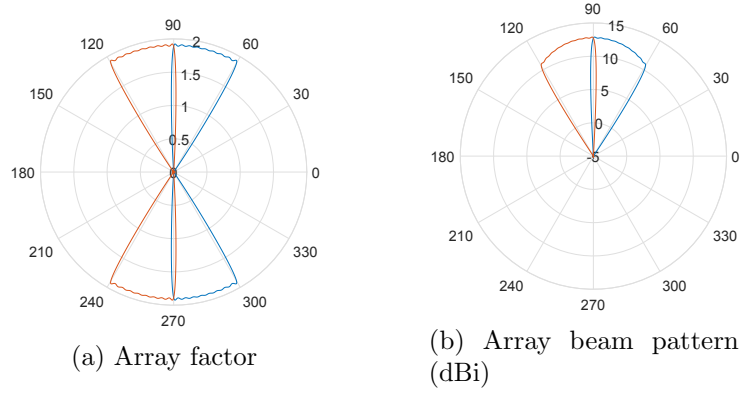


Figure A.6: 2 beam candidates in the proposed beamforming covering 60°

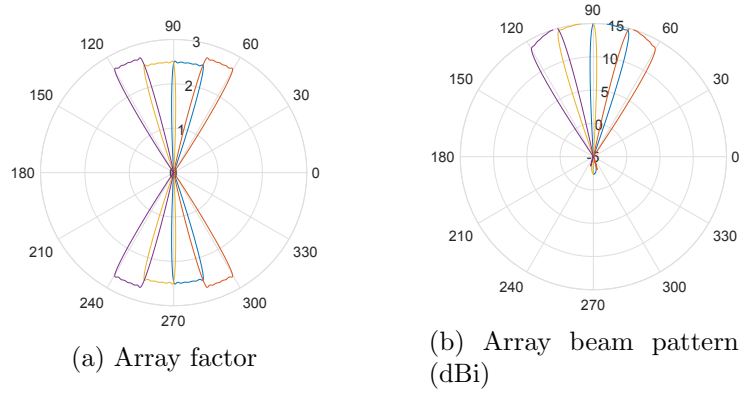


Figure A.7: 4 beam candidates in the proposed beamforming covering 60°

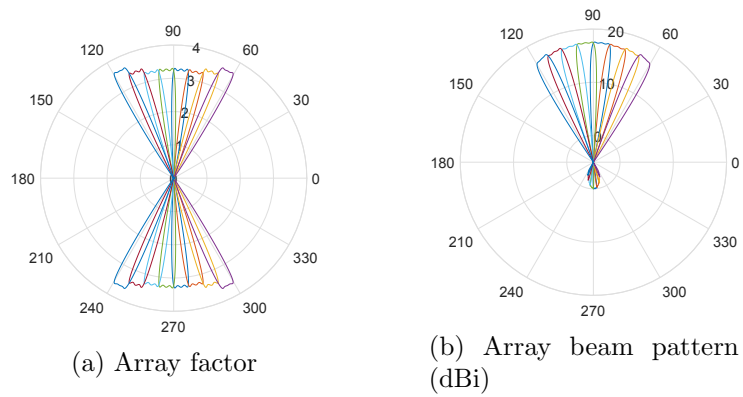
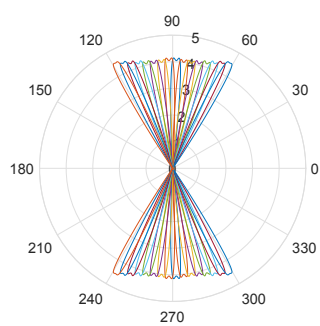
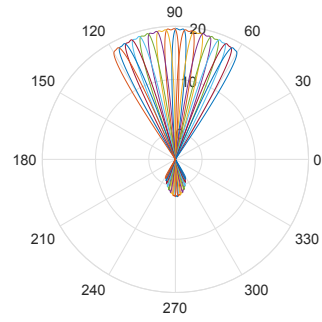


Figure A.8: 8 beam candidates in the proposed beamforming covering 60°

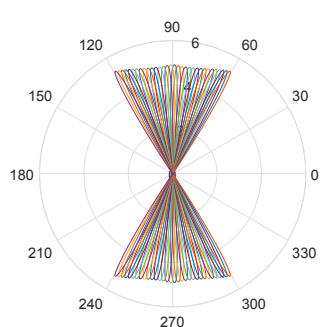


(a) Array factor

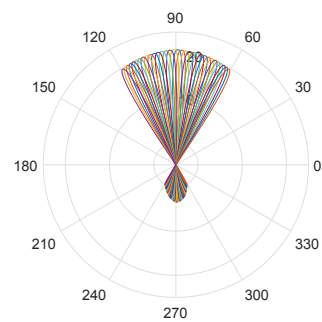


(b) Array beam pattern (dBi)

Figure A.9: 16 beam candidates in the proposed beamforming covering 60°



(a) Array factor



(b) Array beam pattern (dBi)

Figure A.10: 32 beam candidates in the proposed beamforming covering 60°

Appendix B

Pseudo Algorithms

B.1 Hybrid Beamforming Algorithm

Algorithm 3: OMP algorithm for hybrid beamforming [26] [28] [29]

Input : Ideal digital predefined codebook w , restricted RF codebook candidate $w_{RF_{can}}$

Output : Predefined RF codebook w_{RF} , predefined baseband codebook w_{BB}

- 1: $w_{RF} =$ empty matrix
 - 2: $w_{res} = w$
 - 3: **for** $i \leq N_{RF}$ **do**
 - 4: $\Psi = w_{RF_{can}}^H w_{res}$
 - 5: $k = \arg \max_{m=1, \dots, K} (\Psi \Psi^H)_{m,m}$
 - 6: $w_{RF} = [w_{RF}, [w_{RF_{can}}]_{:,k}]$
 - 7: $w_{BB} = (w_{RF}^H w_{RF})^{-1} w_{RF}^H w$
 - 8: $w_{res} = \frac{w - w_{RF} w_{BB}}{\|w - w_{RF} w_{BB}\|_2}$
 - 9: **end for**
 - 10: $w_{BB} = \frac{w_{BB}}{\|w_{RF} w_{BB}\|_2}$
-

Algorithm 4: DDL OMP algorithm for hybrid beamforming [12]

Input : Ideal digital predefined codebook w , restricted RF codebook candidate $w_{RF_{can}}$

Output : Predefined RF codebook w_{RF} , predefined baseband codebook w_{BB}

- 1: $w_{RF} =$ empty matrix
- 2: $w_{RF_{can}} = [w_{RF_{can}}, S(w)]$ $\{S(v)$ is an operator that maps the vector v into one close vector attainable with b -bit RF phase shifters $\}$
- 3: $w'_{RF_{can}} = w_{RF_{can}}$
- 4: $w_{res} = w$
- 5: **for** $i \leq N_{RF}$ **do**
- 6: $\Phi = w'^H_{RF_{can}} w_{res}$
- 7: $k = \arg \max_{m=1, \dots, K+1} |\Phi(m)|$
- 8: $w_{RF} = [w_{RF}, [w_{RF_{can}}]_{:,k}]$
- 9: $w_{BB} = (w^H_{RF} w_{RF})^{-1} w^H_{RF} w$
- 10: $w_{res} = w - w_{RF} w_{BB}$
- 11: $[w'_{RF_{can}}]_{:,k} = [w_{RF_{can}}]_{:,k} - (w^H_{RF} w_{RF})^{-1} w^H_{RF} w_{RF_{can}}$
- 12: **for** $j \geq M + 1$ **do**
- 13: **if** $\|w'_{RF_{can}}\|_2 \neq 0$ **then**
- 14: $[w'_{RF_{can}}]_{:,k} = \frac{[w'_{RF_{can}}]_{:,k}}{\|w'_{RF_{can}}\|_2}$
- 15: **end if**
- 16: **end for**
- 17: $w_{BB} = \frac{w_{BB}}{\|w_{RF} w_{BB}\|_2}$
- 18: **end for**

B.2 Hierarchical Beam-searching Algorithm in the Proposed Beamforming

Algorithm 5: Find the best beam pair $AWV^1 = w(\log_2 K, k_1)$ and $AWV^2 = w(\log_2 K, k_2)$, assuming STA1 and STA2 have the same beam-searching level $L = \log_2 K$

Input : A full set of predefined codebook

$[w(1, 1), w(1, 2)], [w(2, 1), \dots, w(2, 4)], \dots, [w(\log_2 K, 1), \dots, w(\log_2 K, K)]$

Output : Best beam pair $w_1(\log_2 K, k_1)$ and $w_2(\log_2 K, k_2)$

- 1: $\ell = 1; k_1 = 1; k_2 = 1$
- 2: STA1 and STA2 transmit beacons through its quasi-omnidirectional beam $AWV^1 = w(0, k_1)$ and $AWV^2 = w(0, k_2)$ respectively
- 3: STA1 and STA2 detect the beacons and start beamforming
- 4: **while** $\ell \leq L$ **do**
- 5: STA1 sets its AWVs into $AWV_1^1 = w(\ell, 2k_1 - 1)$ and $AWV_2^1 = w(\ell, 2k_1)$ alternately
- 6: STA2 sets its AWV into $AWV^2 = w(\ell - 1, k_2)$
- 7: STA2 measures the signal quality received from AWV_1^1 and AWV_2^1 which are Γ_1^1 and Γ_2^1 respectively
- 8: **if** $\Gamma_1^1 \geq \Gamma_2^1$ **then**
- 9: $k_1 = 2k_1 - 1$
- 10: **else**
- 11: $k_1 = 2k_1$
- 12: **end if**
- 13: STA1 sets its AWV into $AWV^1 = w(\ell, k_1)$
- 14: STA2 sets its AWVs into $AWV_1^2 = w(\ell, 2k_2 - 1)$ and $AWV_2^2 = w(\ell, 2k_2)$ alternately
- 15: STA1 measures the signal quality received from AWV_1^2 and AWV_2^2 which are Γ_1^2 and Γ_2^2 respectively
- 16: **if** $\Gamma_1^2 \geq \Gamma_2^2$ **then**
- 17: $k_2 = 2k_2 - 1$
- 18: **else**
- 19: $k_2 = 2k_2$
- 20: **end if**
- 21: $\ell ++$
- 22: **end while**
- 23: $AWV^1 = w(\log_2 K, k_1)$
- 24: $AWV^2 = w(\log_2 K, k_2)$

Bibliography

- [1] Cisco, “Cisco Visual Networking Index: Global Mobile Data Traffic Forecast Update 2015-2020,” *Cisco Public Information*, February, 2016.
- [2] R. Van Uden, R. A. Correa, E. A. Lopez, F. Huijskens, C. Xia, G. Li, A. Schülzgen, H. de Waardt, A. Koonen, and C. Okonkwo, “Ultra-high-density Spatial Division Multiplexing with a Few-mode Multicore Fibre,” *Nature Photonics*, vol. 8, no. 11, pp. 865–870, 2014.
- [3] W.-F. Alliance, “Wi-Fi CERTIFIED n: Longer-Range, Faster-Throughput, Multimedia-Grade Wi-Fi Networks,” 2009.
- [4] I. C. Society, “Part 11: Wireless LAN Medium Access Control (MAC) and Physical Layer (Phy) Specifications, Amendment 4: Enhancements for Very High Throughput for Operation in Bands below 6 GHz,” *IEEE*, 2013.
- [5] Y. Qi, M. Hunukumbure, M. Nekovee, J. Lorca, and V. Sgardoni, “Quantifying Data Rate and Bandwidth Requirements for Immersive 5G Experience,” in *Communications Workshops (ICC), 2016 IEEE International Conference on*, pp. 455–461, IEEE, 2016.
- [6] R. ITU-R, “P. 676-5: Attenuation by Atmospheric Gases in the Frequency Range 1 to 350 GHz,” *Geneva*, 2001.
- [7] R. W. Heath, N. Gonzalez-Prelcic, S. Rangan, W. Roh, and A. M. Sayeed, “An Overview of Signal Processing Techniques for Millimeter Wave MIMO Systems,” *IEEE Journal of Selected Topics in Signal Processing*, vol. 10, no. 3, pp. 436–453, 2016.
- [8] R. C. Daniels and R. W. Heath Jr, “60 GHz Wireless Communications: Emerging Requirements and Design Recommendations,” *IEEE Vehicular Technology Magazine*, vol. 2, no. 3, pp. 41–50, 2007.
- [9] ITU, “Report ITU-R M.2227, Multiple Gigabit Wireless Systems in Frequencies Around 60 GHz,” 2011.

- [10] T. S. Rappaport, R. W. Heath, R. C. Daniels, and J. N. Murdock, *Millimeter Wave Wireless Communications*. Prentice Hall, 2014.
- [11] L. Chen, Y. Yang, X. Chen, and W. Wang, "Multi-stage Beamforming Codebook for 60GHz WPAN," in *Communications and Networking in China (CHINACOM), 2011 6th International ICST Conference on*, pp. 361–365, IEEE, 2011.
- [12] D. De Donno, J. P. Beltrán, D. Giustiniano, and J. Widmer, "Hybrid Analog-Digital Beam Training for mmWave Systems with Low-Resolution RF Phase Shifters," in *IEEE International Conference on Communications Workshops (ICC) 2016*, pp. 700–705, IEEE, 2016.
- [13] T. He and Z. Xiao, "Suboptimal Beam Search Algorithm and Codebook Design for Millimeter-wave Communications," *Mobile Networks and Applications*, vol. 20, no. 1, pp. 86–97, 2015.
- [14] S. Hur, T. Kim, D. J. Love, J. V. Krogmeier, T. A. Thomas, and A. Ghosh, "Millimeter Wave Beamforming for Wireless Backhaul and Access in Small Cell Networks," *IEEE Transactions on Communications*, vol. 61, no. 10, pp. 4391–4403, 2013.
- [15] Z. Xiao, T. He, P. Xia, and X.-G. Xia, "Hierarchical Codebook Design for Beamforming Training in Millimeter-Wave Communication," *IEEE Transactions on Wireless Communications*, vol. 15, no. 5, pp. 3380–3392, 2016.
- [16] T. Ngo, M. Tummala, and J. McEachen, "Introduction: Switched/Steered Directional Antennas for Networking," in *Wireless Network Performance Enhancement via Directional Antennas: Models, Protocols, and Systems*, pp. 3–19, CRC Press, 2015.
- [17] C. A. Balanis, *Antenna Theory: Analysis and Design*. John Wiley & Sons, 2016.
- [18] R. J. Mailloux, *Phased Array Antenna Handbook*, vol. 2. Artech House Boston, 2005.
- [19] W. L. Stutzman and G. A. Thiele, *Antenna Theory and Design*. John Wiley & Sons, 2012.
- [20] J. Litva and T. K. Lo, *Digital Beamforming in Wireless Communications*. Artech House, Inc., 1996.
- [21] IEEE Standards Association, "IEEE Std 802.15.3c - 2009, Part 15.3: Wireless Medium Access Control (MAC) and Physical Layer (PHY) Specifications for High Rate Wireless Personal Area Networks (WPANs)," *IEEE Std*, 2009.

- [22] I. C. Society, *802.11ad-2012 - IEEE Standard for Information Technology–Telecommunications and Information Exchange Between Systems–Local and Metropolitan Area Networks–Specific Requirements–Part 11: Wireless LAN Medium Access Control (MAC) and Physical Layer (PHY) Specifications Amendment 3: Enhancements for Very High Throughput in the 60 GHz Band*. IEEE, 2012.
- [23] J. Wang, “Beam Codebook Based Beamforming Protocol for Multi-Gbps Millimeter-Wave WPAN Systems,” *IEEE Journal on Selected Areas in Communications*, vol. 27, no. 8, 2009.
- [24] J. Qiao, X. Shen, J. W. Mark, and Y. He, “MAC-layer Concurrent Beamforming Protocol for Indoor Millimeter-wave Networks,” *IEEE Transactions on Vehicular Technology*, vol. 64, no. 1, pp. 327–338, 2015.
- [25] S. J. Orfanidis, *Electromagnetic Waves and Antennas*. Rutgers University New Brunswick, NJ, 2002.
- [26] A. Alkhateeb, O. El Ayach, G. Leus, and R. W. Heath, “Channel Estimation and Hybrid Precoding for Millimeter Wave Cellular Systems,” *IEEE Journal of Selected Topics in Signal Processing*, vol. 8, no. 5, pp. 831–846, 2014.
- [27] S. Rangan, T. S. Rappaport, and E. Erkip, “Millimeter-wave Cellular Wireless Networks: Potentials and Challenges,” *Proceedings of the IEEE*, vol. 102, no. 3, pp. 366–385, 2014.
- [28] O. El Ayach, S. Rajagopal, S. Abu-Surra, Z. Pi, and R. W. Heath, “Spatially Sparse Precoding in Millimeter Wave MIMO Systems,” *IEEE Transactions on Wireless Communications*, vol. 13, no. 3, pp. 1499–1513, 2014.
- [29] O. El Ayach, R. W. Heath, S. Abu-Surra, S. Rajagopal, and Z. Pi, “Low Complexity Precoding for Large Millimeter Wave MIMO Systems,” in *IEEE International Conference on Communications (ICC) 2012*, pp. 3724–3729, IEEE, 2012.
- [30] W. Zou, Z. Cui, B. Li, Z. Zhou, and Y. Hu, “N Phases Based Beamforming Bodebook Design Scheme for 60 GHz Wireless Communication,” *Journal of Beijing University of Posts and Telecommunications*, vol. 35, no. 3, pp. 1–5, 2012.
- [31] J. Palacios, D. De Donno, D. Giustiniano, and J. Widmer, “Speeding Up mmWave Beam Training through Low-Complexity Hybrid Transceivers,” in *IEEE 27th Annual International Symposium on Personal, Indoor, and Mobile Radio Communications (PIMRC) 2016*, pp. 1–7, IEEE, 2016.
- [32] D. De Donno, J. Palacios, and J. Widmer, “Millimeter-Wave Beam Training Acceleration through Low-Complexity Hybrid Transceivers,”

- IEEE Transactions on Wireless Communications*, vol. 16, no. 6, pp. 3646–3660, 2017.
- [33] T. C. Cheston and J. Frank, “Phased Array Radar Antennas,” *Radar Handbook*, pp. 7–1, 1990.
- [34] B. Forman, “Directivity Characteristics of Scannable Planar Arrays,” *IEEE Transactions on Antennas and Propagation*, vol. 20, no. 3, pp. 245–252, 1972.
- [35] M. Golio and J. Golio, *RF and Microwave Passive and Active Technologies*. CRC Press, 2007.
- [36] D. J. Joaquin, *A New Low-Cost Microstrip Antenna Array for 60 GHz Applications*. PhD thesis, Utah State University, 2016.
- [37] J. L. Volakis, *On-Chip Antenna Element and Array Design for Short Range Millimeter-Wave Communications*. PhD thesis, The Ohio State University, 2007.
- [38] P. F. Smulders, “Statistical Characterization of 60-GHz Indoor Radio Channels,” *IEEE Transactions on Antennas and Propagation*, vol. 57, no. 10, pp. 2820–2829, 2009.